Effects of disorder in striped phases of cuprate superconductors and in planar vortex lattices

Inaugural-Dissertation
zur
Erlangung des Doktorgrades
der Mathematisch-Naturwissenschaftlichen Fakultät
der Universität zu Köln

vorgelegt von
Simon Sebastian Bogner
aus Nürnberg

2003

Berichterstatter: Priv. Doz. Dr. S. Scheidl
Prof. Dr. M. Braden
Dr. T. Emig

Tag der mündlichen Prüfung: 11. Juli 2003

Abstract. — Effects of disorder on planar periodic structures in superconductors are examined in the present work. In part one we analyse the role of impurities in the striped phases of cuprate high-temperature superconductors. The geometrical degrees of freedom of the combined charge and spin superstructure in the two-dimensional (2D) copper-oxide planes are first discussed. Pinning by the atomic lattice – which might give rise to commensuration effects – is irrelevant on large length scales in the presence of quenched disorder. As a consequence, the stripes have divergent displacement fluctuations and topological defects are present at all temperatures, implying short-ranged positional order of the stripe array with a finite correlation length even at zero temperature. Lock-in phenomena can exist only as crossovers but not as transitions. These results are in agreement with the glassy nature of stripes observed in experiments.
Secondly, we study the effect of disorder on coupled planar arrays of Luttinger liquids (LLs) as a model for the electronic degrees of freedom of the stripes. In the framework of a renormalisation group analysis, we find that weak inter-LL charge-density-wave couplings are always irrelevant as opposed to the pure system. By varying either disorder strength, intra- or inter-LL interactions, the system can undergo a delocalisation transition between an insulator and a strongly anisotropic metallic state with LL-like transport. The delocalised state can exist other than in one dimension even for a purely repulsive interactions and it is characterised by short-ranged charge-density-wave order, quasi-long-ranged superconducting order along the stripes and short-ranged superconducting order in the transversal direction.

In part two the random $(1+1)$-dimensional fluxline lattice as a model system for vortex glasses (VG) is examined. Using the recently found exact Replica Bethe Ansatz solution [EK01] for a special vortex interaction, we argue against the existence of the transition to a thermally unpinned phase above the VG. The argument is generalised to arbitrary repulsive interactions via the mapping to one-dimensional repulsive fermions. A small window for the transition sharply below the superconducting critical temperature is opened by the introduction of a finite persistence length of a single vortex line. In the phenomenologically related random-field XY model the transition under debate is present but does not leave any signature in the free energy as we calculate in a sideline of the reasoning.
Finally, the relation of the vortex system to the random-bond dimer model is explored in detail. The latter can be simulated with a recently developed polynomial algorithm at a precision far beyond any previous Monte Carlo approach. Data from simulations, which are provided by the collaborating group of C. Zeng (Washington, D.C.), and theory do not only show qualitative but also excellent quantitative agreement for a wide range of observables: the large scale lattice stiffness; the average free energy, internal energy and entropy; moments of the disorder distributed free energy; specific heat. The special model character of the planar VG as a genuine glassy and yet in many aspects solvable system is highlighted.

Contents

A. Introduction

1 Striped phases in cuprate superconductors

High-temperature superconductivity (HTSC) was discovered in 1986 [BM86]. To the present day, a satisfactory understanding of the pairing mechanism in the new material classes has not been achieved. Early hopes for the designability of compounds with ever higher transition temperatures could not be fulfilled. Still, the intense research has greatly advanced the understanding of strongly correlated fermions and made this one of today's thriving fields in condensed-matter physics. The copper-oxide (CuO_2) planes common to all the important high-T_c compounds, the 'cuprates', have been identified as the basic functional building block. The rich phase diagram of HTSC is believed to emerge upon hole doping from the physics of these antiferromagnetic CuO_2 layers, which are often described by the very reduced paradigm model of highly correlated electrons, the Hubbard model. Theoretically, a new ordering phenomenon in doped antiferromagnets had been predicted [Sch89, ZG89, Mac89, EKL90]: the one-dimensional periodic accumulation of the free charges in 'rivers' that simultaneously act as anti-phase boundaries in the surrounding antiferromagnet. After the first experimental observation of these one-dimensional superstructures [TSA$^+$95] the field of stripes physics in the cuprates began to flourish. Not only is the existence of stripes by now experimentally proven in all the important compound classes, their relation to superconductivity is also largely debated. While the static, originally detected stripe structures quite clearly suppress superconductivity, the dynamically fluctuating variant plays an essential role in a class of – still – rather speculative model mechanism for high-temperature superconductivity [KFE98]. The focus of the present work is neither on the microscopic mechanism of the formation of stripes nor on the mechanism of superconductivity. We rather explore the influence of another key ingredient in real-world materials, which is, moreover, generic in doped compounds: disorder. In a first part (Chapter B), the structural properties of a stripe ordered phase are analysed. The preformed stripes are treated as collective quantum objects. Both the underlying periodic lattice and random impurities work against thermal and quantum fluctuations in the effort to pin the stripe array. The periodic potential tends to order the array while disorder pinning roughens the structure. The question in this multiple competition is which mechanism will prove most efficient. A motivation of such an analysis comes from the observation of particularly stable, static stripe structures at certain doping levels that correspond to well-defined stripe spacings [MSFS88]. A lock-in of the stripe superstructure in the underlying periodic atomic potential seems possible. On the other hand, glassy features of the superstructure have also been observed, which suggests a dominant role of disorder [TIU99, DGS$^+$00]. The situation in the present model is complicated with respect to roughening phenomena in disordered classical elastic systems [EN97, EN98] by the presence of quantum fluctuations. On a technical level, the quantum nature can be coded in an extra imaginary time dimension in the Feynman path integral

approach. Disorder is then correlated in time direction which has always prevented a closed renormalisation group (RG) analysis [Bal93]. In order to avoid the known obstacles our approach lies in a suitable successive 'switching on' of mechanisms. The effect of the latest mechanism on the phase diagram one step earlier is analysed with a combination of scaling and RG arguments. Eventually, having chosen a convenient order of steps, we arrive at the qualitative phase diagram for the full model. Disorder shows to be dominant on largest scales while lock-in effects can only be seen in crossover behaviour and cannot establish a phase of their own. A detailed overview of experimental observations in the cuprates – and related nickelate systems – and of the phenomenology of stripes is given in the introductory section of this first part on stripes.

In the second part (Chapter C) we turn to the so far neglected internal degrees of freedom of the 'rivers of charges'. In the limit of sharp distinction between charge-carrier-free regions and the charge stripes, these stripes may be considered as one dimensional electron gases (1DEG). They interact internally, described in the Luttinger liquid picture [Hal81a], and from stripe to stripe by the electron Coulomb repulsion. The coupling to spin degrees of freedom in the embedding antiferromagnet as well as inter-stripe superconducting order-parameter coupling opens a whole variety of possible emerging phases depending on the actual coupling parameters. A model calculation by Emery *et al.* [EK93, EKZ97] showed that the antiferromagnetic environment may induce a gap in the spin sector on the stripes. As a consequence, one-particle hopping between the stripes is no longer necessarily the dominant inter-stripe coupling. A novel two-dimensional non-Fermi liquid seems to be at least possible. This as a starting point, a series of publications tried to give phase diagrams of coupled Luttinger liquids as a model for cuprate superconductors [EFKL00, MKL01, VC01]. The most spectacular consequences are naturally emerging superconducting phases and also a phase where both of the strong, competing instabilities – charge-density-wave coupling and the superconducting order-parameter Josephson coupling – are irrelevant. This 'sliding Luttinger liquid' or 'smectic metal' would be the realisation of a two-dimensional metallic non-Fermi liquid. The caveat is, however, as big as the 'smectic metal' portion of the phase diagram is small. Only very arbitrary finetuning in the on-stripe and inter-stripe interactions which can hardly be related to the original Coulomb potential leads to the remarkable results. In our contribution to the model, we examine the influence of on-stripe disorder on the suggested phase diagrams, both for the finetuned interaction necessary to obtain the smectic metal and for a more realistic interaction derived from the screened Coulomb potential. In the latter case, the phase diagram looks less colourful with no smectic metal present. Generically, disorder reduces the superconducting phase and replaces all of the charge-density-wave phase by a disorder-localised phase with no translational symmetry. The smectic metal survives disorder localisation in the finetuned model in a *small* part of its *small* fraction of the phase diagram as the strongly modified 'disordered stripe metal' (DSM). Other than in the one-dimensional case, delocalisation is possible even for purely repulsive interactions. The delocalised state is characterised by short-ranged charge-density-wave order, the superconducting order is quasi-long-ranged along the stripes and short-ranged in the transverse direction.

2 Planar vortex systems

The effect of disorder on a periodic structure in superconductors – the theme is the same when the glass phase of planar vortex arrays is examined in the second part of the present work. The Abrikisov

or mixed phase of type-II superconductors – and the high-temperature superconductors are strongly-type II – is of eminent technological relevance. An external magnetic field enters the material in the quantised form of fluxlines which order ideally in a regular lattice. Any transport current in the superconductor will induce such a field, rendering fluxlines ubiquitous in practical situations. Disorder plays under these circumstances not a destructive but a constructive role. Impurities – unavoidable anyway – are welcome to pin the vortex array and prevent dissipation from fluxline motion transverse to the transport current. The nature of the vortex state is not left unchanged by disorder. The translational order of the regular lattice is destroyed in what is then a vortex glass (VG). This phase is fascinating from a theoretical point of view also as a model glass system, on par with the extensive field of spin glasses [BY86]. Translational symmetry is broken, metastable states slow down the relaxation and large barriers in between dominate transport characteristics. The energetical favourability of topological defects will depend on the strength of thermal and disorder fluctuations. They will render the phase diagram even richer with the topologically ordered Bragg glass at weak disorder and a possibly multistep melting behaviour [Kie98, BMS$^+$01, AKM$^+$01].
The *planar* vortex array is a compromise model in a good sense. The reduction of the dimension transverse to the vortex lines may seem artificial considering the technological relevance. However, the system is now simple enough to be approached very successfully in the threefold way of modern physics: (i) experimentally, (ii) analytically and (iii) by numerical means. Since long, theory has predicted the planar vortex array to be a generic glassy system, despite the dimensional simplification. The mapping to the random field XY (RFXY) model [Fis89] reveals the existence of a low-temperature disorder-dominated phase [CO82], with all the signatures in static and dynamic correlations of a glass [CS96]. Recently, in a prominent experiment with a thin specimen of a conventional superconductor, such a planar vortex glass has been investigated [BAP$^+$99]. As for the numerical side, an extensive literature has grown on Monte Carlo simulations, mainly of the related RFXY model [BH94, MMRL95, CS95]. Only lately the discovery of the relation to a model of statistical combinatorics, the random-bond dimer model, which can be simulated with polynomial algorithms, has put the planar vortex array in a unique position in the field of vortex (and in many senses related spin) glasses. System of linear sizes up to $L = 512$ can be treated on desktop computers with numerical exact algorithms [ZLH99]. Even the quantitative testing of scaling approaches like the droplet picture of spin glass theory [FH88] seems within reach.
Our contribution is twofold. First, we critically examine the possible transition of the planar vortex glass to an unpinned phase at higher temperatures as implied by the often used mapping to the RFXY model (Section D.2). New exact results for the free energy of the vortex system with a contact interaction that prevents line crossing ('noncrossing only' vortex interaction) [EK01] rule out the transition to the high-temperature phase. We stringently extend the argument to the generic case for a repulsive interaction, a result that had been previously suggested [NLS91] but also often debated. Sharply below the superconducting transition, there is

In a sideline of the reasoning the analytic behaviour of the free energy of the RFXY model throughout the transition, which this system does undergo, is shown.
The second part (Section D.3) is the fruit of a collaboration with the group of Chen Zeng at George Washington University, who study numerically the random-bond dimer model and its direct link to the vortex model. Once the details of the mapping have been clarified, the comparison of the analytical results from Ref. [EK01] to so far unpublished simulations is very gratifying. Not only

for the large-scale behaviour like correlation exponents but also for a wide range of thermodynamic quantities, including response functions and even moments of the disorder distributed quantities, the agreement between theory and simulation is very good. Concerning the latter quantities this is even more surprising as, a priori, one could have imagined a strong dependency on microscopic details, which, of course, differ from the continuum model to the lattice dimers. The benefit is two-directional. On the one hand, the validity of the analytical Bethe Ansatz results in the replica framework are clearly confirmed. At least for the delicate part of the analytical continuation in the replica index, this may not have been anticipated universally. On the other hand, the dimer model is shown to simulate precisely the disordered vortex system on *all* length scales. Questions regarding the vortex glass that cannot be addressed analytically may hence be answered numerically in the dimer model context. To be a bit more speculative, in view of the large number of relations between tiling problems and condensed matter systems [MS02] it might prove profitable in other contexts to have solved with the Bethe Ansatz results a random dimer model exactly.
For a more detailed introduction to the models and the literature we refer to the introductory sections of Chapter D.

3 Relations and methods

The links between the two main parts of the present thesis are manifold. Beyond the relation of the physical systems, all type-II superconductors, and the common emphasis on disorder effects, there is a methodological brace. In the two-dimensional plane, superstructures with a one-dimensional periodicity are subject to the disordering influence of impurities. The problem falls into the class of 'disordered elastic media' that has prospered over the last 15 years in a fruitful interplay with the development of *functional* renormalisation tools [Fis86, NS00, SD00, LWC02]. Prior to rigorous renormalisation group methods comes the use of qualitative scaling arguments in order to clarify the broad large-scale picture in situations with competing mechanisms. The use of both will go hand in hand throughout the following chapters. We also take advantage of the possibility given by the Feynman path-integral approach to quantum mechanics. A quantum statistical physics problem can be rewritten as a classical problem with an extra (imaginary time) dimension. In Chapters B and C, we go the way from quantum mechanics to classical physics, while in Chapter D, the two-dimensional classical line system is mapped onto interacting fermions in one dimension. Also, the method of bosonisation, that allows to write one-dimensional *interacting* fermion systems in the guise of a classical two-dimensional *elastic manifold* is used two-directional. In Chapter C the interplay of stripe *electronic* degrees of freedom with disorder is examined in terms of bosonised, classical fields while in Chapter D, when the possibility of a glass transition in the vortex array is analysed, the mapping of the lines to fermions – and simple results from bosonisation theory there – prove helpful. For the ease of the reader, the presentation of known results from the literature may appear repeatedly if needed at considerably distant points of the thesis.
Numerical methods had to be used at two points. The phase diagrams in Chapter C rely upon solving a large number of integrals numerically, while in Section D.3 the very ill-conditioned Bethe Ansatz integral equation has to be solved numerically in order to extract higher moments of disorder-distributed thermodynamical quantities.
Chapter E briefly states the 'round up' work that had been done on the field of the author's diploma

thesis, the 'Bragg glass phase in impure type-II superconductors'. A long version of the analysis, whose results had already been published, was produced. It may illustrate nicely the applicability of *functional* renormalisation tools, as mentioned above, to disorder vortex physics.

B. Striped phases, the geometrical degrees of freedom

1 Introduction, the phenomenology of stripes

During the last decade evidence emerged from theoretical work [Sch89, ZG89, Mac89, EKL90] and from experiments on cuprates [CAM$^+$91, MAM92, TSA$^+$95, DMD98] and closely related nickelates [HLZ$^+$92, CCC93, TBSL94, LC97] for the existence of striped structures within the $M\mathrm{O}_2$ (M = Cu, Ni) planes. These stripes are highly correlated states of holes which are introduced into the planes by doping and which order into a unidirectional [MDDH00] charge-density wave (CDW, wave length a) that may be accompanied by a simultaneous spin-density wave of period $2a$ in the sublattice magnetisation of the antiferromagnetic metallic spins [TBSL94, KE96, ZKE98]. Qualitatively, one may think of stripes as parallel strings of holes that constitute an antiphase boundary for spin order, see Fig. B.1.

Particular interest in these stripes – see the rapidly growing literature in the field, Fig. B.2 – arises from the possible interplay [EK93] between stripes and superconductivity, In Fig. B.3 a phase diagram of the classical HTSC material is sketched. Fig. B.4 collects stripe signatures for the same material that can be seen in a wide portion of the phase diagram both in the superconducting and in the normal phase. It is important to distinguish between "dynamic" and "static" stripes. While there is evidence that superconductivity can coexist with both dynamic [CAM$^+$91, MAM92, MD99] and static [TAI$^+$97, KHM$^+$99] stripes, static stripes tend to suppress superconductivity [CHM$^+$91, NU92, EKZ97] in contrast to dynamic stripes. Therefore the study of the structure and dynamics of stripes is of principal importance.

In Fig. B.5, typical experimental evidence from neutron scattering for a periodic superstructure is shown. The plot is taken from the classical paper by Tranquada *et al.* The superstructure peaks are given in reciprocal lattice vector units with respect to the orthorhombic unit cell of the CuO_2-plane. If the four-fold rotation symmetry in the plane is not broken, the tetragonal unit cell may equally be used, see Fig. B.6. Stripes in the cuprates were first seen in the $\mathrm{La}_{2-x}\mathrm{Sr}_x\mathrm{CuO}_4$ class of materials. Their detection in the important $\mathrm{YBa}_2\mathrm{Cu}_3\mathrm{O}_{7-\delta}$ and $\mathrm{Bi}_2\mathrm{Sr}_2\mathrm{Ca}_{n-1}\mathrm{Cu}_n\mathrm{O}_{4+2n+\delta}$ families was more difficult, but by now it has been compiled a large amount of evidence for stripes in all major material classes by a wide range of experimental techniques, see Table B.1. $\mathrm{La}_{2-x}\mathrm{Sr}_x\mathrm{CuO}_4$ is a $n = 1$ material, i.e., it has one CuO_2-plane per unit cell and a fairly low maximum critical temperature $T_c = 40K$ compared to $\mathrm{YBa}_2\mathrm{Cu}_3\mathrm{O}_{7-y}$ ($T_c = 93K$) and $\mathrm{Bi}_2\mathrm{Sr}_2\mathrm{Ca}_{n-1}\mathrm{Cu}_n\mathrm{O}_{4+2n+y}$ ($T_c = 100K$). The latter two are $n \geq 2$ materials and are doped interstitially by extra oxygen in contrast to the substitutional strontium doping in the case of $\mathrm{La}_{2-x}\mathrm{Sr}_x\mathrm{CuO}_4$. See Figs. B.7, B.8 for a sketch of the

structure of two representative compounds.

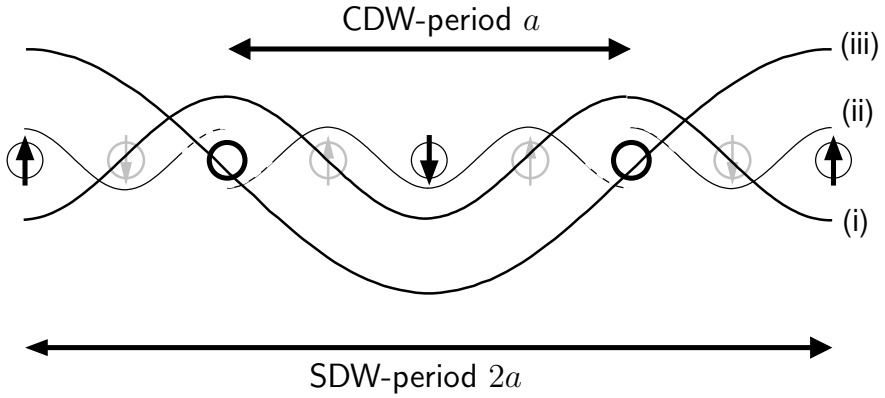

Fig. B.1: Sketch of the charge and spin density wave in the CuO_2-planes, sideview; circles stand for the Cu-sites with thickness proportional to hole concentration. (i) represents the charge modulation, (ii) the antiferromagnetic order with phase shifts at the charge stripes; (iii) illustrates the periodic modulation in the staggered magnetic field (SDW) due to the phase shifts with period $2a$.

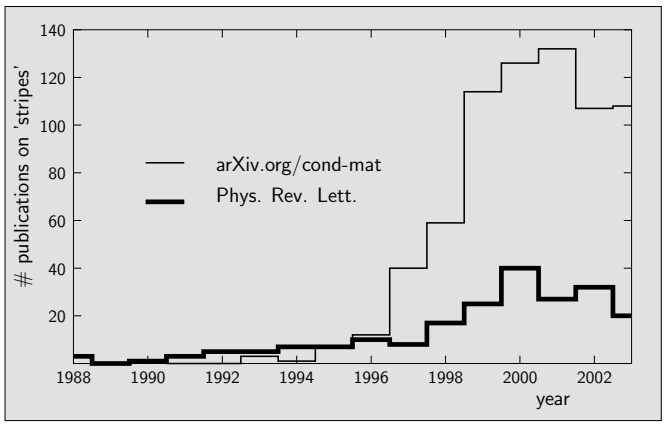

Fig. B.2: Appearance of keywords 'stripes' and 'striped' in title and abstract of publications in Physical Review Letters and in preprints on `cond-mat`; data for 2003 are extrapolated from the first quarter of the year. Note that the Phys. Rev. Lett.-data contain a background of about 3 publications per year from the field of optics rather than highly correlated electronic systems.

Various phenomenological pictures have been developed for the theoretical description of stripes. While charge and spin order are naturally described within a Landau theory [ZKE98], the aspect that stripes act as magnetic domain walls suggests to describe them as string-like objects [ZHvS96, MDHC98]. In the ideally ordered case these strings form a periodic array. Dynamic fluctuations are generated by thermal and quantum effects, whereas potentials tend to suppress dynamic fluctuations while they may reduce or increase static conformations of the stripes.
In such phenomenological models, the crystalline structure of the underlying atomic lattice has to

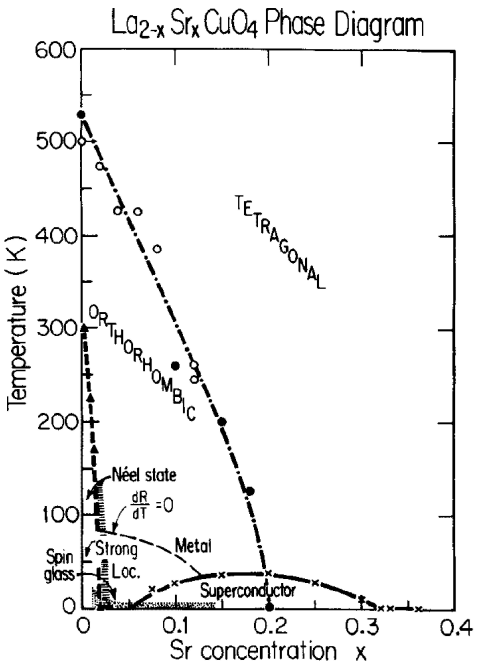

Fig. B.3: Temperature vs doping phase diagram of the high-T_c compound $La_{2-x}Sr_xCuO_4$; from [KBB+92].

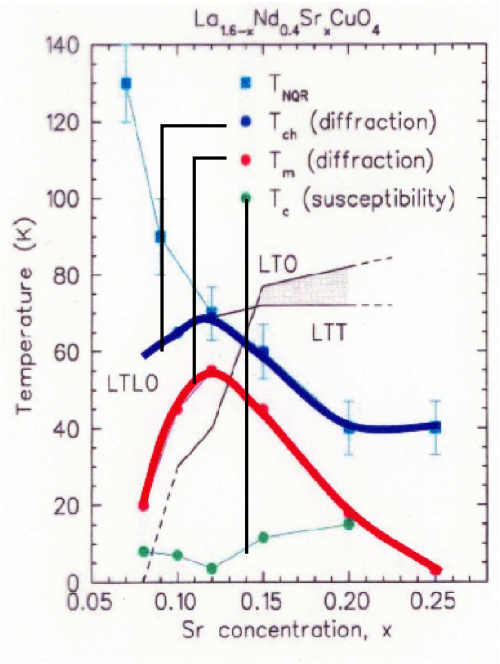

Fig. B.4: Charge (ch) and spin (m) order in the HTSC phase diagram; note the higher energy scale for charge order as compared to magnetic ordering; also note the simultaneous peak in stripe order and dip of superconducting response; from [IUT+00].

be taken into account by a periodic potential with period b in the direction perpendicular to the stripes. Such a potential tends to increase the positional order of the stripe array since is can be the source of lock-in effects [TSA+95, NW96, EKZ97], see Fig. B.9 where the structural transition in Nd-$La_{2-x}Sr_xCO_4$ precedes the appearance of static stripe order. Depending on the crystalline phase of the material [low-temperature orthorhombic (LTO) or low-temperature tetragonal (LTT)] and on the direction of the stripes with respect to the crystal axes, the ratio between the period b and the distance of nearest neighbours can vary.[1] In the cuprates the orientation of the stripes can change with doping: in $La_{2-x}Sr_xCuO_4$ the stripes were found to lie "diagonal" in the elementary CuO plaquette for low doping, while they rotate by 45^o into a "collinear" state for larger doping when the material becomes superconducting [WSE+00, MFY+00], see Fig. B.10. In the nickelates, the stripes appear to be diagonal in general.

In addition to such a periodic potential, the spatially inhomogeneous distribution of dopants provides a disorder potential for the stripes because of the (screened) Coulomb interaction between dopants

[1] Denoting the distance between nearest metal neighbours with d and neglecting the tilt of the oxygen octahedra, one has $b/d = 1$ for collinear stripes and $b/d = 1/\sqrt{2}$ for diagonal stripes. Although the octahedra tilt increases the period of the atomic *structure* in the LTT and LTO phases to twice its value, the period of the stripe *potential* remains the same for symmetry reasons: the atomic structure is modulated only by out-of-plane displacements (alternating "up" and "down") of the oxygen atoms. These displacements do not double the period of the potential since the stripe energy is not sensitive to the direction of the out-of-plane displacement.

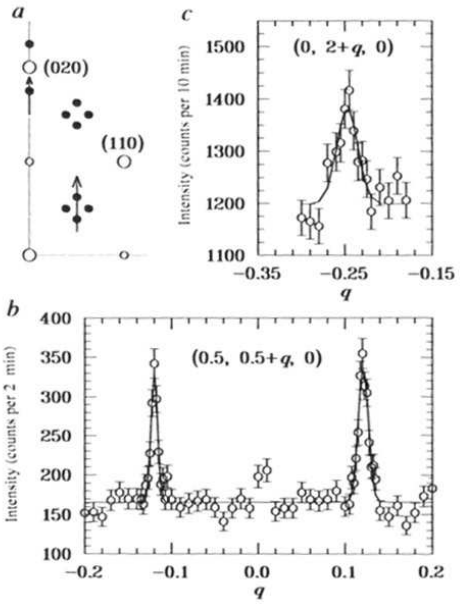

Fig. B.5: Typical superstructure peak in neutron scattering; from [TSA+95].

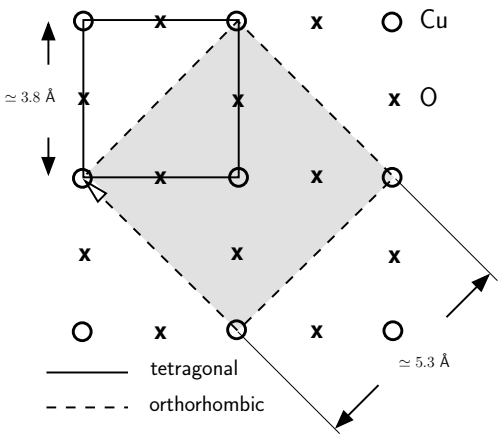

Fig. B.6: Orthorhombic vs tetragonal unit cell of the CuO_2-planes.

method	length scale	time scale	
neutron scattering	couples to spin density		
elastic	$\lesssim 100$Å	10^{-9}–10^{-14}s	
inelastic		$\Delta E \simeq \mathrm{meV} \sim 4 \times 10^{-12} s$	
resonance	relaxation of excited internal or implanted states is observed		
NMR	local	$10^{-3} s$	nuclear magnetic resonance
μSR	"	10^{-4}–10^{-6}s	muon spin resonance
ESR	"	10^{-6}–10^{-10}s	electron spin resonance
NQR	"	static	quadrupole res. ($\rightarrow$ electric field)
X-rays	0.1-10 μm	10^{-13}–10^{-14}s	couples to charge density
ARPES	photo emission; probes Fermi surface, quasiparticle spectrum		
transport	conductivity σ, Hall coefficient R_H, thermoelectric effect		
STM	tunneling microscopy; controversial interpretation [HML+02, HEKK02]		

Table B.1: Experimental techniques and their characteristics.

and holes. For low enough temperatures, these dopants can be considered as quenched. However, not all dopants will contribute to the disorder potential. While substitutional dopants (such as Sr in $La_{2-x}Sr_xCuO_4$) are essentially randomly distributed, interstitial dopants (such as oxygen) may partially organise themselves in homogeneous layers parallel to the CuO_2-planes (this behaviour is called "staging", see [WLK+97]). At higher temperatures ($\approx 10^2 K$), interstitial dopants may become mobile and act as annealed disorder, while substitutional dopants are still quenched.

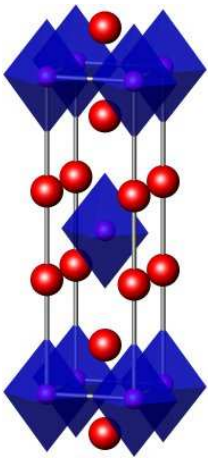

Fig. B.7: Conventional unit cell of La_2CuO_4, showing lanthanum ions and CuO_6 octahedra. Oxygen atoms at the vertices of the octahedra are not shown. The unit cell contains two formula units.

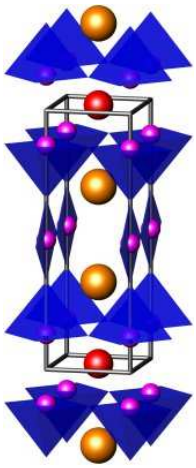

Fig. B.8: Conventional unit cell of $YBa_2Cu_3O_7$, again oxygen atoms are not shown; one formula unit per cell.

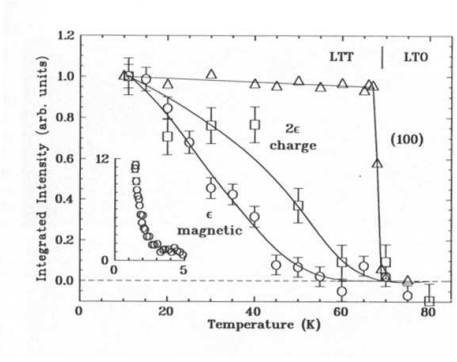

Fig. B.9: Structural phase transition in Nd-$La_{2-x}Sr_xCuO_4$ and evolution of superstructure signals; from [TSA+95].

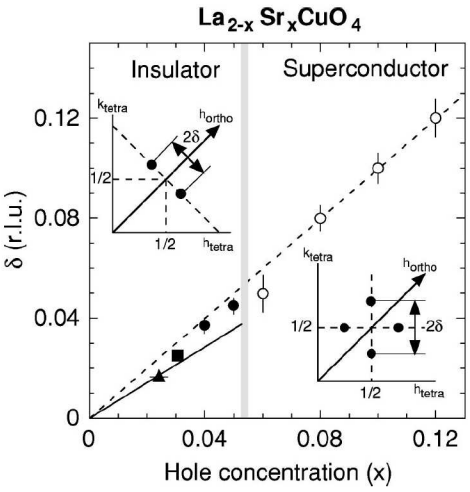

Fig. B.10: Sublattice resonance as a function of doping; the stripe pattern rotates by 45° at the critical doping $x \simeq 0.05$. From [MFY+00].

Pinning by the periodic potential is of particular interest since lock-in effects might explain the special role of certain values for the stripe spacing. In the cuprate system $La_{2-x}Sr_xCuO_4$ a linear relation $\delta \approx x$ between the mismatch δ of magnetic Bragg satellite peaks and the hole doping concentration x is observed from zero doping up to a saturation at $x \approx 0.12$ [YLK+98, MFY+00]. Since the mismatch δ is related to the lattice and CDW periods via $\delta = b/2a$, it allows for a natural explanation [TSA+95] of the "$x = \frac{1}{8}$-problem", which was originally observed in $La_{2-x}Ba_xCuO_4$ [MSFS88]: Since at $\delta = \frac{1}{8}$ the periods of the CDW and the Cu spacings have an integer ratio $p := a/b = 4$

this saturation could be a commensuration effect.[2] Similarly, the nickelate system $La_{2-x}Sr_xNiO_{4+y}$ shows anomalous thermodynamic behaviour at the values $p = 2, 3$ [CHC$^+$94, RGC$^+$96] which seem to be stable over certain respective ranges of the hole concentration $x + 2y$ [CCC93]. Even more, evidence was reported [TBSL94] for plateaus of the mismatch as a function of temperature at rational values $\delta = \frac{3}{22}, \frac{5}{36}$ in $La_2NiO_{4.125}$.
On the other hand, the stripe array can also be pinned by disorder [TIU99, DGS$^+$00]. Therefore it is important to take a closer look at the competitive pinning by the periodic atomic lattice and by disorder in order to understand to what extent lock-in effects can persist. A first step in this direction was made by Hasselmann *et al.* [HNMD99] who focus on a *single* stripe. However, since a single stripe and a stripe array differ in dimensionality one expects qualitatively distinct behaviour of the response of the system to disorder.
The purpose of the analysis in this chapter is to determine the effects of periodic and disorder potentials on the *structural* order of the two-dimensional stripe array on large scales. The internal electronic degrees of freedom are not probed in the present context. We assume them to be integrated out and to determine only the large scale parameters of the stripe description as fluctuating objects. In the next chapter, the point of view will be reversed and the internal degrees of freedom will be in the focus.

The outline of the chapter is as follows. In Section 2 we establish an elastic model for the quantum stripe array with periodic and pinning potentials. The effects of these potentials are discussed in Section 3 in the classical limit. In Section 4 we demonstrate the irrelevance of quantum fluctuations. Our conclusions are drawn in Section 5 where we discuss the relation of our work to previous work, the role of topological defects and implications for experiments.

2 Model, competing mechanisms

We describe the stripe system as an array of interacting quantum strings. The strings are assumed to be aligned in y-direction and to have an average spacing a in x-direction. In the following we ignore topological defects in the array, the role of which will be discussed in Section 5. Then the stripe array can be considered as an elastic system. The displacement field u represents a bosonic collective mode of the electron system. Its fluctuations are governed by a ("reduced") dynamic action [ZHvS96, MDHC98, HNMD99]

$$\mathcal{S} = \frac{1}{\hbar}\int_0^{\hbar/T} d\tau \left\{ \int d^2r \, \frac{\mu}{2}(\partial_\tau u)^2 + \mathcal{H} \right\}. \tag{2.1}$$

τ is the imaginary time and it is set $k_B = 1$. We identify $\mathbf{r} = (x, y)$, μ is a mass density and the Hamiltonian $\mathcal{H}$ has a contribution from the elastic energy

$$\mathcal{H}_{\rm el} = \int d^2r \, \frac{\gamma}{2}(\boldsymbol{\nabla} u)^2$$

with a stiffness constant γ which includes the line tension of the strings as well as their interaction. The main contribution to this interaction will stem from the Coulomb interaction between the stripes,

[2] Note that our usage of the notions commensurate and incommensurate follows the traditional usage in the context of commensurate-incommensurate transitions [Bak82, LNP92]. We distinguish *incommensurability* from a *mismatch* δ of Bragg peaks in the structure factor, whereas in the stripe literature incommensurability is used synonymously to mismatch. Our notions allow to distinguish incommensurate and commensurate states with finite mismatch.

but it will also have contributions of entropic nature. These will, however, differ substantially from the 1+1 dimensional case discussed in later chapters, see [Zaa00] and references therein. We therefore will avoid in the following analysis arguments based on the numerical value of the stiffness constants, even when the classical 1+1 dimensional limit of our 2+1 dimensional model is discussed. A further contribution to the stiffness arises from a crystal field that aligns the stripes in y direction. *A priori*, the stiffness can be anisotropic with an elastic energy density $\propto \gamma_x(\partial_x u)^2 + \gamma_y(\partial_y u)^2$. To simplify the analysis, such an anisotropy can be removed by rescaling the y coordinate. Then the effective isotropic stiffness constant is related to the original anisotropic constants through $\gamma = \sqrt{\gamma_x \gamma_y}$. Note that γ_x is dependent on the stripe spacing a, i.e., on doping. With increasing distance a between the stripes γ will shrink.

We will examine the coupling of the stripe array to the periodic potential $U(x)$ generated by the atomic structure as well as to a random potential $V(x,y)$ due to the interaction between the holes and the dopants which may be considered quenched at low temperatures. The corresponding energy contributions read

$$\mathcal{H}_U = \int d^2r\ \rho(\mathbf{r})U(x), \quad \mathcal{H}_V = \int d^2r\ \rho(\mathbf{r})V(x,y) \tag{2.2}$$

in terms of the stripe density

$$\rho(\mathbf{r},\tau) \simeq \frac{1}{a}\Big\{ \sum_m e^{iQ_m[x-u(\mathbf{r},\tau)]} - \partial_x u(\mathbf{r},\tau)\Big\} \tag{2.3}$$

where $Q_m := 2\pi m/a$ are reciprocal lattice vectors of the stripe array. The elastic and disorder pinning energies of the stripe array are similar to those of vortex lines in planar type-II superconductors. A recent review of the latter system can be found in Ref. [NS00].

U is assumed to be periodic, $U(x) = U(x+b)$, with a period $b < a$ (the modulation along the stripes is negligible for our purposes). For simplicity we take $U(x)$ as an even function (this restriction is for the simplicity of our analysis but not essential for the results)

$$U(x) = -\sum_{n\geq 1} U_n \cos(pQ_n x)$$

with $p > 1$. We assume that the random potential $V(x,y)$ is Gaussian distributed with zero average and a variance

$$\overline{V(\mathbf{r})V(\mathbf{0})} \;=\; \frac{\Delta}{\sqrt{2\pi}\ \xi} e^{-x^2/2\xi^2}\delta(y)$$

with a correlation length ξ and a weight Δ.

Subsequently we will establish the global phase diagram for the total system with a partition sum

$$Z \;=\; \int \mathcal{D}[u]\ e^{-S}.$$

Since the system without pinning provides an important reference point we start with a brief discussion of thermal and quantum fluctuations of the displacement. There is a characteristic length scale $\ell_T := \sqrt{\hbar^2\gamma/T^2\mu}$ beyond which thermal fluctuations dominate over quantum fluctuations. A related temperature scale $T_a := \sqrt{\hbar^2\gamma/a^2\mu}$ is defined by the coincidence $\ell_T = a$. In terms of these scales,

the displacement fluctuations in systems with a large size $L \gg \ell_T$ are obtained as

$$\langle u^2 \rangle \simeq \begin{cases} \dfrac{T}{2\pi\gamma} \ln \dfrac{L}{a} & \text{for } T \gg T_a, \\ \dfrac{T}{2\pi\gamma} \ln \dfrac{L}{\ell_T} + \dfrac{\hbar}{2a\sqrt{\pi\gamma\mu}} & \text{for } T \ll T_a. \end{cases} \tag{2.4}$$

Thus, while the unpinned stripe array is flat (i.e., $\langle u^2 \rangle$ is finite for $L \to \infty$) at $T = 0$, it is logarithmically rough (i.e., $\langle u^2 \rangle \propto \ln L$ for $L \to \infty$) at any finite temperature.

3 Classical limit

For the analysis of the effects of the potentials it is convenient to examine the various limiting cases defined by the relative strength of thermal fluctuations, quantum fluctuations, periodic pinning and disorder pinning. We start from the consideration of the classical limit $\hbar \to 0$ acting on the $\hbar$ appearing explicitly in Eq. (2.1) but not on possible implicit dependences of other model parameters. In this limit temporal fluctuations become negligible and one has to examine the system governed by the Hamiltonian

$$\mathcal{H} \;=\; \mathcal{H}_{\rm el} + \mathcal{H}_U + \mathcal{H}_V .$$

In the absence of the potentials U and V thermal fluctuations lead to an average displacement that diverges logarithmically with the system size L [see Eq. (2.4) for $T_a = 0$] which means that the stripe structure has only quasi-long-range order in the position of the stripes.

3.1 Periodic potential only

To analyse the relevance of a periodic pinning potential we focus on commensurabilities of low order with integer p. In this case the stripe structure can lock into the periodic potential at low temperatures while it unlocks at large temperatures. The transition between these two states is analogous to the roughening transition of crystal surfaces. We follow the standard analysis of the roughening transition (see Ref. [Noz92] and references therein) in order to obtain the transition temperature $T_{\rm R}$. Combining Eqs. (2.2), (2.3) and (2.4) we find an average potential energy

$$\langle \mathcal{H}_U \rangle \;\simeq\; -L^2 \frac{1}{a} \sum_{n \geq 1} U_n \exp\left(-p^2 Q_n^2 \langle u^2 \rangle / 2\right) \tag{3.5a}$$

$$\;\simeq\; -L^2 \frac{1}{a} \sum_{n \geq 1} U_n \left(\frac{L}{a}\right)^{-p^2 Q_n^2 T / 4\pi\gamma} \tag{3.5b}$$

for an infinitesimally weak periodic potential. The lowest harmonic $n = 1$ gives the most relevant contribution to this energy. The stripes are locked when the average potential energy does not vanish in the limit $L \to \infty$, i.e., for temperatures below

$$T_{\rm R} = \frac{2\gamma a^2}{\pi p^2}.$$

The transition temperature increases with increasing strength of the potential since γ is renormalised to larger values. The effective parameters on large length scales $L = ae^l$ are described by renormalisation group (RG) flow equations [Noz92]

$$\frac{d}{dl}U_1 = (2 - \frac{\pi p^2 T}{a^2\gamma})U_1, \tag{3.6a}$$

$$\frac{d}{dl}\gamma = A\frac{2\pi^4 p^2}{\gamma a^2}U_1^2, \tag{3.6b}$$

with a temperature dependent coefficient A which is of order one near the roughening transition. These equations lead to the phase diagram sketched in Fig. B.11. The case with non-integer p

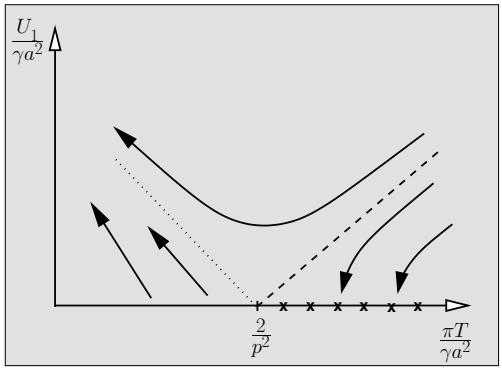

Fig. B.11: Schematic representation of the renormalisation-group flow near the roughening transition according to Eqs. (3.6). The line of crosses represents fixed points where the periodic potential is irrelevant and the stripes are not locked. The dashed line is the phase boundary between the locked and unlocked phase. Arrows indicate the RG flow.

involves the analysis of higher order commensurable states or incommensurable states. In such cases the periodic potential is less relevant than in the low order commensurate cases examined above. Since we find later that the periodic potential is irrelevant in the presence of disorder, for integer $p \geq 2$ this will be true also for non-integer p. For more details on commensurate/incommensurate systems the interested reader is referred to Refs. [Bak82, LNP92].

3.2 Pinning potential only

In order to discuss the relevance of disorder pinning, we start from the Hamiltonian $\mathcal{H}_V$ as given in Eq. (2.2), discard rapidly oscillating terms that are irrelevant on scales much larger than a and keep only the most relevant term $m = 1$ in the sum over harmonics for the density (see Ref. [NS00] or [BEN01] for intermediate steps). After averaging over disorder we find the effective replica pinning Hamiltonian

$$\mathcal{H}_V^{\rm rep} \simeq \sum_{\alpha\beta}\int d^2r \left\{-\frac{\gamma^2\sigma}{2T}\boldsymbol{\nabla}u^\alpha\boldsymbol{\nabla}u^\beta - \frac{\Delta}{a^2T}\cos\frac{2\pi}{a}[u^\alpha(\mathbf{r}) - u^\beta(\mathbf{r})]\right\} \tag{3.7}$$

Disorder couples to the $\partial_x u$ term in the density Eq. (2.3) as a random field and gives rise to the first term in Eq. (3.7) with a value $\sigma = \frac{\pi\Delta}{a^2\gamma^2}$. (Note that strictly speaking this term should contain only $\partial_x u^\alpha \partial_x u^\beta$ in the unrenormalised Hamiltonian; the form written in Eq. (3.7) anticipates that renormalisation generates a random field coupling to *both* components of the gradient.) Similar to the estimate for the roughening temperature above, one can estimate the relevance of $\mathcal{H}_V^{\rm rep}$ from its average with respect to $\mathcal{H}_{\rm el}$,

$$\begin{aligned}\langle \mathcal{H}_V^{\rm rep}\rangle &\simeq -\sum_{\alpha,\beta=1}^{N} L^2 \frac{\Delta}{a^2 T}\exp(-2\pi^2\langle[u^\alpha - u^\beta]^2\rangle/a^2)\\ &= -L^2 N(N-1)\frac{\Delta}{a^2 T}\left(\frac{L}{a}\right)^{-\frac{2\pi}{a^2}\frac{T}{\gamma}},\end{aligned}$$

where we used $\langle u^\alpha(\mathbf{r})u^\beta(\mathbf{r})\rangle = \delta^{\alpha\beta}\frac{1}{2\pi}\frac{T}{\gamma}\ln\frac{L}{a}$. For temperatures above

$$T_{\rm SR} = \frac{\gamma a^2}{\pi}$$

the average disorder energy vanishes on large scales. Below, disorder shows to be relevant and its effects have to be calculated by renormalisation group techniques. Note that

$$T_{\rm SR} \simeq \frac{p^2}{2} T_{\rm R}.$$

This relation becomes an identity if the renormalisation of γ due to the presence of the potentials can be neglected. Then $T_{\rm SR} > T_{\rm R}$ for $p > \sqrt{2}$.

Cardy and Ostlund [CO82] were the first to derive RG equations near the transition and Villain and Fernandez [VF84] studied the flow of parameters to their large-scale values at zero temperature. A concise summary of these two approaches is given in Ref. [NS00]. We combine the flow equations for these two temperature ranges by the interpolation

$$\frac{d\sigma}{dl} = c_1 \frac{a^2\Delta^2}{T^2\gamma^2 a^4 + \Delta(\gamma^2 a^4 + c_2\Delta)}, \tag{3.8a}$$

$$\frac{d\Delta}{dl} = \left(2 - \frac{2\pi T}{\gamma a^2}\right)\Delta - 2\frac{c_2\Delta^2}{\gamma^2 a^4 + c_2\Delta}. \tag{3.8b}$$

The numbers c_1 and c_2 are of order unity and depend only weakly on temperature. γ is not renormalised due to a statistical symmetry [HF94], just like σ does not feed back to Δ. This holds for the replica Hamiltonian (3.7) which is a good approximation on large length scales. Smaller scales will weakly renormalise the stiffness γ to larger values and generate additional irrelevant terms. From the flow equations, $T_{\rm SR} = \gamma a^2/\pi$ is identified as the temperature above which Δ is renormalised to zero. Nevertheless, disorder is marginal for $T > T_{\rm SR}$ since σ takes a finite fixed-point value. Thus, here one has displacement fluctuations

$$\overline{\langle u^2\rangle} = \frac{1}{2\pi}\left(\frac{T}{\gamma} + \sigma\right)\ln\frac{L}{a}.$$

Below the transition temperature ($T \lesssim T_{\rm SR}$), Δ flows to a finite fixed-point value and $d\sigma/dl$ becomes constant. σ thus asymptotically has a logarithmic dependence on the scale L and gives the dominant contribution to the fluctuations

$$\overline{\langle[u(\mathbf{r}) - u(\mathbf{0})]^2\rangle} \sim a^2\chi\ln^2\frac{r}{a}. \tag{3.9}$$

Slightly below $T_{\rm SR}$, $\chi \propto (1 - T/T_{\rm SR})^2$. This squared-logarithmic roughness (3.9) defines the *superrough* (SR) phase. In this phase thermal fluctuations can still give a logarithmic contribution to the correlator (3.9) which, however, is subdominant.

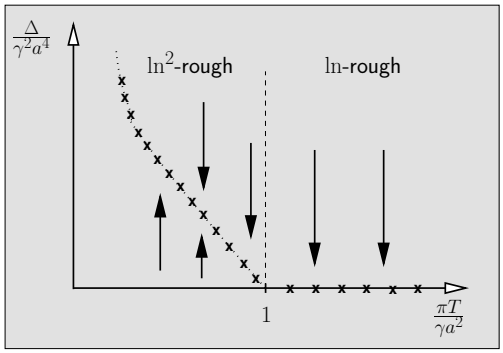

Fig. B.12: Schematic representation of the renormalisation group flow describing the superroughening transition according to Eqs. (3.8). Arrows indicate the RG flow. The dashed line is the phase boundary between the superrough and rough phase. Crosses represent fixed points (note, however, that σ flows to infinity for $T < T_{\rm SR} = \gamma a^2/\pi$).

3.3 Complete potential

In the presence of both a disorder potential and a periodic pinning potential it is not immediately clear which one will prevail in what part of the phase diagram. At first sight it seems to be possible to have a flat phase, a ln-rough phase, or a $\ln^2$-rough phase. We assume that U and V are weak such that a renormalisation of the stiffness γ as well as of $T_{\rm R}$ and $T_{\rm SR}$ is negligible. Then one always has $T_{\rm R} < T_{\rm SR}$ for $p > \sqrt{2}$. Thus, at high temperatures $T > T_{\rm SR}$ the system will be logarithmically rough since both U and V are irrelevant. At intermediate temperatures in the interval $T_{\rm R} < T < T_{\rm SR}$, V is relevant while U is irrelevant with respect to thermal fluctuations. This suggests that the system is superrough. Although we ultimately find this to be true (see below), the argument needs to be refined since it is no longer sufficient that U is irrelevant with respect to thermal fluctuations. Instead, we one has to argue that U is irrelevant at the disorder-dominated, superrough fixed point. Eventually, for $T < T_{\rm R}$ one might expect to find a superrough phase if U is weak compared to V and a flat phase if V is weak compared to U. However, the following arguments show that a flat phase is not stable in the presence of disorder and that superroughness should persist for all $T < T_{\rm SR}$. For the case of a interface in the presence of both a periodic potential and disorder, the equivalent conclusion had already been reached [EN98]. Here, with a periodic medium, the situation is completely analogous for the case $p \geq 2$, still we go through the details for completeness.

In order to argue that a flat phase cannot exist for arbitrarily weak V and that the stripe array is superrough for all $T < T_{\rm SR}$, we show (i) that weak periodic potentials ($U \ll V$) are irrelevant at the superrough fixed point and (ii) that arbitrarily weak disorder ($V \ll U$) will roughen the stripe array even for $T < T_{\rm R}$, i.e. that disorder is relevant at the flat-phase fixed point, which implies that U is renormalised to zero and the system is superrough on large scales.

Consideration (i). For $U \ll V$ the irrelevance of a periodic potential follows from an analysis

in analogy to the one in Section 3.1. We assume that the disorder-induced fluctuations of the displacement field are Gaussian with a correlator $\overline{\langle u^2\rangle} \sim \frac{1}{2}a^2\chi\ln^2(L/a)$ [which is implied by Eq. (3.9)]. This replaces the thermal correlator in Eq. (3.5a). This now leads to

$$\overline{\langle \mathcal{H}_U\rangle} \sim -L^2\frac{1}{a}\sum_{n\geq 1} U_n \left(\frac{L}{a}\right)^{-\pi^2 n^2 p^2 \chi \ln(L/a)}$$

and the average periodic pinning energy vanishes for large system sizes.

Consideration (ii). The situation $V \ll U$ is more subtle. We assume that the stripes are locked into a flat state. We neglect thermal fluctuations which would renormalise U to smaller values. For simplicity of our argument we assume that $p = 2$ although the argument can be generalised to any $p > 1$. In addition, we retain only the most relevant, lowest harmonic of the periodic pinning energy,

$$\mathcal{H}_U \simeq -\frac{U_1}{a}\int d^2r\ \cos\frac{2\pi p}{a}u(\mathbf{r}).$$

In the absence of V all flat states $u(\mathbf{r}) = nb$ with some integer n would be equivalent. Disorder certainly breaks this degeneracy and one might expect the stripe array to find a ground state where $u(\mathbf{r})$ fluctuates only weakly around na with some particular n, say $n = 0$. However, one can show that the ground state is not given by small fluctuations within this particular "valley" $n = 0$ but that solitons (i.e., local areas where $u(\mathbf{r}) \approx \delta n\, b$ with a shift $\delta n \neq 0$, cf. Fig. B.13) are preferred energetically. The proliferation of a large number of such solitons implies the irrelevance of U and hence the superroughness of the stripe array on large scales.

We now examine a disk-like soliton of Radius R and estimate its elastic energy cost and typical gain of pinning energy in order to decide whether such solitons are favourable. From an energetical point of view the creation of $\delta n = 1$ solitons is equivalent to the creation of a magnetic domain in a random-field Ising model. For a strong periodic pinning potential, $U_1 \gg \gamma a$, the soliton has a narrow border of width $\ell_U \approx \sqrt{a\gamma/U_1}b$ and of an energy per unit length $\epsilon \approx \sqrt{U_1 a\gamma}/p$. Thus the elastic energy cost is proportional to the border length, $E_{\rm el} \propto \epsilon R$. In the area of the soliton the strings are exposed to a different disorder potential V (we assume the disorder correlation length to be small, $\xi \lesssim a$). Then the typical energy gain is proportional to the square root of the area $E_V \propto -\sqrt{\Delta R^2/a\xi}$. This gain is larger than the elastic energy cost for solitons of all sizes for a disorder strength beyond a threshold value

$$\Delta_{\rm c} \propto a\xi\epsilon^2.$$

However, for large solitons one has to take into account that the soliton border will be roughened by disorder. The equivalent roughening of domain walls in the random field Ising model was studied in Refs. [Bin83, Nat85]. As a consequence, E_V for the soliton gains a logarithmic correction and wins over the cost in elastic boundary energy for any strength, given a large enough soliton. In other words, the border line tension ϵ is renormalised to zero on a finite length scale

$$\ell_\epsilon \sim a\exp\left(c\frac{a\xi\epsilon^2}{\Delta}\right), \tag{3.10}$$

where c is a constant of order unity. The creation of solitons of a size R larger than ℓ_ϵ is thus energetically favourable. Overlapping solitons of unbounded size imply a roughness of the stripe

array, provided the sum of the shifts $\sum_i \delta n_i$ at a given position increases with the number of solitons (enumerated by the index i) that include this site. In principle, the interaction between solitons could lead to a compensation of the shifts between pairs of solitons. However, the interaction between the solitons is short-ranged on the scale ℓ_U and it cannot compete with a disorder energy that discriminates between a shift $\delta n_i = 1$ and a $\delta n_i = -1$ for each soliton. Although the pinning energy of these two states is identical in the bulk area, the disorder energy of these two solitons is different in the border region and leads to an energy contribution proportional to $\sqrt{R}$. Therefore the multiple creation of large and overlapping solitons leads to uncorrelated contributions to shifts δn and therefore implies the roughness of the stripe array on scales beyond ℓ_ϵ. In this sense U is irrelevant on large scales in the presence of arbitrarily weak V, although on small scales the stripes will be confined to valleys of U. Since U is irrelevant, the stripe array will be superrough as in the absence of U.

Although the case $p = 1$ appears not to be of physical relevance for striped systems, we add as a side remark that for $p = 1$ a flat phase can exist. In this case the elastic energy cost $\propto R$ of a soliton cannot be compensated by a disorder energy which no longer has a bulk contribution $\propto R$ but only a border contribution $\propto \sqrt{R}$.

Strictly speaking, we have shown the irrelevance of U only for integer values of p. Since non-integer rational values of p would correspond to commensurabilities of higher order, they are even more susceptible to the destruction of long-range order by V.

It is interesting to note that the absence of a flat phase for $p > 1$ is peculiar to two dimensions. In dimensions $2 < d < 4$ a flat phase is stable for disorder weaker than a threshold value [EN98, EN99]. Therefore, a stack of planar stripe arrays with a finite coupling between the planes will exhibit also a flat phase for a disorder strength below a certain threshold value.

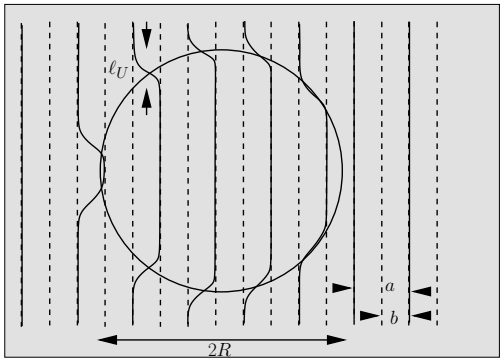

Fig. B.13: Illustration of a soliton of radius R for $p = 2$. Full lines represent the strings of holes of average spacing a, dashed lines are minima of U with spacing $b = a/p$. The soliton width is ℓ_U.

4 Adding quantum fluctuations

Now we finally study how the potentials U and V affect the elastic string model taking into account its quantum mechanical nature. In order to analyse whether these potentials are relevant at all, the scaling arguments used in Section 3 can be applied analogously to the dynamic action. Since the

displacement correlations of the unpinned array are qualitatively different for $T = 0$ (where the array is flat) and $T > 0$ (where the array is rough) these cases will be discussed separately.

4.1 At zero temperature

In this section we focus on the case with disorder but without a periodic potential. Before we turn to the analysis of this case, it is worthwhile to point out that this system is essentially a two-dimensional "Bose glass." Because of an analogy between a d-dimensional bosonic problem at zero temperature and a classical $(d+1)$-dimensional problem a finite temperature [FL89], superconducting vortices in the presence of columnar pinning centers provide another equivalent system that has received a lot of recent attention [NV92, NV93]. The problem at hand, a bosonic one-component displacement field at $T = 0$, is equivalent to a stack of classical elastic layers which was studied by Balents [Bal93]. According to his analysis – which is restricted to dimensions close to $d = 4$ – the displacement field is logarithmically rough. We now focus on two dimensions because characteristic modifications leading to superroughness are to be expected.

The analysis of the disorder pinning is most convenient using the replicated action

$$\begin{aligned} \mathcal{S}_V^{\mathrm{rep}} \simeq \sum_{\alpha\beta} \int d\tau d\tau' d^2r \Big\{ & -\frac{\gamma^2\sigma}{2\hbar^2} \boldsymbol{\nabla} u^\alpha(\mathbf{r},\tau) \boldsymbol{\nabla} u^\beta(\mathbf{r},\tau') \\ & -\frac{\Delta}{a^2\hbar^2} \widetilde{\Delta}[u^\alpha(\mathbf{r},\tau) - u^\beta(\mathbf{r},\tau')] \Big\} \end{aligned} \tag{4.11}$$

where

$$\widetilde{\Delta}(u) = \cos\frac{2\pi}{a}u$$

if we retain only the lowest harmonic of the stripe density as most relevant term as in Eq. (3.7).

For a scaling analysis of this action contribution, we consider a rescaling of space, time, displacement and action quantum according to

$$\mathbf{r} = e^l \mathbf{r}_l, \quad \tau = e^{zl}\tau_l, \quad u = e^{\zeta l} u_l, \quad \hbar = e^{\eta l}\hbar_l$$

with a dynamical exponent z, roughness exponent ζ and action scaling exponent η. In order to analyse the relevance of quantum fluctuation later on we allow for a rescaling of $\hbar$. We note that due to a statistical tilt symmetry the flow equation of γ consists only of the scaling part [HF94]

$$\frac{d}{dl}\gamma = (z - \eta + 2\zeta)\gamma$$

which implies

$$\eta = z + 2\zeta \tag{4.12}$$

at any possible fixed point. If $\eta > 0$ quantum fluctuations are irrelevant on large scales and the fixed point can be called a "classical" ($\hbar_\infty = 0$) fixed point in analogy to the irrelevance of thermal fluctuations for classical systems [Fis86].

To establish the relevance of pinning we note that the action of the unpinned system $\mathcal{S}_{\mathrm{el}}$ is invariant under a rescaling with $z = 1$, $\eta = 0$ and $\zeta = -\frac{1}{2}$. According to Eq. (2.4) the displacement fluctuations are finite for $T = 0$ (this is reflected by the negative value of ζ) which implies

that $\langle \cos \frac{2\pi}{a}[u^\alpha(\mathbf{r},\tau) - u^\beta(\mathbf{r},\tau')]\rangle$ is finite since in the unpinned system $\langle [u^\alpha(\mathbf{r},\tau) - u^\beta(\mathbf{r},\tau')]^2\rangle \simeq \hbar/(a\sqrt{\pi\gamma\mu})$ for $l \to \infty$ and thus disorder is strongly relevant, $\langle \mathcal{S}_V^{\rm rep}\rangle \propto e^{4l}$.

Disorder can be taken into account on a crude level (the "random field" approximation) by retaining in action (4.11) only the harmonic parts bilinear in u. Then this action part is found to be scale invariant together with $\mathcal{S}_{\rm el}$ for $z = 1$, $\zeta = 1$, and $\eta = 3$. To gain qualitative insight into the spatio-temporal correlations we calculate the displacement fluctuations in this random-field approximation. We find

$$\overline{\langle [u^\alpha(\mathbf{r},\tau) - u^\beta(\mathbf{0},0)]^2\rangle} = C_1^{\alpha\beta}(\mathbf{r},\tau) + C_2(\mathbf{r}) \tag{4.13a}$$

with a contribution C_1 from quantum fluctuations and a disorder contribution C_2. $C_1^{\alpha\beta}(\mathbf{r},\tau)$ vanishes for $\alpha = \beta$ and $\mathbf{r} = \mathbf{0}$ and $\tau = 0$ and takes a finite value

$$C_1^{\alpha\beta}(\mathbf{r},\tau) \simeq \frac{\hbar}{a\sqrt{\pi\gamma\mu}} \tag{4.13b}$$

for $\alpha \neq \beta$ or $r \gg a$ or $\tau \gg \sqrt{\mu/\gamma}a$. $C_2(\mathbf{r})$ is rough; its roughness

$$C_2(\mathbf{r}) \simeq \frac{\sigma}{\pi}\ln\frac{r}{a} + \frac{4\pi\Delta}{\gamma^2 a^4}r^2 \tag{4.13c}$$

is dramatically overestimated in this approximation. From this correlation function we recognise that while disorder roughens the displacement in *spatial* directions (consider large r for $\tau = 0$), it preserves the flatness in *temporal* directions (consider large τ for $r = 0$). These qualitative properties should hold even after renormalisation effects due to the anharmonic terms in action (4.11) are taken into account.

Although a systematic renormalisation group analysis is very intricate and beyond the scope of this article, we present arguments in favour of $\eta > 0$ at the true fixed point. First, we use the fact that a fixed point with a periodic correlator $\widetilde{\Delta}(u)$ can exist only for $\zeta = 0$. Thus

$$\eta = z$$

from Eq. (4.12) and it is sufficient to show $z > 0$ for the irrelevance of quantum fluctuations. It is natural to assume that the dynamic exponent is positive, if not diverging on large scales as is typical of glassy systems where the dynamics is governed by tunneling through divergent barriers.

The difficulty [Bal93] to calculate z is related to the fact that $\widetilde{\Delta}(u)$ may become nonanalytic near $u = 0$. While such a nonanalyticity follows from a functional renormalisation group analysis near $d = 4$ [Fis86], it is not clear whether such a nonanalyticity is present in $d = 2$. According to the analysis summarised in Section 3.2, such a nonanalyticity is absent at finite temperature near $T_{\rm SR}$. At zero temperature, the strong coupling analysis of Villain and Fernandez [VF84] misses such a possible nonanalyticity. Therefore we consider both possibilities.

We first assume analyticity of the function $\widetilde{\Delta}(u)$. In this case the "dynamic stiffness" will be renormalised according to

$$\frac{d}{dl}\mu = (2 - z + 2\zeta - \eta)\mu + \beta_\mu[\widetilde{\Delta}]. \tag{4.14}$$

The functional $\beta_\mu[\widetilde{\Delta}]$ represents the vertex corrections arising from the $\mathcal{S}_V^{\rm rep}$. These corrections are expected to be positive since disorder pins the stripes at minima of V, thereby confining the temporal

fluctuations which amounts to an increase of the renormalised μ. If $\beta_\mu[\widetilde{\Delta}]$ is finite at the fixed point, then $\eta = z = 1 + \beta_\mu[\widetilde{\Delta}]/(2\mu^*)$ (μ^* denotes the fixed-point value of μ). Then $\eta > 0$ and the fixed point will be classical.

In case the fixed-point correlator is nonanalytic, the functional $\beta_\mu[\widetilde{\Delta}]$ diverges [Bal93]. This signals a qualitative increase of the dynamic stiffness, which should be described by a kinetic term of the form [Bal93]

$$\mathcal{S}_{\rm kin} = \frac{1}{\hbar}\int_0^{\hbar/T} d\tau \int d^2r\ \nu|\partial_\tau u| \tag{4.15}$$

which is more relevant than the original kinetic term in Eq. (2.1). The coefficient ν would flow according to

$$\frac{d}{dl}\nu = (2 + \zeta - \eta)\nu + \beta_\nu[\widetilde{\Delta}] \tag{4.16}$$

with another functional $\beta_\nu[\widetilde{\Delta}] > 0$. This would imply an even larger dynamical exponent $z = \eta = 2 + \beta_\nu[\widetilde{\Delta}]/\nu^*$ and even stronger irrelevancy of quantum fluctuations.

Thus, in any case $\eta > 0$ and the system flows to the classical fixed point value for $V \neq 0 = U$. Quantum effects will result only in a finite renormalisation of the parameters in the classical system. The most important renormalisation effect concerns an increase of the dynamic stiffness with a possible generation of ν. Although there is no way of handling a kinetic action of the form (4.15), we expect quantum fluctuations on small scales to induce a flat but finite quantum contribution C_1 to the displacement correlation. The classical contribution C_2 will be renormalised as in the absence of quantum fluctuations [the proper correlation can be obtained from equation (4.13c) by inserting the scale-dependent values of Δ and σ as obtained from the flow equations (3.8) without rescaling; in the superrough phase $\sigma \propto \ln r$ and $\Delta \propto (\ln r)/r^2$].

Since the presence of the disorder potential implies the irrelevance of quantum fluctuations, they cannot be expected to modify the competition between U and V as was analysed in Section 3.3. Thus, the quantum array has superrough spatial correlations at $T = 0$.

4.2 At finite temperature

An inspection of the correlator (2.4) of the unpinned system suggests that thermal fluctuations dominate over quantum fluctuations on large scales. In fact, quantum fluctuations are irrelevant at the classical fixed point also for $T > 0$.

This can be seen from the action as follows. The classical fixed points (with both thermal roughness or superroughness) are described by $\zeta = 0$. The finiteness of the time integral implies $z = 0$ and according to Eq. (4.12) also $\eta = 0$. Then the effective "dynamical stiffness" flows to infinity according to Eq. (4.14) or Eq. (4.16). Thereby temporal fluctuations of the displacement are suppressed on large scales, on which the system is described by the static limit

$$\mathcal{S} \to \frac{1}{T}\mathcal{H}.$$

Hence quantum fluctuations will lead only to a renormalisation of the parameters in the classical description. Therefore the scaling arguments that were applied in Section 3 to the Hamiltonian hold also for the dynamic action. We conclude that the system in disorder will be superrough at low

temperatures – without or with an additional periodic potential – while it will be thermally rough at high temperatures.

5 Summary and discussion

So far, we have analysed the stripe array in the elastic approximation, i.e. neglecting dislocations. Before we discuss the relevance of dislocations, we summarise our results. In general, we found quantum fluctuations to be irrelevant in the presence of thermal and/or disorder-induced fluctuations, i.e., to renormalise the classical elastic model only weakly.

In the absence of disorder ($\Delta = 0$), the stripe array locks into a commensurate periodic potential below a roughening temperature $T_{\mathrm{R}} = 2\gamma b^2/\pi = 2\gamma a^2/\pi p^2$. This transition temperature is proportional to the stiffness γ which is implicitly temperature dependent due to entropic contributions [PT79, Zaa00]. At the transition the translational order changes from long ranged to quasi-long ranged (with logarithmic roughness).

The large-scale structure of the stripe array is dramatically influenced by the presence of disorder ($\Delta > 0$). If there were no periodic potential, the stripe array would undergo a superroughening transition at $T_{\mathrm{SR}} = \gamma a^2/\pi$. For $T > T_{\mathrm{SR}}$ the array would be unpinned with $\ln$-roughness, while it would be pinned and superrough for $T < T_{\mathrm{SR}}$. The same scenario holds also in the presence of the periodic potential, from which the stripe array always unlocks (on sufficiently large scales even for arbitrarily weak disorder). Therefore, the array is *rough at all temperatures* for $\Delta > 0$. However, for weak disorder and strong periodic potential the crossover length scale from flat to superrough correlations will be exponentially large, see Eq. (3.10).

Hasselmann *et al.* [HNMD99] previously proposed a phase diagram for a single stripe with flat and disordered phases. To our understanding, the disorder was effectively assumed to have long-ranged correlations, which allows for the existence of a flat phase even for a single stripe. In contrast to this we consider disorder with short-ranged correlations and find that it always roughens the stripe array. Because a single stripe represents an elastic system of lower dimensionality than the stripe array, our finding implies also the roughness of a single stripe in disorder with short-ranged correlations.

Now we come back to discuss the relevance of topological defects in the stripe array, starting with the simplest situation for $U = V = 0$. At low temperatures the stripe array can be considered as a "smectic" with quasi-long-range translational order and long-range orientational order. At a temperature

$$T_{\mathrm{m}} = \frac{\gamma a^2}{8\pi}$$

it would melt [KT73] due to a proliferation of dislocations into a "nematic" liquid with short-range translational order and quasi-long-range orientational order, before the proliferation of disclinations drives a second transition into an isotropic liquid with short-ranged orientational order. While this scenario is well known for classical systems (for a review see e.g. Ref. [Nel83]), its relevance to doped Mott insulators was pointed out by Kivelson, Fradkin, and Emery [KFE98].

It is instructive to compare the melting temperature to the other characteristic temperatures related to the potentials. As pointed out by José *et al.* [JKKN77], distinct melting and lock-in transitions can exist only for $p \geq 4$ since $T_{\mathrm{R}} = (4/p)^2 T_{\mathrm{m}}$. For $p < 4$ they will merge to a single phase transition. The effect of disorder is quite virulent: In the elastic approximation, it makes the system

superrough at temperatures below $T_{\rm SR} = 8T_{\rm m}$. However, superroughness implies that dislocations become energetically favourable [this follows from the flow equations (3.8), see. e.g. Ref. [LG00]]. Therefore, their density will be finite even at zero temperature. Nevertheless, for weak disorder and at low temperatures the length scale where free dislocation appear can be extremely large because of a U that tends to lock the stripes up to exponentially large scales. Since melting in the absence of disorder occurs at a temperature, $T_{\rm m} < T_{\rm SR}$, free dislocations will be present at *all* temperatures. The presence of dislocations reduces the quasi-long-range order (where the satellite peaks have an algebraic singularity due to the $\ln$-roughness; $\ln^2$-roughness corresponds to an algebraic singularity with an exponent that depends weakly on the wave vector) to short-range order with a correlation length of the order of the distance between (free) dislocations. Thus, the saturation of the dislocation density at low temperatures implies also the saturation of the correlation length at a maximum value. This conclusion is consistent with experimental observations in the cuprates [TIU99] (here it was observed in magnetic ordering, which can be destroyed due to a coupling to disorder even without a distortion of the stripe array) as well as in the nickelates [LC97, DGS$^+$00] (here the correlation length is explicitly that of charge order).

Note that the *true* correlation length of charge order $\xi^{\rm C}$ (which we identify with the distance between free dislocations) can be related to the measured width of peaks in the structure function only if the wave-vector resolution is much smaller than $1/\xi^{\rm C}$. Thus, a system without dislocations (with $\ln$- or $\ln^2$-roughness) has an infinite correlation length and the *apparent* correlation length deduced from experiments would be resolution limited. Zachar [Zac00] recently proposed an explanation of the observed apparent correlation lengths in terms of chaotic fluctuations of the distance between neighbouring stripes (see also Ref. [TIU99]), excluding explicitly a key role of dislocations. However, this argument is based on the assumption of non-integer p and cannot account for the finite correlation length observed for integer p in the nickelates [LC97, DGS$^+$00][3] and the cuprates [YLK$^+$98]. It is interesting to note, that the systems, for which a finite correlation length is measured are indeed the ones with quenched disorder deriving from substitutional Sr doping. The hypothesis of chaotic stripe distance fluctuations also cannot explain why the transverse correlation length (along the stripes) – which apparently is not resolution limited [NIF$^+$99] – can be finite. Even more, the fact that longitudinal and transverse correlation lengths are roughly of the same size [vVN$^+$98, NIF$^+$99] is consistent with their relation to the dislocation density.

The relevance of disorder even in the presence of periodic pinning is consistent with the quenched nature of the stripe *structure* observed in experiments [TIU99, DGS$^+$00]. Concerning the *spin dynamics* one has to keep in mind that the mere displacement of stripes (which act as phase boundaries for magnetic domains) does not lead to a frustration and glassy behaviour of spins [ZOK$^+$01]. However, stripe dislocations do induce such a frustration. Thus, our conclusion about the presence of dislocations is consistent with glassy spin dynamics as seen by local experimental techniques [YHC99, HSI99]. A detailed study of magnetic fluctuations is beyond the scope of the present approach which focuses on order in the charge sector of the stripe array.

As both the roughening transition is washed out by disorder and the superroughening transition is washed out by the presence of dislocations, no sharp transition will exist in the thermodynamic limit. Nevertheless, crossover phenomena may be observable. For weak disorder and/or strong lattice po-

[3] Note also that in the nickelates the charge correlation length is *larger* than the spin correlation length by roughly a factor 4 [LC97], while it should be *smaller* in the absence of topological defects according to Ref. [Zac00].

tential the stripe array appears to be locked to the lattice potential up to very large length scales. It "unlocks" also on finite scales with increasing temperature or decreasing lattice potential. An apparent lock-in transition was observed [TSA$^+$95] in $La_{2-x-y}Nd_ySr_xCuO_4$ where the strength of the lattice potential corresponds to the Nd concentration. Since $T_{\rm SR} \gg T_{\rm m}$ the density of free dislocations will be high near $T_{\rm SR}$ so that reminiscences on finite scales of the superroughening transition are unlikely to survive.

Since the array has short-range order at all temperatures for $\Delta > 0$ we expect the absence of commensurate/incommensurate transitions (identified from fluctuations on asymptotically large length scales). Nevertheless, the experimental observations of anomalies at particular values of p can be related to the effects of U on finite length scales.

In view of our conclusion about the absence of commensuration effects we comment on the $\delta = \frac{1}{8}$ problem, i.e., the observation that $\delta = 1/2p$ apparently saturates at $\delta = \frac{1}{8}$ near a doping $x = 0.125$ of the cuprates. If this were a commensuration effect as suggested previously [TSA$^+$95, NW96], one would expect to observe the value $\delta = \frac{1}{8}$ around $x = \frac{1}{8}$, i.e. above ($x > \delta$) and below ($x < \delta$) the matching $x = \delta$. To the best of our knowledge (see the data collected in Fig. 7 of Ref. [YLK$^+$98]), there is no evidence for data with $x < \delta$. As pointed out by Yamada *et al.* [YLK$^+$98], the saturation of δ coincides with a saturation of the effective hole concentration in the CuO_2-planes beyond a certain doping level $x \approx 0.12$. Thus it is conceivable that other mechanisms limit the effective hole concentration and lead to a plateau in δ.

Interestingly, evidence for a similar saturation effect has been reported for $YBa_2Cu_3O_{6+y}$ at $\delta = 1/10$ corresponding to $p = 5$ [DMHD01]. While Dai *et al.* argue that the saturation of δ is *not* caused by a saturation of y in this material, we are not aware of any significant data with $y < \delta$ which would support a lock-in mechanism giving rise to this saturation.

At this point we want to address the question to what extend our analysis (so far restricted to two-dimensional arrays) applies to materials consisting of coupled stacks of layers. Such a coupling is expected [EK93] because of the Coulomb interaction. In principle, it may give rise to a crossover from two-dimensional behaviour at small length scales to three-dimensional behaviour on large scales. As a consequence, a true unlocking transition might exist [EN98, EN99]. Indeed, scattering experiments [SBT$^+$95, TAI$^+$96, vVN$^+$98] provide evidence for interlayer correlations. However, the correlations extend only over a few layers which thus behave like one effective layer. We therefore expect our two-dimensional analysis to apply also to these material classes.

In conclusion, we have pointed out the relevance of disorder for a stripe array even in states where its period is commensurate with the atomic structure. We found that on large scales pinning by disorder dominates over pinning by the atomic structure. This induces the superroughness of the array and, on sufficiently large scales, the presence of free dislocations even at low temperatures, which explains the saturation of the correlation length observed in experiments.

In the next chapter the focus is shifted from the large scale structure to the electronic degrees of freedom in the stripes picture.

C. Striped phases, the electronic degrees of freedom

1 Introduction, possible 2D non-Fermi-liquid metal and the role of disorder

Quasi-one-dimensional electron liquids play a paradigmatic role in describing the conductive properties of a variety of physical systems such as organic conductors [Jer91], quantum-Hall systems [vHS00], and striped phases in high-T_c compounds [ZG89, EKZ97]. Recent studies of weakly coupled Luttinger liquids (LL) have provided evidence for the stability of non-Fermi-liquid metallic behaviour in more than one dimension [EFKL00, VC01, MKL01] as opposed to results for an isotropic 2D Fermi gas [ER90]. This remarkable result comes from inter-LL interactions that in a suitable combination with the interactions within the LLs suppress single particle/Cooper pair tunneling and also the instability towards charge-density wave formation. Earlier studies either excluded hopping [LRK77], treated all inter-LL interactions separately as weak perturbations [KG76] or focused on single particle tunneling for strong repulsive intra-LL interactions only [Wen90]. In Refs. [EFKL00, VC01, MKL01] it was shown that backscattering and particle hopping processes between the LLs can be irrelevant for sufficiently strong inter-LL forward scattering. The resulting state was called "sliding Luttinger liquid" (SLL). For a large range of interactions, these processes can be partially relevant and lead to charge-density wave (CDW), transverse superconductor (SC) or Fermi Liquid (FL) phases [EFKL00, VC01, MKL01]. Experiments have provided evidence for 1D transport in high-T_c compounds [NEU99, ASKL99, ALS02]. Theoretically, novel and to date essentially unexplored behaviour can arise from disorder, which is induced by doping in these materials.

Here, we examine the role of electron scattering by a random impurity potential. For a single LL it was shown [Ape82, AR82, GS88] that a delocalisation transition can occur with increasing electron attraction and that repulsive interactions always lead to localisation. On the other hand, for coupled LLs, a simple scaling analysis suggests that disorder would be irrelevant at least in the SLL phase [MKL01]. However, using a renormalisation-group (RG) analysis, we show that disorder profoundly modifies the characteristic properties of these systems. It turns out that a delocalisation transition persists in analogy to single LLs. Where Josephson inter-stripe couplings are irrelevant, the delocalised phase can be identified with a new state of matter, which we call disordered stripe metal (DSM). In contrast to the SLL state of the pure system, even in this delocalised phase, there exists only short-ranged longitudinal CDW order due to impurity forward scattering. Because of this scattering process, we also find a strong tendency towards the destruction of transverse CDW order. Thus, the novel DSM state combines short-ranged CDW order and quasi long-ranged longitudinal

superconducting order with LL-like transport properties. Interestingly, it has a much wider stability region in comparison to the pure system's SLL state.

2 The general model: coupled one-dimensional electron gases

We assume a spin gap in the LLs, as present in stripes in high-T_c compounds [EKZ97] and focus hence on the low-energy *charge* excitations. For stripes (labelled by j) that do not couple to each other these excitations can be described in the language of bosonisation by the *bosonic* phase fields $\hat{\Phi}_j$ and their conjugate momenta $\pi\hat{\Pi}_j = \partial_x\hat{\Theta}_j$. The phase field determines the modulation of the charge density in the Luttinger liquid around the average value ρ_0 and the dual field is consequently related to the current,

$$\hat{\rho}_j(x) - \rho_0 = -\frac{1}{\pi}\frac{\partial\hat{\Phi}_j}{\partial x} + \frac{1}{\sqrt{2}\pi\alpha}\cos[2k_{\mathrm{F}}x - \sqrt{2}\hat{\Phi}_j]. \tag{2.1}$$

$$\hat{\jmath}_j(x) = v_J\hat{\Pi}_j.$$

Both the kinetic energy and Coulomb interaction of the orginal fermions on the stripes translate to a harmonic path-integral action for the bosonic fields

$$\begin{aligned} S^0 &= \frac{1}{2\pi}\sum_j\int_{x\tau}\Big[v_J(\partial_x\Theta_j)^2 + v_N(\partial_x\Phi_j)^2 - 2i\partial_\tau\Phi_j\partial_x\Theta_j\Big] \\ &= \frac{1}{2\pi}\int_{\mathbf{Q}}\Big[v_N q_\parallel^2|\Phi_{\mathbf{Q}}|^2 + v_J q_\parallel^2|\Theta_{\mathbf{Q}}|^2 - 2iq_\parallel\omega\ \Phi_{\mathbf{Q}}\Theta_{-\mathbf{Q}}\Big], \qquad (2.2) \\ S^0\Big|_\Phi &= \frac{1}{2\pi K}\sum_j\int_{x\tau}\Big[\frac{1}{u}(\partial_\tau\Phi_j)^2 + u(\partial_x\Phi_j)^2\Big] \qquad (2.3) \\ S^0\Big|_\Theta &= \frac{K}{2\pi}\sum_j\int_{x\tau}\Big[\frac{1}{u}(\partial_\tau\Theta_j)^2 + u(\partial_x\Theta_j)^2\Big]. \qquad (2.4) \end{aligned}$$

The latter two version of the action result from the integration over the Θ- and the Φ-field, respectively, and the characteristic velocities v_N and v_J – which are renormalised by intra-stripe forward scattering with respect to to the free-fermion value $v_N = v_J = v_{\mathrm{F}}$ – are expressed in terms of the conventional Luttinger liquid interaction parameter $K = \sqrt{v_J/v_N}$ and the velocity $u = \sqrt{v_J v_N}$. Backward scattering is irrelevant, like any quantity that is a function of the gapped spin fields only. We have used as definition of the Fourier transformation

$$\begin{aligned} \Phi_j(x,\tau) &=: a\int_{-\pi/a}^{\pi/a}\frac{dq_\perp}{2\pi}\int_{-\Lambda}^{\Lambda}\frac{dq_\parallel}{2\pi}\int_{-\infty}^{\infty}\frac{d\omega}{2\pi}e^{i\omega\tau+iq_\perp(aj)+iq_\parallel x}\Phi_{\mathbf{Q}} \\ &= \int_{q_\perp q_\parallel\omega}e^{i\omega\tau+iq_\perp(aj)+iq_\parallel x}\Phi_{\mathbf{Q}} \end{aligned}$$

with $\mathbf{Q} := (\omega, q_\parallel, q_\perp)$, a the stripe spacing and Λ the ultraviolet cutoff in the direction along the stripes. Note that Fourier transformation in the transverse direction ($\perp$) does not change the dimensionality.

For an introduction to the method of bosonisation and the details of the conventions used here, see Appendix 1; our notation follows the review article Ref. [Voi95].

Forward and backward scattering by weak *impurities* (denoted by IFS and IBS, respectively) is described in terms of the action [GS88]

$$S^{\mathrm{IFS}} = -\frac{\sqrt{2}}{\pi}\sum_j \int_{x\tau} \eta_j(x)\partial_x\Phi_j, \tag{2.5a}$$

$$S^{\mathrm{IBS}} = \frac{1}{\pi\alpha}\sum_j \int_{x\tau} \left\{\xi_j(x)e^{i(\sqrt{2}\Phi_j - 2k_{\mathrm{F}}x)} + \mathrm{h.c.}\right\}. \tag{2.5b}$$

$\eta_j(x)$ and $\xi_j(x)$ are Gaussian random variables with zero mean and correlations $\overline{\eta_i(x)\eta_j(x')} = \frac{1}{2}D_\eta\delta_{ij}\delta(x-x')$ and $\overline{\xi_i^*(x)\xi_j(x')} = D_\xi\delta_{ij}\delta(x-x')$ and α is the infinitesimal regularisation length of bosonisation. Forward scattering can be identified as the coupling of the slowly varying first term of the density, see Eq. (2.1), to a short-range correlated disorder potential, while the second term in Eq. (2.1) accounts for impurity backward scattering. The disorder strength parameters $\mathcal{D}_\eta, \mathcal{D}_\xi$ are both determined by the original disorder potential. We write them independently, however, since they will be separated by the RG flow below. On the replica level the corresponding disorder action contributions read

$$S_n^{\mathrm{IFS}} = \frac{\mathcal{D}_\eta}{2\pi^2}\sum_{j;ab}\int_{x\tau\tau'} \partial_x\Phi^a_{j,x,\tau}\partial_x\Phi^b_{j,x,\tau'}$$

$$S_n^{\mathrm{IBS}} = \frac{\mathcal{D}_\xi}{(2\pi\alpha)^2}\sum_{j;ab}\int_{x\tau\tau'} \cos[\sqrt{2}(\Phi^a_{j,x,\tau} - \Phi^b_{j,x,\tau'})].$$

Coulomb repulsion couples the charge density on different stripes. We first include forward scattering density-density interactions between the stripes, i.e., coupling of the slowly varying first terms of Eq. (2.1). Indirect contributions from electron-phonon interactions may be included here and the corresponding action reads

$$S^V = \frac{1}{2\pi}\sum_{i\neq j}\int_{x\tau}\partial_x\Phi_i V_{i-j}\partial_x\Phi_j. \tag{2.6}$$

In principle, analogous couplings between $\partial_x\Theta_j$ can be added [EFKL00, VC01, MKL01], but are dropped for simplicity. Their inclusion can be achieved by an obvious generalisation of our analysis, and will not modify our main results. Since S^V is bilinear in Φ_i, it can be included in the momentum-space representation of the action S^0 by replacing v_N in Eq. (2.2) by the $q_\perp$-dependent velocity $\tilde{v}_N(q_\perp) = v_N + V_{q_\perp}$ with the Fourier transformed inter-stripe coupling $V_{q_\perp} = \sum_j e^{-iq_\perp(ja)}V_j$. The Luttinger parameter is then generalised to

$$\tilde{K}(q_\perp) = \sqrt{v_J/\tilde{v}_N(q_\perp)} = K/\sqrt{1 + V_{q_\perp}/v_N} \tag{2.7}$$

and intra-stripe forward scattering is included in the harmonic action

$$S^0 + S^V\Big|_\Phi = \frac{1}{2\pi}\int_{\mathbf{Q}} |\Phi_{\mathbf{Q}}|^2 \frac{1}{\tilde{K}}\Big[\frac{1}{\tilde{u}}\omega^2 + \tilde{u}q_\parallel^2\Big], \tag{2.8}$$

$$S^0 + S^V\Big|_\Theta = \frac{1}{2\pi}\int_{\mathbf{Q}} |\Theta_{\mathbf{Q}}|^2 \tilde{K}\Big[\frac{1}{\tilde{u}}\omega^2 + \tilde{u}q_\parallel^2\Big]. \tag{2.9}$$

The restriction to low energy excitations underlying bosonisation obviously requires the stability condition $v_N + V_{q_\perp} > 0$.

Besides these forward scattering processes, the Coulomb coupling of the oscillating terms in the density Eq. (2.1) gives the transverse CDW coupling and pair-hopping reflects the SC Josephson coupling between stripes

$$S^{\mathrm{CDW}} = \sum_{i\neq j} \mathcal{C}_{i-j} \int_{x\tau} \cos\left[\sqrt{2}(\Phi_i - \Phi_j)\right], \tag{2.10a}$$

$$S^{\mathrm{SC}} = \sum_{i\neq j} \mathcal{J}_{i-j} \int_{x\tau} \cos\left[\sqrt{2}(\Theta_i - \Theta_j)\right]. \tag{2.10b}$$

Since we assume the presence of a spin gap, single electron hopping is irrelevant and can be ignored [EKZ97, BC91].

It should be noted that by use of the bosonisation formula for the fermionic field operator, see Appendix 1, the translation of any of the above couplings from fermionic to bosonised language can be shown rigorously.

For the pure system without S^{IFS} and S^{IBS}, a specific interaction V_i in Eq. (2.6) can render the CDW and SC couplings irrelevant in an intermediate region of K, leading to the SLL phase found in Refs. [EFKL00, VC01]. The interaction must be sufficiently strong and has to include at least nearest and next-nearest neighbours.

In the presence of disorder, the scattering off impurities has to be taken into account. Let us first focus on the effect of impurity forward scattering (2.5a) in the absence of any inter-stripe couplings of type (2.10). This process then changes the SLL phase as described by $S^0 + S^V$ into the disordered stripe metal (DSM). Introducing replicated fields and averaging over disorder still leads to a bilinear action with correlations

$$\langle \Phi^a_{\mathbf{Q}} \Phi^b_{-\mathbf{Q}} \rangle = \frac{\pi\delta^{ab}}{\omega^2/v_J + \tilde{v}_N(q_\perp)q_\parallel^2} + \frac{D_\eta \delta(\omega)}{\tilde{v}_N^2(q_\perp)q_\parallel^2}, \tag{2.11a}$$

$$\langle \Theta^a_{\mathbf{Q}} \Theta^b_{-\mathbf{Q}} \rangle = \frac{\pi\delta^{ab}\tilde{v}_N(q_\perp)/v_J}{\omega^2/v_J + \tilde{v}_N(q_\perp)q_\parallel^2} \tag{2.11b}$$

where upper indices a, b are replica labels and the definition of the delta function is $\int d\omega\ \delta(\omega) = 2\pi$. Note that the impurity forward scattering amplitude D_η does not enter the $\langle\Theta\Theta\rangle$-correlations. Any physical quantity that can be written in the Θ-field only will thus be untouched by forward scattering of any strength.

3 Renormalisation

We now examine the relevance of CDW and SC couplings and of impurity backward scattering (IBS) with respect to the DSM state in an RG analysis. To first order, we will find that the DSM parameters $\tilde{K}, \tilde{u}$ are renormalised only by impurity backward scattering and not by CDW and SC couplings. In Refs. [GS88, GS89] this renormalisation is determined for a single Luttinger liquid in a real-space RG scheme, whereas here we prefer the momentum-shell approach in which the inter-stripe couplings can be treated very conveniently. The two approaches are compatible if in the momentum-shell RG the Θ-field is integrated out *before* the feedback from disorder is determined. Not following this prescription leads to dramatically unphysical consequences. It is, however, not easy to find a priori a justification for this RG 'recipe' other than by comparison with the trusted real-space approach. The

problem is explored in detail in Appendix 2 where real- and momentum-space RG are contrasted. The flow equations (3.19) at the end of the section are the main results of this chapter and will be used to derive the phase diagrams below. In order to follow the general line of argument, the following derivation of Eqs. (3.19) may be skipped.

In momentum-space RG, the fields are decomposed in a rapidly varying part ($>$) with modes from a momentum shell of with Λdl sharply under the longitudinal cutoff $\Lambda \sim 1/\alpha$ and a slowly varying part ($<$)

$$\Phi_j(x,\tau) = \Big\{ \int_{|q_\parallel|<\Lambda e^{-dl}} \frac{dq_\parallel}{2\pi} e^{iq_\parallel x} + \int_{\Lambda e^{-dl}<|q_\parallel|<\Lambda} \frac{dq_\parallel}{2\pi} e^{iq_\parallel x} \Big\} \int_{q_\perp \omega} e^{i\omega\tau + iq_\perp (ja)} \Phi_{\mathbf{Q}} =: \Phi_j^< + \Phi_j^>.$$

The latter are integrated out defining a renormalised action $S'_<$ that only depends on the slowly varying fields

$$Z = \int \mathcal{D}[\Phi,\Theta] e^{-S_{<,>}} = \int \mathcal{D}[\Phi^<,\Theta^<] \int \mathcal{D}[\Phi^>,\Theta^>] e^{-S_{<,>}} =: \int \mathcal{D}[\Phi^<,\Theta^<] e^{-S'_<}. \qquad (3.12)$$

Anharmonic ($a.h.$) contributions to the action feed back according to

$$\begin{aligned} \Delta S_< &:= S'_< - S_< = -\ln \langle e^{-(S^{a.h.}_{<,>} - S^{a.h.}_<)} \rangle_{>,0} \\ &= \langle S^{a.h.}_{<,>} - S^{a.h.}_< \rangle_{>,0} - \frac{1}{2} \langle (S^{a.h.}_{<,>} - S^{a.h.}_<)^2 \rangle_{>,0} + \mathcal{O}\big((S^{a.h.})^3\big) \end{aligned}$$

Here, the integration of the rapid modes has been rewritten as an average with respect to the harmonic part of the action.

We now analyse the feedback of each of the anharmonicities $S^{\rm IBS}, S^{\rm CDW}, S^{\rm SC}$ separately, which is consistent to first order. Averages are for the moment to be understood with respect to the harmonic action of the modes in the shell. For the disorder feedback one has

$$\begin{aligned} \Delta S^{\rm IBS}_< &= \langle S^{\rm IBS}_{<,>} - S^{\rm IBS}_< \rangle \\ &= \frac{\mathcal{D}_\xi}{(2\pi\alpha)^2} \sum_{j;ab} \int_{x\tau\tau'} \cos[\sqrt{2}\,\Delta\Phi^<] \, \langle \cos[\sqrt{2}\,\Delta\Phi^>] - 1 \rangle \end{aligned} \qquad (3.13)$$

with $\Delta\Phi^> := \Phi^{a,>}_{j,x,\tau} - \Phi^{b,>}_{j,x,\tau'}$ and the analogue for $\Delta\Phi^<$. We use

$$\begin{aligned} \langle (\Delta\Phi^>)^2 \rangle &= 2 \int_{\mathbf{Q}}^> \Big\{ \langle \Phi^a_{\mathbf{Q}} \Phi^a_{-\mathbf{Q}} \rangle - \langle \Phi^a_{\mathbf{Q}} \Phi^b_{-\mathbf{Q}} \rangle e^{i\omega\,\Delta\tau} \Big\} \\ &= 2dl\,\Lambda \int_{\omega q_\perp} \frac{\tilde{K}}{\omega^2/\tilde{u} + \Lambda^2 \tilde{u}} \Big(1 - \delta^{ab} e^{i\omega\,\Delta\tau} \Big) \\ &= dl\,\Lambda \int_{q_\perp} \tilde{K}(q_\perp) \Big(1 - \delta^{ab} e^{-\omega\,\Delta\tau} \Big) \end{aligned}$$

with $\Delta\tau := \tau - \tau'$ to get

$$\begin{aligned} \langle \cos[\sqrt{2}\,\Delta\Phi^>] \rangle &= e^{-\langle (\Delta\Phi^>)^2 \rangle} \\ &= 1 - dl \int_{q_\perp} \tilde{K}(q_\perp) + \delta^{ab} dl \int_{q_\perp} \tilde{K}(q_\perp) e^{-\Delta\tau \tilde{u} \Lambda}. \end{aligned}$$

The second term of the last expression gives upon insertion into Eq. (3.13) the renormalisation of impurity backward scattering

$$d\mathcal{D}_\xi = -dl \int_{q_\perp} \tilde{K}. \qquad (3.14)$$

There is an additional feedback to the action from the third term

$$\Delta S = dl \frac{\mathcal{D}_\xi}{(2\pi\alpha)^2} \Big(\int_{q_\perp} \tilde{K} \Big) \sum_{j;ab} \delta^{ab} \int_{x\tau\tau'} e^{-\Delta\tau \tilde{u}\Lambda} \cos[\sqrt{2}\, \Delta\Phi^<] \, .$$

A gradient expansion $\cos[\sqrt{2}(\Phi^a_\tau - \Phi^a_{\tau'})] = 1 - (\partial_\tau \Phi^a)^2 \Big|_\tau (\Delta\tau)^2 + \mathcal{O}(\Delta\tau^3)$ brings the latter term to a form that matches the harmonic action

$$\Delta S = dl \frac{\mathcal{D}_\xi}{\pi^2 \alpha^2 \Lambda^3} \Big(\int_{q_\perp} \tilde{K}/\tilde{u}^3 \Big) \sum_{j:a} \int_{x\tau} (\partial_\tau \Phi^a_{j,\tau})^2 .$$

We read off by comparison with Eq. (2.3) the parameter renormalisation

$$dv_J = -dl \frac{2 v_J}{\pi \alpha^2 \Lambda^3} D_\xi \int_{q_\perp} \tilde{v}_N^{-2}(q_\perp).$$

Since $\tilde{v}_N = n_N + V_{q_\perp}$ is not renormalised to first order, the latter flow equation can be rewritten in terms of $K = \sqrt{v_J / v_N}$

$$dK = -dl \frac{K}{\pi \alpha^2 \Lambda^3} D_\xi \int_{q_\perp} \tilde{v}_N^{-2}(q_\perp). \tag{3.15}$$

Similarily, we integrate over modes in the momentum shell in the charge-density-wave and Josephson couplings

$$\begin{aligned}
\Delta S^{\mathrm{CDW,m}}_< &= \langle S^{\mathrm{CDW,m}}_{<,>} - S^{\mathrm{CDW,m}}_< \rangle \\
&= \mathcal{C}_m \sum_{j;a} \int_{x\tau} \cos[\sqrt{2}\, \Delta\Phi^<_m] \, \langle \cos[\sqrt{2}\, \Delta\Phi^>_m] - 1 \rangle \\
&= dl \int_{q_\perp} (1 - \cos[maq_\perp]) \Big\{ \tilde{K}(q_\perp) + \frac{2\mathcal{D}_\eta}{\pi\Lambda \tilde{v}_N^2(q_\perp)} \Big\} \\
&\quad \times \; \mathcal{C}_m \sum_{j;a} \int_{x\tau} \cos[\sqrt{2}\, \Delta\Phi^<_m], \qquad (3.16) \\
\Delta S^{\mathrm{SC,m}}_< &= dl \int_{q_\perp} (1 - \cos[maq_\perp]) \tilde{K}^{-1} \; \mathcal{J}_m \sum_{j;a} \int_{x\tau} \cos[\sqrt{2}\, \Delta\Theta^<_m] \qquad (3.17)
\end{aligned}$$

with $\Delta\Phi^>_m = \Phi^{a,>}_{j+m} - \Phi^{a,>}_j$. Here we have used

$$\begin{aligned}
\langle (\Delta\Phi^>_m)^2 \rangle &= dl \frac{2\Lambda}{\pi} \int_{q_\perp} (1 - \cos[maq_\perp]) \int_\omega \Big\{ \frac{\pi \tilde{K}}{\omega^2/\tilde{u} + \Lambda^2 \tilde{u}} + \frac{\mathcal{D}_\eta \delta(\omega)}{\tilde{v}_N^2 \Lambda^2} \Big\} \\
&= dl \int_{q_\perp} (1 - \cos[maq_\perp]) \Big\{ \tilde{K} + \frac{2\mathcal{D}_\eta}{\Lambda \pi \tilde{v}_N^2} \Big\}, \\
\langle (\Delta\Theta^>_m)^2 \rangle &= dl \int_{q_\perp} (1 - \cos[maq_\perp]) \tilde{K}^{-1}
\end{aligned}$$

Note that different from the impurity backward scattering the forward scattering contribution to the $\langle \Phi\Phi \rangle$-correlations does not drop out in the calculation of the CDW feedback.

After each integration step, the cutoff in the stripe direction has to be readjusted to its original value and also the time direction is rescaled as to keep the harmonic part of the action scale-invariant

$$\begin{aligned}
q_\perp &\to q'_\perp = q_\perp \\
q_\parallel &\to q'_\parallel = q_\parallel e^{dl} \\
\omega &\to \omega' = \omega e^{dl}.
\end{aligned} \tag{3.18}$$

Renormalisation due to rescaling and the integration feedback Eqs. (3.14), (3.15), (3.16), (3.17) combine to the RG equations of flow

$$\frac{dD_\xi}{dl} = (3-\Delta^{\rm IBS})D_\xi, \tag{3.19a}$$

$$\frac{dD_\eta}{dl} = D_\eta, \tag{3.19b}$$

$$\frac{dK}{dl} = -\frac{1}{\pi\alpha^2\Lambda^3}KD_\xi\int_{q_\perp}\tilde{v}_N^{-2}(q_\perp), \tag{3.19c}$$

$$\frac{d\tilde{v}_N}{dl} = 0, \tag{3.19d}$$

$$\frac{d\mathcal{C}_m}{dl} = (2-\Delta_m^{\rm CDW})\mathcal{C}_m, \tag{3.19e}$$

$$\frac{d\mathcal{J}_m}{dl} = (2-\Delta_m^{\rm SC})\mathcal{J}_m, \tag{3.19f}$$

with the scaling dimensions

$$\Delta^{\rm IBS} = \int_{q_\perp}\tilde{K}(q_\perp), \tag{3.20a}$$

$$\Delta_m^{\rm CDW} = \int_{q_\perp}(1-\cos[mq_\perp])\Big\{\tilde{K}(q_\perp)+\frac{2D_\eta}{\pi\Lambda\tilde{v}_N^2(q_\perp)}\Big\}, \tag{3.20b}$$

$$\Delta_m^{\rm SC} = \int_{q_\perp}(1-\cos[mq_\perp])\tilde{K}^{-1}(q_\perp). \tag{3.20c}$$

4 Phase diagrams, generic features

In the *absence of disorder* ($D_\xi = D_\eta = 0$), K preserves its unrenormalised value $\sqrt{v_J/v_N}$. Then the scaling dimensions (3.20) reproduce the expressions given in Ref. [MKL01]. For weak inter-stripe interactions $V_{q_\perp} \ll v_N$ the system is in the SC phase for $K \gtrsim 1$, whereas it is in the CDW phase for $K \lesssim 1$. For a suitable choice of a strong interaction $V_{q_\perp}$, an intermediate range of K can exist where all SC and CDW couplings are irrelevant and the system is in the SLL phase. The stability of the SLL phase is determined by the conditions $K > K^{\rm CDW} = 2/\min_m\{c_m^+\}$ and $K < K^{\rm SC} = \min_m\{c_m^-\}/2$. Hereby we define

$$c_m^\pm \equiv \int_{q_\perp}[1-\cos mq_\perp]\left(\frac{v_N}{\tilde{v}_N}\right)^{\pm 1/2}.$$

In the *presence of disorder*, the strength of impurity forward scattering D_η increases exponentially under the RG flow. This has two important consequences. First, the CDW order along the stripes becomes now short-ranged as can be easily seen from the second term in Eq. (2.11a). Second, it implies an exponential increase of $\Delta_m^{\rm CDW}$ for all m, i.e., the *irrelevance of weak CDW couplings*. Thus, impurity scattering transforms the SLL and CDW phases of the pure system into different phases. If impurity backward scattering (IBS) is irrelevant – this is the case in the entire stability region of the SLL [MKL01] – a novel phase is present which we call DSM phase. Unlike for the SLL, the stability of the DSM for small K is no longer limited by the CDW couplings but by IBS. Its phase boundary is determined by the relevance of SC couplings at large K and the relevance of IBS at small K. IBS leads to *localisation* for a bare IBS strength D_ξ larger than a critical value $D_{\xi,c}$

(that depends on intra- and inter-stripe interactions). In this case D_ξ diverges and K goes to zero under renormalisation. For $D_\xi < D_{\xi,c}$, the system is *delocalised*, $D_\xi \to 0$ and K saturates at a finite value $K^* = K^*(D_\xi)$. For K below the critical value $K_c = 3/c_\infty^+$, infinitesimal disorder produces localisation ($D_{\xi,c} = 0$). For $K > K_c$, the system remains delocalised at finite disorder strength, $0 < D_\xi < D_{\xi,c}$.

To determine the phase boundary $D_{\xi,c}$ of the localisation transition for $K > K_c$, we integrate the flow Eqs. (3.19a) and (3.19c). In terms of the dimensionless disorder strength $\mathcal{D} = D_\xi/(\pi^3 \Lambda v_N^2)$ we obtain

$$\mathcal{D}(K_l) = \mathcal{D}_0 + \frac{c_\infty^+}{c}(K_l - K_0) - \frac{3}{c}\ln\frac{K_l}{K_0} \tag{4.21}$$

with

$$c \equiv \int_{q_\perp} \left(\frac{v_N}{\tilde{v}_N}\right)^2.$$

The critical disorder strength then follows from the condition that $\mathcal{D}(K) = 0$ at its minimum at $K = 3/c_\infty^+ = K_c$:

$$\mathcal{D}_{0,c} = \frac{c_\infty^+}{c}(K_0 - K_c) + \frac{3}{c}\ln\frac{K_c}{K_0}. \tag{4.22}$$

In the delocalised phase, the renormalised value K^* of K can be obtained from Eq. (4.21) with $\mathcal{D}(K^*) = 0$. The phase boundary at large K between DSM and SC phase is given by the condition $K^* < K^{\mathrm{SC}} = \min_m\{c_m^-\}/2$, and the boundary at small K between the DSM and the localised phase is described by Eq. (4.22).

The actual form of the phase diagram and, more importantly, the stability range of the SLL or DSM phase depends on the interaction $V_{q_\perp}$ under consideration. To be specific, we will consider in the following two models for this interaction.

4.1 Model A: interaction yielding a rich phase diagram

A minimal model that renders simultaneously all SC- and CDW-couplings irrelevant for some parameter region was suggested by Vishwanath *et al.* [VC01]. It assumes an inter-stripe interaction forward scattering leading to

$$\tilde{K}(q_\perp) = \kappa/[1 + \lambda_1\cos(q_\perp) + \lambda_2\cos(2q_\perp)].$$

Within this model, the three parameters κ, λ_1 and λ_2 implicitly determine the intra- and inter-stripe interaction. The corresponding Luttinger parameter is given by $K^2 = \kappa^2/(1 + (\lambda_1^2 + \lambda_2^2)/2)$, and the inter-stripe potential V_i has a range of four stripe spacings. In analogy to Ref. [MKL01], we rewrite λ_1 and λ_2 as

$$\begin{aligned}\lambda_1 &= -\frac{4(1-\Delta)\cos q_0}{1 + 2\cos^2 q_0},\\ \lambda_2 &= \frac{1-\Delta}{1 + 2\cos^2 q_0},\end{aligned}$$

such that $\tilde{K}(q_\perp)$ takes its maximal value κ/Δ at $q_\perp = q_0$. By adjusting Δ to small values, CDW couplings are suppressed, while small κ gives negative scaling dimensions for SC-couplings, as pointed out by Mukhopadhyay *et al.* [MKL01]. One thus indeed finds regions in (q_0, κ, Δ)-phase space, where

the system is stable against all inter-stripe couplings of type (2.10) and is thus in the SLL phase. This is demonstrated in Fig. C.1, which may be compared to similar plots in Refs. [VC01, MKL01]. For sufficiently small Δ, windows of q_0 exist where the system evolves from a phase coherent SC

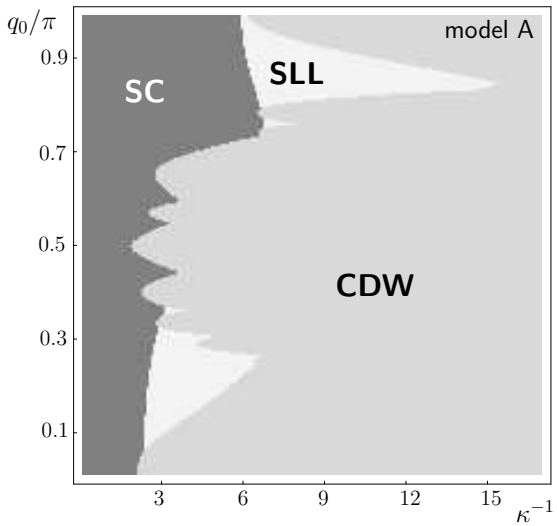

Fig. C.1: Phase diagram of model A for $\Delta = 10^{-3}$ in the absence of disorder. For large K, the system forms a 2D superconductor while it is a 2D CDW for small κ. The intermediate SLL exists only for suitable values of the parameter q_0.

through the 2D metallic SLL to a charge ordered CDW state with decreasing parameter κ. Here and in the following, when both SC and the CDW couplings compete, the one that is most strongly relevant is assumed to determine the phase. The actual boundary between two such strong coupling phases might differ within a narrow corridor. Note however, that boundaries to either the DSM or SLL phase are obtained also quantitatively correctly.

Now disorder is added while all other parameters are unchanged. The CDW and the SLL phases of the pure system become indistinguishable and merge to the metallic, short-range CDW-ordered 'disordered stripe metal' (DSM). Backscattering off impurities leads to localisation in a large portion of the former CDW phase. The SC phase shrinks through downward renormalisation of κ by disorder (note that κ and K differ by a factor that is not renormalised). In Fig. C.2, the boundaries between the three phases are given both for infinitesimal and for finite disorder. The latter shifts the boundaries to larger κ.

A cut through Figs. C.1 and C.2 at fixed q_0 but with varying disorder is shown in Fig. C.3. The SLL and CDW phases exist only for $\mathcal{D} = 0$. A delocalised phase can exist – due to inter-stripe forward scattering – even for purely repulsive interactions (for example, $q_0 = 0.85\pi$, $\Delta = 10^{-3}$ and $\kappa \lesssim 1.42$ corresponds to repulsive on-stripe *and* repulsive inter-stripe interactions), as opposed to the strictly one dimensional electron gas with delocalisation for $K > 3$ corresponding to strongly attractive interactions. However, the inter-stripe interactions corresponding to the values of Δ, κ, q_0 where the SLL or DSM exist may not be very realistic because of their strength.

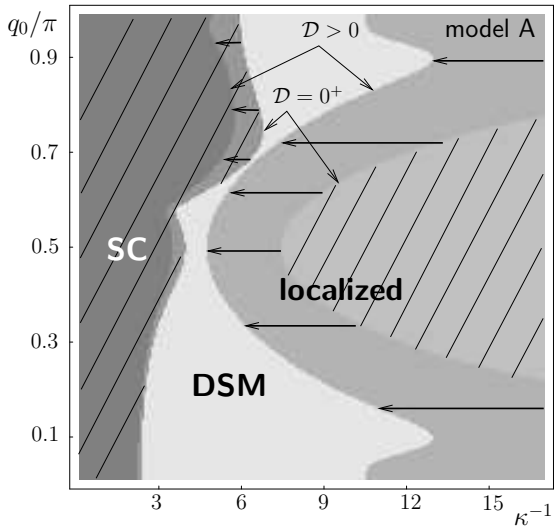

Fig. C.2: Phase diagram for model A with $\Delta = 10^{-3}$ in the presence of disorder for two disorder values. The comparison of the phase boundaries at infinitesimal disorder $\mathcal{D} = 0^+$ and finite disorder $\mathcal{D} = 5 \cdot 10^{-11}$ reflects the disorder induced renormalisation of κ.

4.2 Model B: realistic interaction

Model A is constructed specifically in a way such that the inter-stripe forward scattering interactions (2.6) give rise to a non-monotonous $\tilde{K}(q_\perp)$ which allows for the simultaneous irrelevance of CDW and SC couplings in the absence of disorder. For a large range of parameters q_0 and Δ, this potential has oscillatory character in real space, which also may not be very realistic.
A physically motivated choice for a potential that is monotonous both in real and Fourier space may be the screened Coulomb potential

$$V(r) \quad = \quad \frac{A}{r} e^{-\mu r}$$

which we consider as model B. In Fourier space this model reads

$$V_{q_\perp} \quad = \quad -A \ln \left[1 + e^{-2\mu} - 2e^{-\mu} \cos q_\perp \right] .$$

Due to the stability condition $V_{q_\perp}/v_N > -1$, see Eq. (2.7), there is a critical amplitude $A_c(\mu)$, above which the model breaks down.
Fig. C.4 displays the stability of the model with respect to weak inter-stripe CDW and SC couplings in the absence of disorder. No SLL is found, the system shows for all μ and A a direct transition from the SC to the CDW phase for decreasing K. The addition of disorder leads to the phase diagram in Fig. C.5. As opposed to model A, impurity backscattering completely covers the CDW phase and thus leaves only two phases, the localised one and the SC phase. In contrast to the competition between CDW and SC couplings, the localisation boundary is not given by the most relevant bare coupling. Since even weakly relevant IBS renormalises K to small values, the disorder scaling dimension decreases while the Josephson coupling, provided a small enough bare value, ultimately becomes irrelevant, see Eqs. (3.19). Hence the boundary is given by the onset of relevance of IBS

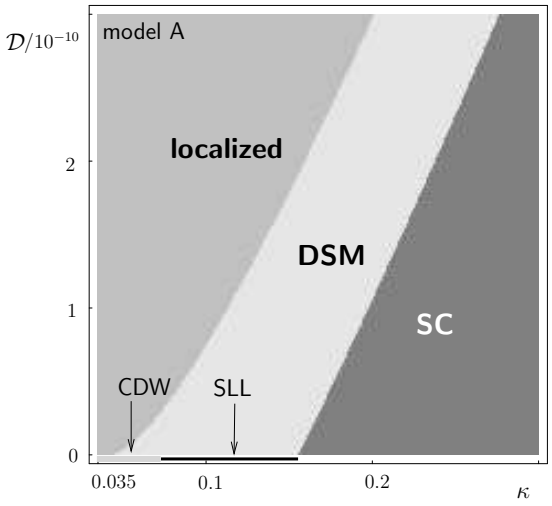

Fig. C.3: Phase diagram for model A in the plane spanned by disorder and interaction parameter κ for fixed inter-stripe interactions with $q_0 = 0.85\pi$ and $\Delta = 10^{-3}$. With increasing disorder strength $\mathcal{D}$, the boundaries of the DSM phase move to larger κ keeping a nearly constant distance.

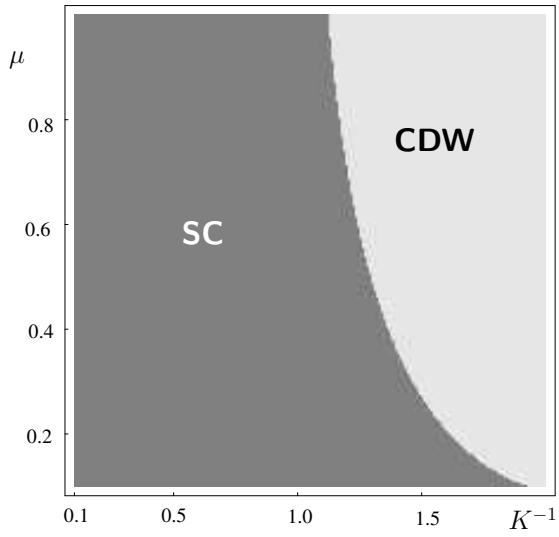

Fig. C.4: Phase diagram for model B for $A = 0.78 v_N$ without disorder.

with respect to the pure system. It moves to larger K for increasing disorder. No DSM phase is found now. Formally, the absence of a minimum of $V_{q_\perp}$ inside the interval $(0, \pi)$ makes up for this latter qualitative difference in models A and B.

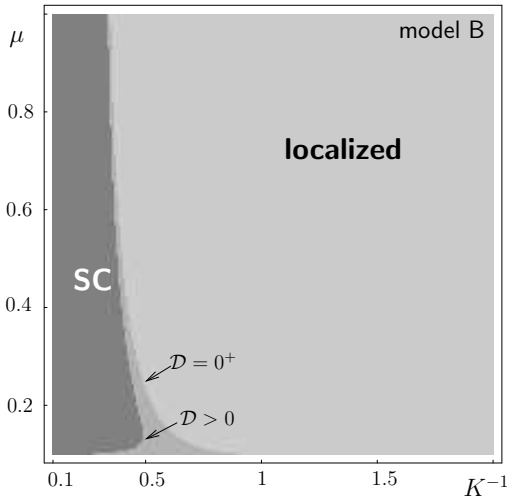

Fig. C.5: Phase diagram for model B for two disorder values $\mathcal{D} = 0^+$ and finite disorder $\mathcal{D} = 10^{-3}$ and infinitesimal Josephson coupling $\mathcal{J} = 0^+$; $A = 0.78 v_N$;

5 Correlations

Having established the generic topology of phase diagrams, we now address the nature of the possible phases. First we consider the *delocalised DSM phase*. It is described by the correlations (2.11) with the bare IFS amplitude D_η and the renormalised effective K^* (in general, one has to use the renormalised but unrescaled quantities). We find a linear growth of the fluctuations of Φ with longitudinal system size L, $\overline{\langle \Phi_j^2(x,\tau)\rangle}_L = (c/2\pi^2) v_N^{-2} D_\eta L$, which leads to short-ranged longitudinal CDW correlations like for single LLs. On the other hand, IFS does not affect the quasi long-ranged longitudinal superconducting order (fluctuations of Θ) of the pure system. Equally, the conductivity along the stripes is not affected by IFS since $\eta_j(x)$ is time independent [GS88]. From a linear-response calculation we obtain the LL-like conductivity

$$\sigma(\omega, q_\parallel, q_\perp) = \frac{2e^2}{\pi\hbar} \frac{i\omega}{(\omega + i0^+)^2/v_J^* - \tilde{v}_N(q_\perp) q_\parallel^2},$$

representing a longitudinal metal. Here, ω represents a real frequency in contrast to Matsubara frequencies in Eqs. (2.11). Notice that $v_J^* = v_N K^{*2}$. To extract physical observables from this expression, the order of limits is crucial. In a situation where a constant field is applied, one should set $q_\parallel = 0$ before asking for the static $\omega \to 0$-limit, which exhibits the Drude peak of a pure, ideal conductor. More realistic, however, is a measurement of the *conductance* in a finite geometry. To this end, one integrates the current-current correlation function over the *finite* length of a given conductor. The frequency may then be sent to zero to obtain the conductance as the conductivity per unit length [FL81]. Since K^* jumps from a finite value to zero at the localisation transition, $\sigma(\mathbf{q})$ behaves discontinuously there. In the transverse direction, CDW and SC correlations will be short-ranged since the corresponding couplings are irrelevant. In the presence of a spin gap (which suppresses single particle hopping) the irrelevance of the couplings also signals that the DSM is a transverse insulator.

The *localised phase* is less amenable to an analytic description since the divergence of IBS would necessitate a strong-coupling analysis. However, if the SC coupling is irrelevant, the localisation transition and the localised phase share the qualitative properties of their 1D counterparts. The inter-stripe couplings will lead to merely quantitative renormalisation effects. Whether the localised phase is a random antiferromagnet or a pinned CDW depends on the mechanism generating the spin gap. The longitudinal localisation length $L_{\rm loc}$ can be estimated analytically when the transition line is approached from the localised side. For $K < K_c$, $L_{\rm loc} \simeq \Lambda^{-1}\mathcal{D}_0^{-1/(3(1-K/K_c))}$. For $K > K_c$, $L_{\rm loc} \simeq \Lambda^{-1}\exp(\tilde{c}/\sqrt{c(\mathcal{D}_0 - \mathcal{D}_{0,c})})$ with $\tilde{c}$ a numerical factor of order unity. Thus, the inter-stripe interactions influence the localisation length quantitatively, but the qualitative behaviour found [GS88] for the localisation transition in a single LL persists.

6 Discussion and outlook

In summary, we have examined impurity effects in arrays of coupled LLs. The competition between impurity backscattering, CDW and SC couplings allows for three different phases: a localised phase, a superconducting phase, and the disordered stripe metal. The latter two phases are delocalised since IBS scattering is irrelevant. While for a single stripe delocalisation occurs only for strongly attractive on-stripe interactions ($K \gtrsim 3$), for a coupled stripe array delocalisation is possible also for purely *repulsive* on-stripe and inter-stripe interactions (forward scattering).

The delocalised DSM phase is metallic in longitudinal direction and insulating in transverse directions. Its correlations for CDW order are short-ranged in all directions whereas superconducting correlations are quasi long-ranged along the stripes and short-ranged in the transversal direction. These experimentally accessible features should allow to identify the disordered stripe metal and to distinguish it from the SLL phase.

In the above analysis we have determined the phase diagram from a stability analysis of a Gaussian fixed point – representing the stripe array with forward scattering by interactions and impurities – with respect to CDW and SC couplings as well as impurity backward scattering. This stability analysis, reflected by the flow equations (3.19) which are linear in D_ξ, $\mathcal{C}_m$, and $\mathcal{J}_m$, requires the weakness of these couplings. In principle, this approach does not cover strong-coupling phenomena: sufficiently strong couplings might drive transitions into SC or CDW phases which are less susceptible to disorder than the SLL.

Although we cannot consistently access such strong coupling phenomena via our flow equations, they nevertheless can be used to determine crossovers related to the *relative* strength of non-Gaussian couplings. Since all CDW couplings are irrelevant at the DSM fixed point, we raise the question of whether a CDW phase can be reestablished if CDW couplings are sufficiently strong in comparison to disorder. We focus on the region where a CDW coupling $\mathcal{C}_m$ is relevant in the absence of disorder and where IBS is irrelevant (i.e., $\delta \equiv 2 - \Delta_m^{\rm CDW} > 0$ and $\Delta^{\rm IBS} > 3$ for the bare parameters).

Irrespectively of the relative strength of CDW couplings and IBS, the presence of disorder implies a continuous growth of D_η and thus also of $\Delta_m^{\rm CDW}$ which implies the irrelevance of $\mathcal{C}_m$ only on sufficiently large scales. Thus the question is, whether D_η increases fast enough to achieve $\Delta_m^{\rm CDW} > 2$ before a strong-CDW coupling regime is entered. This regime is entered when the dimensionless coupling $\hat{\mathcal{C}}_m \equiv \mathcal{C}_1/(\Lambda^2 v_N)$ becomes of order unity under renormalisation before the disorder contribution

to Δ_m^{CDW} becomes of order δ. For weak $V_{q_\perp}$ or $m \gg 1$, this is the case if

$$\hat{\mathcal{C}}_m \gtrsim \left(\frac{2cD_\eta}{\pi \Lambda v_N^2 \delta} \right)^\delta .$$

For CDWs (quasi-)long-ranged charge correlations can exist in the presence of disorder only in $D > 2$ dimensions like for vortex lattices [NS00]. Then the fermions would form a pinned (localised) Wigner crystal. However, in $D = 2$, the formation of CDW order is prohibited by the proliferation of dislocations [VF84], which ultimately render the CDW coupling irrelevant on sufficiently large scales.

In the previous two chapters, the two sectors of geometrical and electronic on-stripe degrees of freedom were discussed separately, one of them assumed to be integrated out at a time. One can imagine, that the coupling does not only determine the effective parameters of the sector under consideration, but may even generate qualitatively new terms. These important questions deserve an independent thorough analysis. Steps into this direction have been taken in Refs. [KFE98, TP00] but further efforts certainly are desirable.

D. Planar vortex lattices

1 Introduction

The existence of a vortex glass (VG) in type-II superconductors is of crucial importance for their performance. This disorder dominated phase has been the subject of intense research for decades [NS00]. The vortex glass plays a paradigmatical role in the field of disordered systems. In face of the challenges the VG poses, theoretical concepts of great generality and applicability have been developed, of which the wide field of functional renormalisation may serve as an example. With its famous relatives, the spin glass models [BY86], there has been a fruitful interplay. Some theories have been designed in parallel, e.g., the droplet or scaling picture of ground-states and excitations [FH88, NS00], some have been adapted from one field to the other and the VG may play the role of a testing ground, e.g., for replica symmetry breaking schemes [LG95]. Other than for spin glass models there is no lack of experimental realisations of the VG [CFY$^+$93, ZMK$^+$95, SMR$^+$01].

In this context, the *planar* vortex glass plays an exceptional role. A thin layer of a superconductor of the second type is placed in a magnetic field parallel to a long axis of the material. Above a lower critical field H_{c_1} which diverges with vanishing layer thickness [Abr64], it becomes energetically favourable for the magnetic field to enter the layer in the form of vortices carrying a flux quantum, just like for a bulk superconductor. Field energy with respect to the situation where the magnetic field is expelled from the material is gained, while a – lower – amount of superconductor condensation energy at the flux line positions is lost. The restricted geometry reduces the immediate technological relevance of the model to practically zero, however, on the other hand the model thus becomes basic enough to be analytically tractable while still retaining the generic features of a vortex glass[1]. Both in static and in dynamical properties, the glassy nature of the phase will be reflected, e.g. by the decrease of translational order and by nonlinear response. Other unambiguous characteristics of the glass phase are the anomalous nature and statistics of thermodynamic quantities [EK00]. Recently, the glassy behaviour of the magnetic response of a planar vortex lattice has been demonstrated experimentally for a mesoscopic film of the conventional superconductor 2H-$NbSe_2$ [BAP$^+$99]. Exact numerical calculations of thermodynamic quantities for very large systems will be presented below, highlighting the third approach to the system aside analytical calculations and experiments. Given all this, ideally, an analogy to the field of exactly solvable 1D quantum systems which have advanced the understanding of strongly correlated systems can here be seen for vortex glasses.
Moreover, the theory underlying the vortex system can be applied to a broad class of other systems like steps on a vicinal surface [MS64], polymers [dG68], domain walls [PT79] and possibly the striped phases of the previous sections.

[1] The planar vortex glass model for that reason has been called a 'baby spin glass' (M. Mezard).

Our analysis will have two main themes. In the following Chapter 2, the possible thermally driven transition from the VG to a free, unpinned phase will be examined. This transition is present in a model where the vortex interaction is described in elastic approximation (the random-field XY model, short RFXY model), see Section 2.1. Since the exact disorder averaged free energy for the vortex system with hard-core repulsion as only interaction is known and analytical [EK01], it would be interesting to know about signatures of the transition in the RFXY free energy. We find, however, in Section 2.2 that the transition is not signalled by any nonanalyticities. Our point, the absence of the glass transition, thus does not come 'for free' by the analytical nature of the exact free energy. In the following Section 2.3 we argue how the strength of thermal fluctuations is overestimated by the elastic approximation to the vortex interaction, which allows for line intersections. The exact solution for the 'noncrossing only' model is then combined with the renormalisation group argument to show the relevance of disorder at all temperatures, Section 2.4. We generalise this result of a stable VG phase to models of noncrossing lines with arbitrary repulsive interactions in Section 2.5. The final Section 2.6 acts as a caveat. Due diligence in the treatment of the small-scale cutoff opens a window for stronger thermal fluctuations. If this may suffice to depin the lattice is discussed for realistic system parameters.

Chapter 3 explores the relation of the random-bond dimer model to the vortex lattice. The dimer model is introduced (Section 3.1) and the mapping between the seemingly diverse systems is explained in detail (Section 3.1.3). Large scale simulations of the dimer model have been performed by the group of C. Zeng. A recently developed algorithm allows to compute thermodynamic quantities in polynomial time and makes simulations possible even for size 512×512 at thousands of disorder configurations. In Section 3.2 thermodynamic quantities measured in the simulations are compared to predictions of the above mentioned exact solution by Emig and Kardar [EK01]. The agreement of correlations, thermodynamic potentials, their momenta with respect to the random disorder distribution and of response functions is striking. The two approaches thus benefit from each other. On the one hand, the replica Bethe Ansatz approach by Emig and Kardar with no resort to replica symmetry breaking is confirmed, the difficult analytical continuation in the replica index included. Some new light is shed on the old problem of the free energy of a directed polymer in a disordered environment. On the other hand, the dimer model is shown to simulate the physics of line lattices down to the lattice cutoff whereas beforehand it had not been clear, if nonuniversal quantities with contributions from all scales should not likely be dominated by very diverse physics at small scales. The dimer model seems to allow for quantitative testing of droplet picture or scaling theory predictions as several orders of magnitude of system size are within reach.
Throughout the following we use – as in the previous chapters – angular brackets $\langle \ldots \rangle$ in order to denote thermal averages and the overline $\overline{\ldots}$ for disorder averages.

2 Absence of a glass transition in the (1+1)-dimensional line lattice

Thermal fluctuations compete against the VG. This raises the question of the existence of a glass transition at a finite temperature T_g [Fis89]. However, the literature on this subject is rather contradictory [NL91, HF94, ZLH99]. Major support, both analytical and numerical, for a finite T_g comes from the phenomenologically related random field XY model which has a finite T_g transition [CO82, GL94]. However, considering the entropic vortex interaction, the absence of a finite T_g transition has been predicted under certain assumptions as well [NL91]. In this chapter, we will review the arguments given in the literature, try to clarify the problem and suggest a conclusive answer.
To become specific we introduce the model description. Consider a lattice of self-avoiding directed elastic lines of density $\rho = 1/a$ in (1+1) dimensions. Each line is characterised by its position $x_i(z)$ and line tension g. The lines interact via a short-ranged repulsive pair potential $U(x)$ that does not allow them to cross. Quenched disorder couples locally to the lines via the random potential $V(\mathbf{r})$, $\mathbf{r} = (x, z)$, which is assumed to have short-ranged correlations $\overline{V(\mathbf{r})V(\mathbf{r}')} = \Delta\delta_{\xi_d}(\mathbf{r}-\mathbf{r}')$. Whenever the disorder correlation length ξ_d is the smallest length-scale in the problem, it can safely assumed to be zero. The total energy then reads

$$H = \int dz \sum_i \left\{ \frac{g}{2}\left(\frac{dx_i}{dz}\right)^2 + \sum_{i,j\neq i} U(x_i - x_j) + V(x_i, z) \right\}. \tag{2.1}$$

This model can be considered the continuum version of lines placed on the bonds of a rectangular lattice [KN85]. Below, we will also consider the effect of the small scale cutoff inherent to any condensed matter system. The lines will then have a finite persistence length ξ (not to be confused with ξ_d), corresponding to *persistent* random walks in the lattice model.

2.1 Mapping to the XY model and the non-crossing condition

The line lattice in the continuum limit is usually treated within a two-dimensional (2D) elastic theory for the displacement field $u(\mathbf{r})$ so that the line positions are $x_i(z) = ia + u(ia, z)$. The Hamiltonian is

$$H_{\text{el}} = \int d^2r \left\{ \frac{c_{11}}{2}(\partial_x u)^2 + \frac{c_{44}}{2}(\partial_z u)^2 + \rho(\mathbf{r})V(\mathbf{r}) \right\} \tag{2.2}$$

with compression modulus $c_{11} = aU''(a)$, tilt modulus $c_{44} = g/a$ and line density $\rho(\mathbf{r}) = \sum_i \delta[x - x_i(z)]$.
Upon rescaling

$$z \;\rightarrow\; z' = \left(\frac{c_{11}}{c_{44}}\right)^{1/2} z \tag{2.3a}$$

$$u \;\rightarrow\; \phi = \frac{2\pi}{a} u \tag{2.3b}$$

and retaining of only the most relevant term from $\rho(\mathbf{r})$ written as a Fourier series in $u(\mathbf{r})$, the model becomes equivalent[2] to the random-field XY model without vortices [Fis89]

$$H = \int d^2r \left\{ \frac{J}{2}(\nabla\phi)^2 + \tilde{V}(\phi(\mathbf{r}),\mathbf{r}) - \vec{\mu}(\mathbf{r})\nabla\phi(\mathbf{r}) \right\} \tag{2.4a}$$

$$J = \left(\frac{a}{2\pi}\right)^2 \sqrt{c_{11}c_{44}} \tag{2.4b}$$

The random variables $\tilde{V}$ and $\vec{\mu}$ are Gaussian with zero mean and variance

$$\overline{\mu_i(\mathbf{r})\mu_j(\mathbf{r}')} = \sigma\delta_{\xi_d}(\mathbf{r}-\mathbf{r}') \tag{2.5a}$$

$$\overline{\tilde{V}(\phi,\mathbf{r})\tilde{V}(\phi',\mathbf{r}')} = h^2\cos(\phi-\phi')\delta_{\xi_d}(\mathbf{r}-\mathbf{r}'), \tag{2.5b}$$

$$h^2 = 2\frac{\Delta}{a^2}\left(\frac{c_{44}}{c_{11}}\right)^{1/2}$$

$$\sigma = \frac{h^2a^2}{8\pi}.$$

After replication – the version we will need in the next section on renormalisation – we get

$$H_n = \sum_{ab}\int d^2r \left\{ \frac{1}{2}J\,\nabla\phi_a^2\delta_{ab} - \frac{\sigma}{2T}\partial_x\phi_a\partial_x\phi_b - \frac{h^2}{2T}\cos[\phi_a-\phi_b] \right\}. \tag{2.6}$$

Cardy and Ostlund [CO82] were the first to show in a renormalisation group (RG) scheme that disorder is relevant for temperatures below $T_g = 4\pi J$. The renormalised strength of disorder scales with size L as $\Delta(L) \sim L^{\lambda_{\rm dis}}$,

$$\lambda_{\rm dis} = 2\left(1-\frac{T}{4\pi J}\right) = 2\left(1-\frac{\pi T}{a^2\sqrt{c_{11}c_{44}}}\right). \tag{2.7}$$

Perturbatively in the distance from the transition temperature $\tau = 1 - T/T_g$, a finite fixed point for the disorder strength Δ is found for $\tau > 0$ at which σ of Eq. (2.5a) runs to infinity. Above the transition ($\tau < 0$) the lines are thermally free. In Fig. D.1 the flow of disorder Δ is sketched. Since the boundary of the VG phase is given by the condition $\lambda_{\rm dis} = 0$, the existence of a glass transition crucially depends on the *large scale* stiffness J. While in the XY model J stays the same on all length scales due to a statistical symmetry [CO82, HF94], its asymptotic value for the vortex model of Eq. (2.1) is a priori not known. Below, we will address this question and argue against a finite temperature transition. The scaling dimension of disorder[3] will remain to be the central criterion. The RFXY renormalisation group will not be *replaced* but *complemented* by a renormalisation of the stiffness. It will be checked that the small parameter τ of the RG remains small under the modification.

What are the manifestations of the glass transition in the RFXY model? In equilibrium, the hallmark of the VG are the displacement correlations [GH82]. For $T < T_g$, the RG predicts

$$C(\mathbf{r}) = \overline{\langle (u(\mathbf{r})-u(\mathbf{0}))^2\rangle} \sim \ln^2(|\mathbf{r}|/a)$$

[2] We follow largely the notation of [NS00].

[3] The scaling dimension of disorder can be obtained equally by an average of the disorder term with the free Hamiltonian; thereby the scaling of disorder compared to the elastic energy is described.

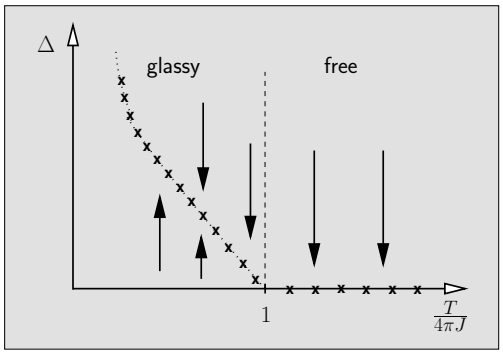

Fig. D.1: Schematic representation of the renormalisation group flow near the glass transition in the RFXY model. Arrows indicate the RG flow. The dashed line is the phase boundary between the glassy and the thermal phase. Crosses represent fixed points (note, however, that σ flows to infinity for $T < T_g = 4\pi J$).

in contrast to the thermal correlations

$$C(\mathbf{r}) = \frac{a^2 T}{4\pi^3 J} \ln(|\mathbf{r}|/a) \tag{2.8}$$

for $T > T_g$. In the glassy phase, thermal fluctuations of $\delta u(\mathbf{r}) = u(\mathbf{r}) - \langle u(\mathbf{r})\rangle$ around the pinned state $\langle u(\mathbf{r})\rangle$ are equally described by Eq. (2.8). A measurement of these latter correlations – if not experimentally maybe in simulations, see below – would provide for the large scale stiffness. Although thermal correlations do not indicate the transition directly they thus carry information on the phase in their amplitude. Recently, simulations both at $T = 0$ [ZMS96] and close to T_g [ZLH99] confirmed the anomalous displacements and thus provided strong support of the RG theory. The limitations of earlier Monte Carlo simulations [BH94, MMRL95, CS95] could hereby be overcome. Dynamical properties as, e.g., the local autocorrelation function, have also been used to identify the transition, leading at weak disorder to the same result for T_g as given by the static RG condition $\lambda_{\rm dis} = 0$ [CS96]. However, direct signatures of the transition in the free energy have not been studied so far. Using the known mapping of the XY model onto a vector Coulomb gas [CO82] one can derive the RG flow of the free energy as shown in [Kos74] for the pure XY model. This is done in the next section in a variation of the original derivation of the flow equations.

2.2 The free energy of the XY model at the glass transition

In this section, we want to consider the glass transition in the RFXY model, Eq. (2.2), (2.6), in more detail. We are especially interested in the behaviour of the free energy at the transition, i.e., whether any signature of the transition in form of a nonanalyticity can be found. To this end we will briefly go through the steps of the real space RG of [CO82] and identify the contribution to the free energy of an infinitesimal RG step. In the spirit of Kosterlitz' calculation of the free energy of the pure XY model [Kos74], these contributions will be integrated over all length scales and give us the free energy closely above and below the transition point. In order to follow the line of argument of the chapter, the technicalities in this section may be skipped. Eq. (2.19) at the end of the section contains the main result.

Below, the original value of renormalised parameters will be denoted by the subscript '0', the length

scale dependent value by 'l'.

At the heart of the RG procedure is the famous identification of spin wave and topological charge degrees of freedom [Kos74].[4] The topological excitations would be missed by a naive gradient expansion of the cos-term in Eq. (2.6). One way to do better and retain the periodicity is to use the Villain approximation

$$e^{K\cos(\phi_a(\mathbf{r})-\phi_b(\mathbf{r}))-K} \simeq \frac{1}{\sqrt{2\pi K_V}}\sum_m e^{i(\phi_a(\mathbf{r})-\phi_b(\mathbf{r}))m-\frac{m^2}{2K_V}},$$

that introduces one discrete degree of freedom $m \in \mathbb{Z}$ for each tuple $(a,b;\mathbf{r})$. In the limit of small K, which we will need around the transition, K_V is related to the original K by $K_V = \frac{1}{2\ln(2/K)}$. For the moment, positions are discretised with a spacing corresponding to the small length-scale cutoff of the theory. The replica partition function may thus be written as

$$\overline{Z^n} = \text{const} \times \big(\Pi_{a;\mathbf{r}}\int d\phi_{a;\mathbf{r}}\big)e^{-H_0[\{\phi\}]/T}\Pi_{a,b;\mathbf{r}}\big(\sum_{m_{a,b;\mathbf{r}}} z^{m^2_{a,b;\mathbf{r}}}e^{im_{a,b;\mathbf{r}}(\phi_a-\phi_b)}\big)$$

H_0 is the harmonic part of the Hamiltonian Eq. (2.6) and the fugacity $z = e^{\beta\mu} = e^{-\frac{1}{2K_V}}$ in original parameters is

$$z = \frac{a_0^2 h_0^2}{4T^2}.$$

In the next step we integrate out the 'spin wave' degrees of freedoms and retain a theory for the charges,

$$\overline{Z^n} = \text{const} \times \det(\mathcal{M})^{-1/2} \times \big(\Pi_{a,b;\mathbf{r}}\sum_{m_{a,b;\mathbf{r}}} z^{m^2_{a,b;\mathbf{r}}}\big)e^{\sum_{\mathbf{r},\mathbf{r}'}\sum_{ab,cd} T\tilde{J}^{-1}_{bd} m_{a,b;\mathbf{r}}m_{c,d;\mathbf{r}'}G(\mathbf{r}-\mathbf{r}')}. \qquad (2.9)$$

The charges interact logarithmically via the two dimensional Green's function

$$G(\mathbf{r}) = \frac{1}{2\pi}\ln[|\mathbf{r}|/a] \qquad (2.10)$$

with coupling parameter $\tilde{J}^{-1}_{ab} = -\sigma + \delta_{ab}J$. $\mathcal{M}_{\mathbf{q},\mathbf{q}';a,b} = q^2\delta_{\mathbf{q},\mathbf{q}'}(J\delta_{a,b} - \sigma\cos^2\theta)$ is the harmonic coupling matrix, θ the angle between the z- and x-axis, and the contribution of these harmonic modes to the disorder part of the free energy density is analytic, see Appendix 3,

$$\lim_{n\to 0}\frac{1}{n\tilde{A}}\ln\det\mathcal{M}^{-1/2} \quad = \quad c(J,T) + \frac{1}{\xi_x\xi_z}\frac{\sigma}{4J}. \qquad (2.11)$$

Remember $\frac{\sigma}{J} = \frac{\pi\Delta_0}{c_{11}Ta_0^2}$ and note that the size of the original line system A had been rescaled to obtain the size of the RFXY model $\tilde{A} = A\times(c_{11}/c_{44})^{1/2}$. ξ_x, ξ_z denote the small scale cutoff lengths in the respective directions in the isotropised model.

On each lattice site $\mathbf{r}$, due to the symmetry $m_{a,b} = -m_{b,a}$ there are only $n(n-1)/2$ (n is the replica index) independent scalar charges. These may be combined to a vector charge $\vec{m}_{\mathbf{r}} = \sum_{a<b} m_{a,b;\mathbf{r}}\hat{e}_{ab}$ in the vector space spanned by the set $\{\hat{e}_{a<b}\}$. If the sum in the exponent of Eq. (2.9) is considered a quadratic form, the scalar product $\hat{e}_{ab}.\hat{e}_{cd} = \frac{1}{2}(\delta_{ac} + \delta_{bd} - \delta_{ad} - \delta_{bc})$ is implied. It follows $\hat{e}_{ab} + \hat{e}_{ac} = \hat{e}_{bc}$ for $a < b$, i.e., the set of basis vectors $\{\hat{e}_{a<b}\}$ is overcomplete and only $n-1$ of them

[4] Although rather the mathematical structure of our replica Hamiltonian than the physics is similar, we will use the terms 'spin wave' and 'topological charge' in order to signify the terms concisely.

are independent. The above symmetry also requires $\sum_{a,b} m_{a,b} = 0$, which allows to keep in $\tilde{J}_{ab}^{-1}$ only the term $J^{-1}\delta_{ab}$. The charge part of the partition function becomes thus the vector Coulomb gas

$$\begin{aligned}\overline{Z^n} &= \sum_M \frac{z^M}{M!} \Pi_{i=1}^M \int_{D_{a_0}} \frac{d^2 r_i}{a_0^2} e^{-\tilde{H}_c} \\ -\tilde{H}_c &= TJ^{-1} \sum_{i \neq j} \vec{m}_{\mathbf{r}_i} \vec{m}_{\mathbf{r}_j} G(\mathbf{r}_i - \mathbf{r}_j).\end{aligned}$$

Here the vector charges have already been restricted to the smallest possible values $\vec{m}_i^2 = 0, \pm 1$, since higher charges will be irrelevant at the transition. $\sum_M$ sums over configurations with $M = \sum_i \vec{m}_i^2$ unit vector charges labelled by the index i. A finite interaction energy in the thermodynamic limit further requires overall charge neutrality. It has thus been reparametrised the sum over vector charges of size $0, \pm 1$ on each site to a sum over all values $M/2$ of unit vector charge pairs, which are then arranged in the plane. Of course, the lattice constant a_0 sets a limit to how close they may come to each other, symbolised by the restriction on the position integrals. $\int_{D_{a_0}} d^2 r_i$ integrates over the plane apart from spheres of radius a_0 around positions $\mathbf{r}_k, k < i$.

Now we take terms with $M + 2$ charges containing a pair of opposite charges at a distance just above the cutoff, $|\delta \mathbf{r}| \in (a_0, a_0 + \mathrm{d}a_0)$, and integrate over the position of such a pair by use of Kosterlitz' decomposition

$$\Pi_i \int_{D_{a_0}} d^2 r_i = \Pi_i \int_{D_{a_0'}} d^2 r_i + \frac{1}{2} \sum_{k \neq l} \left(\Pi_{i \neq k,l} \int_{D_{a_0}} d^2 r_i \right) \int_{\bar{D}_{kl}} d^2 r_k \int_{\delta_k(l)} d^2 r_l.$$

where $a_0' = a_0 + da_0$, $\bar{D}_{kl}$ is the plane bar spheres around points k, l and $\delta_k(l)$ is the halo $|\mathbf{r}_k - \mathbf{r}_l| < da_0$. We again get a term with M charges

$$\begin{aligned}\overline{Z^n} &= \sum_M \frac{z^M}{M!} \left(\Pi_i \int_{D_{a_0'}} \frac{d^2 r_i}{a_0^2} \right) \left\{ 1 + \frac{z^2}{a_0^4} 2\pi a_0 da_0 n \left(\tilde{A} - \frac{a_0^2 T^2}{4\pi J^2} \sum_{kl} \vec{m}_k \vec{m}_l G(\mathbf{r}_k - \mathbf{r}_l) \right) \right\} \\ &\quad \times \exp[TJ^{-1} \sum_{ij} \vec{m}_i \vec{m}_j G(\mathbf{r}_i - \mathbf{r}_j)].\end{aligned}$$

Upon reexponentiation we have

$$\begin{aligned}\overline{Z^n} &= \exp[\frac{z^2}{a_0^4} 2\pi a_0 da_0 n \tilde{A}] \sum_M \frac{z^M}{M!} \left(\Pi_i \int_{D_{a_0'}} \frac{d^2 \mathbf{r}_i}{a_0^2} \right) \\ &\quad \times \exp\left[(TJ^{-1} - \frac{nT^2}{4\pi J^2} \frac{z^2}{a_0^4} 2\pi a_0^3 da_0) \sum_{ij} \vec{m}_i \vec{m}_j G_{a_0}(\mathbf{r}_i - \mathbf{r}_j) \right]. \qquad (2.12)\end{aligned}$$

At this point, the standard RG 'philosophy' requires to adjust the length scale in order to keep the cutoff a_0 fixed and the theory form invariant. Our goal, however, is to simply perform the partition sum step by step, we therefore only do the integration step of the RG and do not rescale. We have though, in order to be able to do the above integration step iteratively, to adjust the cutoff in the free Green's function Eq. (2.10) to $a_0' = a_0 + da_0$ so that it complies with the cutoff in the integrals

$$G_{a_0}(\mathbf{r}) = \frac{1}{2\pi} \ln[|\mathbf{r}|/a_0] = \frac{1}{2\pi} \ln[|\mathbf{r}|/a_0] + \frac{1}{2\pi} \ln \frac{a_0'}{a_0} = G_{a_0'}(\mathbf{r}) + \frac{1}{2\pi} \ln \frac{a_0'}{a_0}.$$

With overall charge neutrality in mind, the last term gives a contribution $\exp[TJ^{-1}dl\sum_{i\neq j}] = \exp[-TJ^{-1}Mdl]$ to the partition function. This term renormalises z. Note that no length is rescaled at any point. After many integration steps the cutoff will have grown to say a_l with the flow parameter

$$l = \ln \frac{a_l}{a_0},\ a_l = a_0 e^l.$$

It measures the progress of the integration of the partition function. A subtlety arises in this scheme. The factor $1/a_0^4$ in the feedback of the integration has its origin in the integral measure $d^2\mathbf{r}/a_0^2$ of the pair of charges that we integrated out. Upon interation of the integration, this is the only appearance of the original a_0, any other cutoff will have grown to a_l.
The equations of flow can now be read off. The exponential in front of the integral is independent of the charges and contributes to the average free energy density $\overline{f}$

$$\begin{aligned} \frac{d}{dl} f_n(l) &= -T\frac{2\pi}{a_0^2} n z^2 e^{2l}, \\ f_n(l=0) &= 0, \\ \overline{f} &= \tilde{A}^{-1} \lim_{n\to 0} \frac{1}{n} \ln \overline{Z^n} = \lim_{n\to 0} \frac{1}{n} f_n(\infty). \end{aligned}$$

The fugacity z and hence the disorder strength flows according to

$$\frac{d}{dl} z = -2\frac{T}{4\pi J} z + 2(n-2)e^{2l} z^2.$$

Here, the adjustment of the cutoff in the Green's function provides for the linear term stems, as mentioned above, while for the quadratic term the perturbation expansion has to be performed to second order, the fusion of two charges giving a new unit charge (note the non-Cartesian metric in the space of vector charges) [CO82]. The length rescaling in the standard RG would give an extra linear term $2z$, indicating the transition at $T = T_g = 4\pi J$. Note that the solutions to the equations without, $z(l)$. and with rescaling, $\tilde{z}(l)$, are related by $z(l) = \tilde{z}(l)e^{-2l}$.
We can read the flow equation for J from the prefactor of the Green's function in Eq. (2.12). In the limit $n \to 0$,

$$\frac{d}{dl} J = \lim_{n\to 0} n\frac{Tz^2}{2} = 0,$$

which is valid to all orders as the statistical 'tilt' symmetry [HF94, SVBO88] of the replicated Hamiltonian shows [HF94, SVBO88] . The flow of σ in this scheme is tied to the flow of J by the invariance of $\lambda_0 = J - n\sigma$ and it is finite and positive. λ_0 is the eigenvalue of the coupling matrix $\tilde{J}_{ab}$ corresponding to the constant eigenvector, which does obviously not couple to disorder. This mode is thus Gaussian and cannot be renormalised.
The flow equation for the fugacity closes on itself and has the solution

$$z(l) = e^{-2l} \frac{2\tau/[2\tau/z_0 + 2(n-2)]}{e^{-2\tau l} - 2(n-2)/[2\tau/z_0 + 2(n-2)]}$$

with $\tau = 1 - T/T_g$ and the initial value

$$z_0 = \frac{\Delta_0}{2T^2}\sqrt{\frac{c_{44}}{c_{11}}}. \tag{2.13}$$

In the limit of interest $n \to 0$ the solution simplifies to

$$\lim_{n\to 0} z(l) = \frac{e^{-2l}\frac{2\tau}{2\tau/z_0-4}}{e^{-2\tau l} + \frac{1}{\tau/(2z_0)-1}}.$$

We use this latter form in the integration for the free energy

$$\begin{aligned} f_n(l=\infty) &= -T\frac{2\pi n}{a_0^2}\int_0^\infty dl\ z^2(l)e^{2l} \\ &= -T_g\frac{2\pi n}{a_0^2}\int_0^\infty dl\ (1-\tau)z^2(l)e^{2l}. \end{aligned} \tag{2.14}$$

Two cases need to be considered separately.
(i) Below the glass transition, $\tau > 0$: Upon the reparametrisation $x := \exp[-2l]$, the integral over the flow parameter can be performed and we have

$$\begin{aligned} \frac{a_0^2}{2\pi T_g}\overline{f}(\tau>0) &= \lim_{n\to 0} f_n^>(l=\infty)\frac{a_0^2}{2\pi nT} \\ &= -\frac{\tau^2}{8}\ {}_2F_1(2,1/\tau;1+1/\tau;1-\tau/(2z_0)) \end{aligned} \tag{2.15}$$

with the hypergeometric function ${}_2F_1(a,b;c;z)$, see e.g. Ref. [AS74].
(ii) Above the glass transition, $\tau < 0$: Upon reparametrisation $x := \exp[2l]$ we get

$$\begin{aligned} \frac{a_0^2}{2\pi T_g}\overline{f}(\tau<0) &= \lim_{n\to 0} f_n^<(l=\infty)\frac{a_0^2}{2\pi nT} \\ &= -\frac{2\tau^2}{(4-2\tau/z_0)^2(1-2\tau)}\ {}_2F_1(2,2-1/\tau;3-1/\tau;\frac{1}{1-\tau/(2z_0)}) \end{aligned} \tag{2.16}$$

It is difficult to find a combined closed expression for all temperatures and equally difficult to expand either of the expressions Eqs. (2.15), (2.16) in τ. Moreover, an expansion of the above result for the trusted region of small disorder is not easy since disorder comes in the combination z_0/τ which is not small near the transition at $\tau = 0$. One can thus not immediately make a statement about the analytical behaviour of $\overline{f}$ at the transition. However, we can give a power series that proves to be the Taylor series of $\overline{f}$ at the transition $\tau = 0$. To this end, we expand the integrand of Eq. (2.14) around $\tau = 0$ and integrate after the expansion term by term. The resulting expression is automatically analytical which does, of course, not imply the analyticity of the free energy as two limits have been exchanged. In order to clarify this question, we compare the resultant power series ($\mathrm{series}_\tau^m[\dots]$ stands for the power series of order m around τ)

$$P_m(\tau) := -\int_0^\infty dl\ \mathrm{series}_{\tau=0}^m[(1-\tau)z^2e^{2l}] = -\sum_{i=0}^m c_k\tau^k \tag{2.17}$$

of order m with the original expression Eqs. (2.15), (2.16) for the free energy. We find for the scaling behaviour of the difference

$$\frac{a_0^2}{2\pi T_g}\overline{f} - P_m(\tau) = \mathrm{const}_m\ \times \tau^{m+1} + \mathcal{O}(\tau^{m+2}) \tag{2.18}$$

for any m considered, both for $\tau \gtrless 0$ with the same constants const_m. In Fig. D.2, this fact is illustrated and the free energy itself is plotted in Fig. D.3. Eq. (2.17) gives hence the manifestly

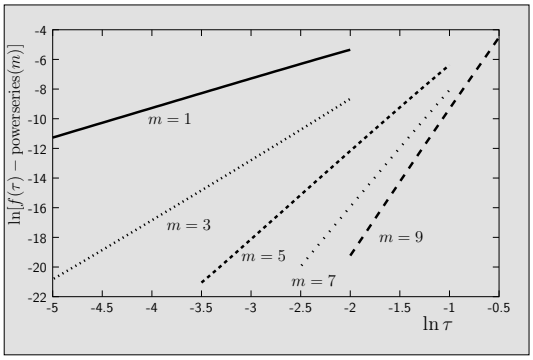

Fig. D.2: Free energy minus Taylor expansion of order $m = 1, 3, 5, 7, 9$, respectively, in double-logarithmic plot.

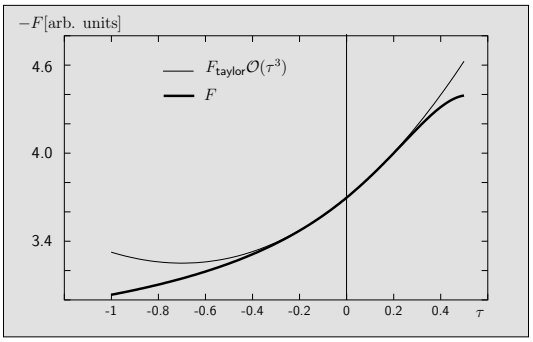

Fig. D.3: Free energy of the RFXY model above and below the transition and one Taylor approximant.

analytical form of the *free energy* at the transition. Since the renormalisation scheme was based on the assumption of small disorder $z_0 \propto \Delta_0$, see Eq. (2.13), only the leading term in Δ_0 of the free energy can be trusted literally. We expand the coefficients $\{c_k\}$

$$\begin{aligned} c_0 &= \frac{1}{4} z_0 - \frac{1}{8} e^{1/(2z_0)} E_1\left(1/(2z_0)\right) \\ c_1 &= \frac{1}{64 z_0}\left(2(1-2z_0)z_0 + (8z_0 - 1) e^{1/(2z_0)} E_1\left(1/(2z_0)\right)\right) \\ &\dots \end{aligned}$$

of the series Eq. (2.17) in z_0, where $E_1(x) := \int_1^\infty \frac{dt}{t} e^{-t/x}$ is the exponential integral,

$$\{c_k\} = z_0^2 \{1/2, 1/2, 1, 2, 4, 8, 16, 32, \dots, 2^{k-2}\} + \mathcal{O}(z_0^3),$$

sum up the leading terms and get

$$\begin{aligned} \overline{f} &= \frac{2\pi T_g}{a^2} P_\infty(\tau) \\ P_\infty(\tau) &= -\frac{z_0^2}{2} \frac{1-\tau}{1-2\tau} + \mathcal{O}(z_0^3). \end{aligned}$$

It has been checked that the rearrangement of the double expansion in τ and z_0 – first we expand in τ and then collect the z_0^2-contributions from all terms – leads to no complications. We obtain the same result by an expansion of the integrand in Eq. (2.14) with respect to z_0 and subsequent integration, which can be performed independent of the sign of τ.

For the ease of notation we have written above $\overline{f}$ where only the contribution from the 'charge part' of the Coulomb gas Hamiltonian was considered. We now collect all disorder contribution to the free energy, as there are (see Eq. (2.6))

(i) the one we just calculated from the $\cos(\phi_a - \phi_b)$-term with $a \neq b$,

(ii) the trivial one with $a = b$, and

(iii) the 'spin-wave' term proportional to σ. In total, the disorder contribution to the free energy density with respect to the *vortex lattice volume*, remember the rescaling Eq. (2.3a), is

$$\overline{f_{\text{dis}}} = -\frac{\Delta^2 \rho^2}{4T^3} \left(\frac{c_{44}}{c_{11}}\right)^{1/2} \frac{\pi}{(1-2\tau)} - \frac{\Delta \rho^2}{T} - \frac{\pi}{2} \frac{\Delta \rho^3}{\xi_\parallel c_{11}} + \mathcal{O}(\Delta^3). \tag{2.19}$$

Note that in the spin wave contribution the cutoff lengths of Eq. (2.11) have been related to the respective length scales of the line lattice $a, \xi_\parallel$ as $\xi_x = a, \xi_z = \xi_\parallel \sqrt{c_{44}/c_{11}}$.

The free energy of the RFXY model is analytical in the temperature at the transition. Although we have shown this strictly speaking only for small initial disorder Δ, the result holds generally. Larger original disorder at temperatures around the transition will be renormalised on finite scales to small values, see Fig. D.1, where our calculation is valid. Following the flow trajectory over a *finite* distance l cannot produce a nonanalyticity and the flow to the fixed points does not either as we have shown. Consequently, in the original vortex system no signature of a transition can be expected in the free energy. The absence of any nonregularities – as observed below in Section 2.4 – will hence not suffice to rule out the transition from the glassy to a thermally free phase. On physical grounds, there is good reason for the regular behaviour of the free energy in the RFXY model. A nonanalyticity in the thermodynamic potential would reflect a divergence of the correlation length of the system, as it is the case, e.g., in the Kosterlitz-Thouless (KT) thermal melting transition where an essential singularity in the free energy is calculated in the spirit of the present analysis [Kos74]. In the melting problem, the quasi-long-range order of the low-temperature phase with no intrinsic length scale is destroyed by the proliferation of topological defects at higher temperatures. Beyond the transition, a finite correlation length indicates short-range order. Coming from high temperatures, the correlation length diverges at the KT-transition. The present case is different: both below and above the transition, correlations have no intrinsic length scale, they are of logarithmic type with, however, different powers. The correlation length is infinite on both sides of the transition and this leaves no room for a divergence which could leave its trace in the free energy. One might also argue with the topology of the RG flow diagram. In the present case, two starting points on the left and right of the phase separatrix stay close throughout the flow, while in the KT-problem two closeby initial vortex fugacities flow to fixed points that are largely separated. The σ-field, which does flow to distant fixed points in the present problem, cannot produce a singularity as we have shown above.

2.3 Shortcomings of the elastic approximation

The elastic approximation of the vortex interaction allowed in Section 2.1 for the mapping of disordered lines to the RFXY model. It was essential for the RG calculation to be mathematically viable. However, some of the physics is swept under the carpet in this procedure. The statistical symmetry which assures nonrenormalisation of the stiffness J and hence the elastic moduli of the line lattice, is artificial. In the x-direction, this symmetry is broken by the original vortex interaction. For the hard-core repulsion of the lines this becomes most obvious but any non-harmonic part in the interaction would do so just as well. We review the argument leading to the statistical symmetry and rewrite the Hamiltonian in the form

$$H = \frac{1}{2} \int d^2r \left\{ c_{11,0} (\frac{\partial}{\partial x} u)^2 + c_{44,0} (\frac{\partial}{\partial z} u)^2 \right\} + H_{\rm dis} + H_{\rm n.h.}. \tag{2.20}$$

The elastic moduli are microscopic constants – denoted by the subscript – and we are interested in their values at large scales, which possibly are renormalised by pointlike uncorrelated disorder (dis) and nonharmonic (n.h.) contributions to the vortex interaction. Now the system size is controlled in horizontal direction by the addition of a linearly growing contribution to any displacement configuration

$$u \to u + \epsilon x, \tag{2.21}$$

which implies for the mean line distance

$$a \to a(1+\epsilon). \tag{2.22}$$

The definition of the *effective* compression modulus at finite temperature is, see [LL69],

$$c_{11} = a\frac{\partial^2}{\partial a^2}(af(a)). \tag{2.23}$$

For the present purpose we rewrite

$$c_{11} = \frac{1}{a}\frac{\partial^2}{\partial \epsilon^2}\frac{F(\epsilon)}{mL_z} \tag{2.24}$$

with m the number of lines and free energy $F = fL_zL_x$. In the case of a purely harmonic vortex interaction, the dependence of F on ϵ is simple. The elastic part of Eq. (2.20), H_0, transforms under Eq. (2.21) as

$$H_0 \to H_0 + \epsilon^2\frac{c_{11,0}}{2}L_xL_z + \epsilon c_{11,0}\int d^2r\frac{\partial}{\partial x}u. \tag{2.25}$$

The third term of course vanishes for periodic boundary conditions. The lines see before and after the transformation a disorder environment with the same statistics. This is the 'statistical symmetry' mentioned above and its effect is most easily seen in the replica form of disorder energy, see Eq. (2.6). There, the disorder average is already taken and the shift drops out in the difference of two replica fields. Thus the only dependence on ϵ is the quadratic field independent term of Eq. (2.25). We readily get

$$c_{11} = c_{11,0}, \tag{2.26}$$

i.e., the nonrenormalisation of the compression modulus. The same argument with $u \to u+\epsilon z$ works for the tilt modulus, which the symmetry derives its name from for historical reasons.

We now consider an additional vortex interaction under the transformation, e.g., one that penalises line crossing

$$\begin{aligned} H_{\text{n.h.}} &= \sum_i c\int dz\,\delta[x_{i+1}(z)-x_i(z)] = \sum_i c\int dz\,\delta[a+u_{i+1}(z)-u_i(z)] \\ &\to \sum_i c\int dz\,\delta[a(1+\epsilon)+u_{i+1}(z)-u_i(z)]. \end{aligned}$$

The dependence on ϵ does not drop out and the compression modulus c_{11} will be renormalised, while the tilt modulus $c_{44} = g/a$ remains untouched by this interaction and indeed is a constant. [5] A quantitative analysis is very difficult.

It is clear where the physical origin of the scale dependent contributions to c_{11} lies [NLS91]. The fluctuating lines repel each other much stronger than described by an elastic term once they get close enough. A crossing would cost a large amount of energy and an idealised hard-core repulsion forbids it altogether. The lattice configurations may thus be heavily restricted, going unnoticed, however, in the elastic approximation to the energy. For low temperatures, the scale above which lines have fluctuated far enough to explore the same regions and 'collide' is large and the error of the elastic approximation is small. The correction is, however, a monotonic function of the fluctuation

[5] For a interaction that is nonlocal in z, c_{44} can be renormalised weakly. This effect, however, can be neglected in what follows.

amplitude and hence of the two sources of fluctuations, temperature and disorder strength.
Stressing this origin of the stiffness contributions, we will in the following talk of entropic and steric stiffness renormalisation with thermal and disorder origin, respectively.
Fortunately the above RG approach is not invalidated in its application to the line lattice altogether by its shortcoming with respect to the stiffness renormalisation. Rather, the missing flow equation may be supplemented by other means and the treatment remains valid as long as the expansion parameter τ continues to be small. Note that τ becomes scale dependent via $\tau = 1 - T/T_g, T_g = 4\pi J = \sqrt{c_{11}c_{44}}a^2/\pi$. In the following section we will review the exact derivation of the asymptotic large scale stiffness in the presence of disorder and thermal fluctuations. The small parameter will still be controlled and small, and hence the RG scaling dimension of disorder Eq. (2.7) will still be a reliable guide to the phase diagram.
Before doing so we illustrate here the underlying physics by looking at the simplified case of thermal renormalization of the stiffness in the pure system. The lines are characterised by a single line stiffness g and they interact only by a hard-core repulsion. With Eq. (2.23) the free energy density – for a given size – will give us the stiffness and thus the scaling dimension of disorder – on the respective scale. There is a very intuitive estimate of the interaction part of the free energy. The typical length l_c on which a collision of two lines occurs can be estimated from $a^2 = \langle \delta x^2(z = l_c)\rangle = T/g\, l_c \Rightarrow l_c = a^2 g/T$, with $\delta x(z) := x_i(z) - x_i(0)$. Every collision 'reflects' the lines and thus reduces the number of possible configurations by a factor of 2 with respect to the noninteracting case. These factors multiply and one can estimate the entropy reduction due to collisions as $\Delta S = -\ln 2\ L_z/l_c\ L_x/a$. The change of free energy density thus is $\Delta f = -A^{-1}T\Delta S = \ln 2\, T^2/(ga^3)$. This is the only interaction effect. The single line contributions to the free energy density being $\propto \rho = 1/a$, we have according to Eq. (2.23) an entropically generated compression modulus $c_{11} = \text{const}\ \times T^2/(ga^3)$. Certainly, the constant will not be obtained numerically correct by this argument, but it should be of order one.
Upon insertion of c_{11}, the scaling dimension of infinitesimal disorder Eq. (2.7) shows to be independent of temperature and it is really up to numerical factors on which side of the transition the system is. One can become quantitative by use of the analogy of a 2D statistical physics problem to a 1D quantum problem. In this case, the quantum problem is a text book one. The hard core repulsion is satisfied by considering the 1D spinless free fermions. Position being their only quantum number they cannot cross. Qua the mapping given in Table D.1 one observes that for the free energy density in the thermodynamic limit only the quantum-mechanical ground state contributes. Integration of the density of states $D(\epsilon) = a/h(2m/\epsilon)^{1/2}$ up to the Fermi edge $\epsilon_F = h^2/(8ma^2)$ yields $E_0 = Nh^2/(24ma^2)$. The equivalence of the dimensionless partition functions (cl: classical, qm: quantum mechanical),

$$-\frac{F}{T} = \ln Z^{\mathrm{cl}} = \ln Z^{\mathrm{qm}} = -\frac{\beta\hbar}{\hbar}E_0,$$

together with the mapping of Table D.1 give for the free energy $F/L_z \leftrightarrow E_0$ of the line system

$$f = \frac{\pi^2}{6}\frac{T^2}{g}\rho^3.$$

The asymptotic compression modulus renormalized by thermal fluctuations thus is

$$c_{11}^{\mathrm{th}} = \frac{\pi^2 T^2}{ga^3}. \tag{2.27}$$

model	stiffness	system size	temperature
lines	g	L_z	T
free fermions	m	$\beta\hbar$	$\hbar$

Table D.1: Relation between parameters of pure vortex lattice and free fermions from the formal equivalence of the partition function for lines and the Feynman path integral for fermions. Note that dimensions are not conserved.

In the disorder scaling dimension Eq. (2.7), one curiously finds $\lambda_{\rm dis} = 0$, i.e., marginal disorder at all temperatures. The effective thermal fluctuation strength is temperature independent, since the entropically generated stiffness J increases linear in temperature and just cancels the usual linear dependence of thermal fluctuations amplitude $\propto T/J$. Neglecting disorder and more complicated interaction contributions to the large scale stiffness, we conclude that the system is at the transition at *all* temperatures. Physically, it will be up to the effects neglected so far, which mechanism to prevail: thermal fluctuations or disorder pinning. These effects that tilt the system to the one or the other side may be small and the situation is comparable to an unstable equilibrium.

Summarising, we may say that line collisions renormalise the stiffness and thus reduce the washing out of the pinning potential in a way that might not allow for a thermal free phase at all. These collision events are misjudged in the elastic approximation that fails to penalise line crossing by an adequately large energy. The weight of these unphysical configurations in the elastic model can be quantified. We look at the nearest neighbour correlations

$$\begin{aligned}\langle \delta u^2\rangle := \langle [u(x+a,z)-u(x,z)]^2\rangle &= \frac{a^2}{(2\pi)^2}\langle [\phi(x+a,z)-\phi(x,z)]^2\rangle \\ &= \frac{2Ta^2}{(2\pi)^4 J}\int_{-\infty}^{\infty} dq_z \int_{-\pi/a}^{\pi/a} dq_x (1-\cos[q_x a])\frac{1}{\mathbf{q}^2} \\ &\simeq \frac{1.64}{4\pi^3}\frac{a^2 T}{J} = \frac{T}{T_g}(0.41a)^2.\end{aligned}$$

Weak disorder is effectively very small around the transition and can be treated in perturbation theory. It gives a correction of order $\Delta(c_1 + \ln[c_2\Delta + 1])$, with constants $c_i = \mathcal{O}(1)$, to the above calculation with only elastic energy. Compared to Lindemann numbers in other problems, the value of 0.41 is rather large[6] and corresponds at $T = T_g$ to a fraction of 1.5% of configurations where the two lines collide at the given value for z. At $T = 1.5T_g$ this number is $\simeq 5\%$. Exactly these crossing configurations lead in a correct treatment to an effective stiffening of the lattice so that thermal fluctuations cannot unpin the lines from impurities.

At the very end of this chapter with various qualitative arguments, we comment on the following scenario, that might be used for a justification of the 'naive' elastic approximation to the (1+1) dimensional line lattice. The line lattice with the hard-core repulsion as only interaction has a vanishing microscopic compression modulus $c_{11,0}$. Thus on smallest scales an elastic approximation would make no sense. However, on any intermediate scale a finite c_{11} will have developed. Why

[6] Of course, the concept of a Lindemann number assumes an effective mechanism for melting, usually the generation of topological defects. These are highly penalised energetically in this model where a line would have to leave the (1+1)-dimensional plane in order to produce a topological charge.

not map the system on this scale to the random field XY model and start the RFXY renormalization scheme here, with effective finite elastic constants? Of course one runs into problems since in doing so the further renormalisation of the elastic constants is neglected. We can calculate the finite size corrections to the effective asymptotic compression modulus, remembering the mapping of the classical system size to the quantum mechanical temperature $L_z \to \hbar\beta$. A Sommerfeld expansion [Lan69] in the small parameter

$$\kappa = \frac{1}{\beta\epsilon_F} = \frac{2}{\pi^2}\frac{ma_0^2}{\hbar^2\beta} \to \frac{2}{\pi^2}\frac{ga^2}{L_z T}$$

translates straightforwardly to finite size corrections in the classical statistical model. We find with

$$c_{11}^{\rm th}(L_z) = \frac{\pi^2 T^2}{ga^3}\left\{1 - \frac{\pi^4}{4}\kappa^2 - \frac{3\pi^6}{180}\kappa^4 + \mathcal{O}(\kappa^6)\right\} \tag{2.28}$$

negative corrections as could have been expected. They give a negative disorder scaling dimension on any finite scale. Only on largest scales, the entropic renormalisation of the stiffness renders infinitesimal disorder marginal. It is thus important to take into account the entire flow of the compression modulus, which is monotonously growing over all scales. Cutting off the renormalisation by hand on an intermediate scale, as the harmonic approximation does, is misleading. Thermal fluctuations would be overestimated.

2.4 Non-crossing interaction and disorder: the exact free energy

The model of interacting fluxlines in the plane that has been used in many of the arguments above is obtained by reduction of the interaction to the non-crossing condition, i.e. choice of $U(x) = c\delta(x)$ with $c \to \infty$ in Eq. (2.1). For this simplified but – with respect to the glass transition – still generic model, an exact solution has been found by Emig and Kardar [EK01], which is something very rare in the field of disordered interacting systems and a major achievement.

In the replica approach the challenge is to find the disorder averaged replicated partition function in the limit of small n. It contains information not only on the disorder averaged free energy but also on all the cumulants $\overline{F_c^j}$ of its distribution, using

$$\ln \overline{Z^n} = \sum_j \frac{(-n)^j}{j!}\frac{\overline{F^j}_c}{T^j}. \tag{2.29}$$

Difficulties typically arise for the limit $n \to 0$ once an expression for Eq. (2.29) has been found for integer n. For an unambiguous analytical continuation, additional information beyond the values at integer n is required.

Just like in the pure case the two-dimensional line problem can be mapped onto a one-dimensional quantum problem. With m lines in the original problem, after replication there are $n \times m$ particles in quantum language. The noncrossing condition of vortices may again be satisfied by Fermi statistics with respect to particles of the same, say, colour n whereas particles of different colour obey Bose statistics upon permutation. Disorder pinning appears then in the guise of an attractive interaction between particles of different colour n. The quantum problem is thus that of $n \times m$ attractive particles with mixed symmetry, mathematically speaking SU(n) attractive fermions. The free energy of the vortex problem is in the thermodynamic limit related to the quantum ground state energy E_0

$$\ln \overline{Z^n} = -\frac{E_0(n)L_z}{T} + n\frac{L_x}{a}\ln Z_0. \tag{2.30}$$

Z_0 is the partition function of a single line with no disorder. The mapping along Table D.1 is implied. Emig and Kardar now realised that thanks to the ultralocal correlation of disorder and the implied contact interaction of the SU(n) quantum problem a solution by Bethe Ansatz (BA) might be possible. Indeed, they derived the BA equations in the thermodynamic limit, given here in the continuous form

$$nk = \int_{-K}^{K} dk' g_n\left[(k-k')l_d\right]\rho(k') \tag{2.31a}$$

with integral kernel

$$g_n[x] = 2\sum_{m\geq 0} \arctan[\frac{nx}{m^2+nm+x^2}]. \tag{2.31b}$$

The length $l_d = T^3/(g\Delta) =: 1/c$ is the second characteristic length scale in the quantum problem next to the average particle distance a. It describes the size of clusters of n particles, which may be considered generalised Cooper pairs, and its inverse c serves at fixed temperature and stiffness as a measure for disorder strength.

From the solution $\rho(k)$ the ground state energy (which has dimensionality EL^{-1} after the mapping of Table D.1) is obtained via integration

$$E_0 = \frac{T^2 L_x c^2 \rho}{24g} n(1-n^2) + \frac{nT^2 L_x}{2g}\int_{-K}^{K} dk\; k^2\rho(k). \tag{2.31c}$$

Note that the first term is linear in the density and contributes to disorder energy of single lines. In the above equations, the integral boundary K is fixed selfconsistently by the density

$$\rho = \int_{-K}^{K} dk\; \rho(k). \tag{2.31d}$$

The solution to the limit of Eq. (2.31a) for $n \to 0$ gives the exact average free energy density [EB03]

$$\overline{f} = \overline{f_0}\rho + \frac{\pi^2}{6}\frac{T^2}{g}\rho^3 + \frac{\Delta}{2T}\rho^2. \tag{2.32}$$

with single line contributions

$$\overline{f_0} = C(g)T - \frac{\Delta}{2\xi_d T} + \frac{g\Delta^2}{24T^4}. \tag{2.33}$$

that were first derived by Kardar and Nelson [KN85, Kar87]. Finite size corrections to these latter terms have been calculated in Refs. [BO90, BD87]. Eq. (2.32) is one of the main result of the Replica BA (RBA) solution and much of the following will build upon it. It is noteworthy that the thermally generated entropic term – second term in Eq. (2.32) – and the steric term from disorder fluctuations – third term – are simply additive and do not couple and that there are no additional contributions. From the interaction part of the exact free energy the large scale stiffness can be derived via Eq. (2.23) as

$$c_{11} = \frac{\pi^2 T^2}{ga^3} + \frac{\Delta}{Ta^2} = c_{11}^{\rm th}\left(1 + \frac{ag\Delta}{\pi^2 T^3}\right). \tag{2.34}$$

The scaling dimension of disorder Eq. (2.7) hence is positive for all temperatures

$$\begin{aligned}\lambda_{\rm dis} &= 2\left(1 - \frac{\pi T}{a^2\sqrt{c_{11}c_{44}}}\right)\\ &= 2\left\{1 - \left(1 + \frac{ag\Delta}{\pi^2 T^3}\right)^{-1/2}\right\} > 0.\end{aligned}$$

We see that the effect of disorder makes the difference for the glassy phase at al temperatures with respect to the pure situation where thermal fluctuations alone render the system marginal. A priori, it could also have been imagined the scenario where disorder enlarges the compression modulus on the one hand but reduces the part induced by thermal fluctuations. This is not the case and no transition to an unpinned phase is possible. The Vortex glass is stable.

A natural limit to the validity of the RBA results is set by the mapping of a given problem (many lines in disorder/one polymer in disorder) to a one-dimensional quantum problem which is then solved by Bethe Ansatz. The natural length scale in the quantum problem is the width l_d of cluster or 'n-string', being a superposition of the BA generalised momentum eigenstates. If $l_d = T^3/(g\Delta)$ becomes of the order of the disorder correlation length ξ_d, the simplification of ultra-locally correlated disorder is no longer justified. This assumption, however, is essential for the Bethe Ansatz to solve. The Bethe Ansatz results shown above therefore become are valid only at high temperatures or small disorder

$$T \gtrsim T^* = (\Delta g \xi_d)^{1/3}. \tag{2.35}$$

Below this scale a modified replica symmetry breaking solution has been suggested in Ref. [KD98] for a single line whose predictions, however, could not be tested to date. For the interacting line system the modifications at low temperatures implied by the replica symmery breaking solution can be adapted [EK01].

We conclude this section on the exact RBA results by the presentation of a simple argument from which the steric part of Eq. (2.32) can be obtained qualitatively. The spirit is similar to the argument given in the previous Section 2.3 for the entropic stiffness.
In the presence of impurities, the total energy which will be a compromise between elastic and disorder energy. Single line fluctuations are limited by the noncrossing constraint. Therefore a typical scale in x-direction is the mean line distance a. In z-direction the corresponding scale is l_c defined by the disorder induced single line fluctuations $a^2 = \langle \delta x(z = l_c)^2 \rangle = (\Delta/(gT))^{2/3} l_c^{4/3}$ with roughness exponent $\zeta = 2/3$ [HHF85, KZ87, Kar87] and $\delta x(z) := x(z) - x(0)$. In equilibrium, both energies will contribute equally. The scaling of the elastic energy is easily written $U = L_z m \times g/2 \times a^2/l_c^2$ with m the number of lines. We immediately get the scaling behaviour of the effective compression modulus $c_{11} = a\frac{\partial^2}{\partial a^2}(af(a)) \propto \Delta/(Ta^2)$, which compares nicely to the exact expression Eq. (2.32).

2.5 General interaction

So far we have considered only the very short range limit of a repulsive vortex interaction. In this section, we allow for a general repulsion over a nonzero range, including long range interactions, while intersections and overlap of lines are still assumed to be energetically prohibited. What will be the effect of a finite range interaction on the glass transition? We again focus on the scaling dimension of disorder Eq. (2.7) $\lambda_d = 1 - \frac{T\pi}{a^2\sqrt{c_{11}c_{44}}}$. While the interaction will not renormalise the tilt modulus $c_{44} = g/a$, the compression modulus will be affected. Two mechanisms compete. A finite range interaction allows for the definition of a microscopic compression modulus

$$c_{11,0} = a\frac{\partial^2}{\partial a^2} U(a) > 0,$$

compared to $c_{11,0} = 0$ for the noncrossing-only case. The energetic part of the stiffness is thus increased, thermal fluctuations are suppressed and disorder becomes more relevant. But then the

entropic fluctuation induced part of the stiffness is also suppressed by which the relevance of disorder is reduced. What will be the net effect? A larger or smaller effective stiffness as compared to the situation with the noncrossing interaction only? In order to separate effects, let us split the interaction potential, which certainly diverges at $x = 0$ and is otherwise a smooth function, into a part solely realizing the noncrossing constraint and the residual interaction $U_r(x)$

$$U(x) = c\delta(x) + \mu U_r(x).$$

c is very large and the factor μ has been included so that we can tune in and out (in Gedanken) of the 'reference state' $\mu = 0$, for which infinitesimal disorder is marginal.
As in Section 2.3, we map the classical lines onto quantum particles and disorder is assumed to be infinitesimal. Statistics assure noncrossing and we arrive at one-dimensional spinless fermions with the repulsive interaction $\mu U_r(x)$. The compressibility[7]

$$\kappa = -\frac{1}{L}\frac{\partial L}{\partial p} = \frac{1}{L}\left(\frac{\partial^2 E_0}{\partial L^2}\right)^{-1} = \frac{1}{\rho^2}\frac{\partial \rho}{\partial \mu}$$

is nothing but the inverse compression modulus in the line language

$$1/\kappa \leftrightarrow c_{11}.$$

The double arrow indicates that the mapping of Table D.1 has been invoked and $L = L_x$.
Weak interaction of the fermions can be treated quantitatively, e.g. by means of bosonisation. For a review see Ref. [Voi95], in Appendix 1 a sketch of the method is given. The compressibility is obtained easily as

$$\kappa = \frac{a^2}{\pi\hbar v_N}$$

with the renormalised Fermi velocity

$$v_N = v_F + \frac{1}{2\pi\hbar}(g_4 + g_2 - g_1) = v_F + \frac{\mu}{2\pi\hbar}\Big(2\tilde{U}_r(0) - \tilde{U}_r(2k_F)\Big),$$

that has contributions g_2, g_4 from forward scattering (momentum transfer $q \simeq 0$) and backward scattering g_1 (momentum transfer $q \simeq 2\pi k_f$). Note that in the literature the g_1 contribution for the spinless case is usually included in g_2. Also the nonharmonic backscattering of the spinfull case is not present without spin. With $k_F = \pi/a$ and $v_F = \hbar k_F/m$, we get in the limiting case of a hard-core repulsion only $\mu = 0$, of course, $\kappa^{-1} = \hbar^2\pi^2/(a^3 m) \to \pi^2 T^2/(a^3 g) = c_{11}^{\rm th}$, see Eq. (2.27).
At finite μ the net effect on the compression modulus is

$$c_{11} = c_{11}^{th} + \delta c_{11}^{i.a.} = c_{11}^{th} + \frac{\mu}{2a^2}\Big(2\tilde{U}_r(0) - \tilde{U}_r(2\pi/a)\Big) > c_{11}^{th}, \tag{2.36}$$

where the last inequality is a simple consequence of a repulsive $U_r(x)$ that implies, in one dimension, $\tilde{U}_r(0) > 0$ and $|\tilde{U}_r(0)| > |\tilde{U}_r(2k_{\rm F})|$. The large scale compression modulus is increased by a repulsive interaction with respect to the value $c_{11}^{\rm th}$ for the noncrossing only (or free fermion) case, where disorder is marginal. Strictly speaking we have shown this only for small μ, as bosonisation is good only in the limit of small interaction energy compared to kinetic energy, i.e., $\delta c_{11}^{i.a.} \ll c_{11}^{th}$. However, for larger μ it is easy to argue. The compressibility of the Fermi system will be a *monotonic* function

[7] Sometimes $\frac{\partial \rho}{\partial \mu}$ alone is called compressibility.

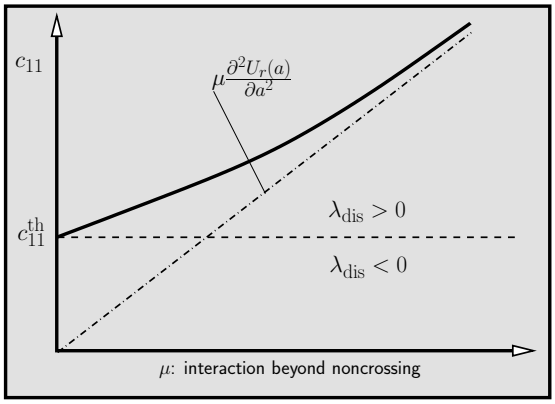

Fig. D.4: Effective compression modulus vs repulsive vortex-interaction strength.

of μ. Without an underlying lattice, no spin and no magnetic field no resonances are possible that would be the only way around an increasing 'stiffening' of the system with increasing repulsion. The picture of Fig. D.4 emerges where the compression modulus cannot become smaller than the marginal value c_{11}^{th}, i.e., even if the effect of disorder on the large scale stiffness is neglected $\lambda_{\rm dis} > 0$. We have also included in the figure the limit of large μ and long-range interaction $U(x)$. Then the electrons will become classical and form a Wigner crystal and their compressibility can simply be obtained in harmonic approximation to the nearest neighbour interaction $\kappa^{-1} \propto \mu\frac{\partial^2 U_r(a)}{\partial a^2}$.

We thus can summarise: Arguing the stability of the glassy phase, we see that the case with only the noncrossing interaction is in fact a worst case scenario. *Any* additional repulsion may reduce the entropic stiffness but in total makes disorder more relevant and Eq. (2.36) even allows us to quantify the effect for weakly repulsive potentials. No glass transition is possible.

2.6 Effect of small length scale cutoff and application to materials

The effect of a finite single line persistence length ξ is now added which is given by the UV cuttoff inherent to any condensed matter system. In our case the superconductor coherence length sets a cutoff for vortex fluctuations, as it is the basic length scale over which the superconducting order parameter can vary and we identify it with the fluxline persistence length. The effect of the UV cutoff $\Lambda = \pi/\xi$ on correlations of a single line is easily calculated to be

$$\langle [x_i(z) - x_i(0)]^2 \rangle = \frac{T}{g}(z - \xi), \tag{2.37}$$

for $z \gtrsim 2\xi$. The same result is obtained by a position space calculation considering a correlated random walk where the 'persistence' of individual line wandering can be analysed very intuitively, see Appendix 4. We use these correlations in the simple scaling argument for the entropically renormalized stiffness of Section 2.3 and compare to the random walk of a line without a cutoff. There is a shift of $-T/g\ \xi$ in the wandering amplitude. Hence, line collisions will be rarer and the effective compression modulus will be smaller than in the reference state that renders disorder marginal. We have identified a mechanism working in favour of the free phase in contrast to the finite disorder and repulsive interaction contributions of the previous sections. To become quantitative,

the modified collision length l_c as defined from Eq. (2.37) by $\langle[x_i(l_c)-x_i(0)]^2\rangle \stackrel{!}{=} a^2$ is used in the scaling arguments for the thermal entropic contribution to c_{11} as discussed above. The analogue is done for the disorder entropic term and the lowest order corrections in ξ/a together with the other contributions to the compression modulus is given as

$$c_{11} = c_{11}^{\rm th} + c_{11}^{\Delta} - \delta c_{11}^{\xi} + \delta c_{11}^{i.a.}, \tag{2.38a}$$

$$\delta c_{11}^{\xi} = \left(\frac{10}{3}\frac{\pi^2 T^3}{g^2 a^4} + \frac{35}{4}\frac{\Delta_0^{3/2}}{T^{3/2}a^{5/2}}\right)\frac{\xi}{a} = \left(c_{11}^{\rm th}\frac{10}{3}\frac{T}{ga} + c_{11}^{\Delta}\frac{35}{4}\sqrt{\frac{\Delta_0}{agT}}\right)\frac{\xi}{a} \tag{2.38b}$$

$$\delta c_{11}^{\Delta} = \frac{\Delta_0}{Ta^2} \tag{2.38c}$$

$$\delta c_{11}^{i.a.} = \frac{1}{a^2}\left(\tilde{U}_r(0) - \frac{1}{2}\tilde{U}_r(2\pi/a)\right). \tag{2.38d}$$

$c_{11}^{\rm th}$ is the reference which renders infinitesimal disorder marginal. The superscript $i.a.$ stands for the effect of repulsive 'interaction' beyond the noncrossing condition, as in Section 2.5. Note that from here the interaction strength parameter μ is set to one. The only effect favouring the thermal phase is the reduction of the stiffness by a finite persistence length ξ. Therefore, at the possible transition point T_g this term has to equal the other two terms, which increase pinning

$$\delta c_{11}^{\rm th}(T_g) \stackrel{!}{=} \delta c_{11}^{\Delta}(T_g) + \delta c_{11}^{i.a.}.$$

In the limit $\tilde{U}(0) \ll \Delta/T$, we get

$$T_g = 0.42(g^2\Delta a^2)^{\frac{1}{4}}\left(\frac{a}{\xi}\right)^{\frac{1}{4}}.$$

For the opposite limit $\tilde{U}(0) \gg \Delta/T$ we try to quantify the interaction term. The usual interaction potential between vortices $U(\mathbf{r})$ in the three dimensional bulk from Ginzburg-Landau theory [Bra77] is [8]

$$U(\mathbf{r}) = \frac{\Phi_0^2}{4\pi\mu_0\lambda^2}\frac{\exp[-r/\lambda]}{r}, \tag{2.39a}$$

$$\tilde{U}(\mathbf{q}) = \frac{\Phi_0^2}{\mu_0}\frac{1}{1+\lambda^2 q^2}, \tag{2.39b}$$

with Φ_0 the flux quantum, μ_0 the vacuum permeability and λ the penetration depth. It is modified when the vortices are confined to a quasi-2D layer of width d perpendicular to the magnetic field, where the effective two dimensional interaction potential in momentum space becomes [Abr64, Kie93]

$$\tilde{U}(\mathbf{q}) = \frac{\Phi_0^2}{4\mu_0\lambda}\frac{1}{\sqrt{1+\lambda^2 q^2}}\tanh[\frac{d}{2\lambda}\sqrt{1+\lambda^2 q^2}]. \tag{2.40}$$

The comparison of Eq. (2.40) with the reduction of the three dimensional (3D) potential Eq. (2.39b) to the plane

$$\int_{q_z}\tilde{U}_{3D}(q_x,q_y,q_z) = \frac{\Phi_0^2}{4\mu_0\lambda}\frac{1}{\sqrt{1+\lambda^2 q^2}} \tag{2.41}$$

[8] Often this equation is written in CGS units, where the flux quantum becomes $\sqrt{4\pi/\mu_0}\Phi_0^{\rm SI} = \Phi_0^{CGS}$; this is easily seen from the energy density $w = B_{\rm CGS}^2/(8\pi) = B_{\rm SI}^2/(2\mu_0)$.

shows how the confinement to the plane *softens* the vortex lattice for $d \ll \lambda$.
We use this potential in formula (2.38d) in order to estimate $\delta c_{11}^{i.a.}$. The fact that the noncrossing contribution has not been subtracted from the potential before the Fourier transform does not disturb. For the purpose of the moment we only evaluate the potential at small momenta while the noncrossing physics is reflected at largest momenta. We thus have

$$\delta c_{11}^{i.a.} > \frac{\tilde{U}_r(0)}{2a^2} \simeq \frac{\Phi_0^2}{8\mu_0\lambda^2}\frac{d}{a^2} \tag{2.42}$$

for $d \ll a$. Ginzburg-Landau theory further tells us $c_{44} = g/a = \Phi_0^2/(4\mu_0\lambda^2)\ d/a^2$, exactly twice the right hand side of Eq. (2.42), again note the softening with small sample width. We get as a bound for the transition temperature in the limit $\Delta T \ll \tilde{U}(0)$

$$T_g > 0.16\left(\frac{a}{\xi}\right)^{\frac{1}{3}} ag = 0.16\left(\frac{a}{\xi}\right)^{\frac{1}{3}} \frac{\Phi_0^2 d}{4\mu_0\lambda^2}.$$

The softening of the lattice both with decreasing sample thickness d and increasing temperature (remember $\lambda = \lambda_0(1-T/T_c)^{-1/2}, \xi = \xi_0(1-T/T_c)^{-1/2}$) seems to make a transition at a temperature smaller than the superconductor critical temperature T_c possible. The system of course cannot be made arbitrarily thin as the lower critical field, at which fluxlines start to enter the layer, diverges with vanishing layer thickness $H_{c_1} \propto 1/d^2$ and matches the upper critical field H_{c_2} at $d \simeq \xi(T)$ [Abr64]. In a realistic geometry, $d \simeq 1\mu$m, see Ref. [BAP$^+$99]. In order to derive an estimate for a lower bound to the transition temperature we choose the limiting values $\lambda_0 \simeq 1\mu$m, $\xi_0 = \lambda_0/\kappa$ with $\kappa \simeq 5$ for the conventional superconductor used in Ref. [BAP$^+$99], $a/\xi_0 \simeq 1$ and $T_c < 100$K. We find

$$T_g > 0.99T_c.$$

This is very close to the critical temperature given the conservative approximations that were made. A transition very close to T_c, however, cannot be ruled out strictly, especially not for the strongly type II HTSC with $\kappa \simeq 10^2$.
Dislocations in the present context can only be generated by lines that leave the sample after crossing only a fraction of its length. Such topological defects in the vortex array cannot be excluded strictly since with the glassy $\ln^2$-roughness their proliferation is energetically favourable even at zero temperature, see, e.g., the discussion at the end of Section 5. However, the scale which sets their average density will be very large, corresponding to a large core energy. In the experiment of Ref. [BAP$^+$99], single flux lines could be observed entering the sample. The discrete response for each such occurrence was in all cases of the same amplitude, indicating that the lines enter the film over its whole width and do not leave the sample in the middle.

3 The random-bond dimer model and the (1+1)-dimensional line lattice

In the previous chapter the planar vortex array was analysed theoretically with a focus on the glass transition. Here, we make use of the close relation to the random-bond dimer model in order to verify the above RBA results by the comparison of a range of thermodynamic quantities in the two models. The random-bond dimer model falls into the class of combinatorial problems in statistical physics that study complete coverings of manifolds by building blocks of a given shape [Fis61, Wu03]. Its relation to the physics of vortex lattices is not very obvious although in practice very simple [Fis84]. Also, quantum versions of the dimer model on a variety of lattice geometries have been successfully linked to a wide range of condensed matter problems, e.g. quantum Ising antiferromagnets, see Ref. [MS02] and references therein. It has also been discovered lately by Propp *et al.* [EKLP92] that the combinatorial problem of the classical random-bond dimer model on the square lattice can be treated with *exact* numerics very effectively. Zeng and collaborators at George Washington University, Washington, D.C., have implemented this algorithm and can compute thermodynamic quantities of the random-bond dimer model with polynomial dependence of computation time on the system size. The results below are the product of a close collaboration with the group at Washington, who have provided the simulation data for the dimer model.
The models and their mapping are explained in detail in the following section before analytical predictions are compared to simulations and the results are interpreted.

3.1 The models and the mapping

3.1.1 Vortex system

We consider the vortex line array of Chapter 2 in the limit of a contact interaction between the lines that does not allow them to intersect. The lines are confined to a plane at an average distance $a = 1/\rho$. A single line is characterised by its position $x_i(z)$ and line tension g. Quenched disorder couples locally to the lines via the random potential $V(\mathbf{r})$, which is assumed to have short range correlations $\overline{V(\mathbf{r})V(\mathbf{r}')} = \Delta\delta(\mathbf{r}-\mathbf{r}')$. The total energy is then written

$$H = \int \sum_i \left\{ \frac{g}{2}\left(\frac{dx_i}{dz}\right)^2 + c\sum_{i,j\neq i}\delta(x_i - x_j) + V(x_i, z) \right\} \tag{3.43}$$

with $c \to \infty$. Although considerably simpler, this model of self-avoiding lines is still generic with respect to thermodynamics and the phase diagram of (1+1)-dimensional vortex lattices, as argued above in Section 2.5.

3.1.2 Dimer model

The dimer model is defined as follows: Choose a subset (whose elements are called dimers) of the bonds on a square lattice with lattice constant b and linear size L such that every of the $L^2 = N$ lattice sites (labelled by (ij)) is touched by exactly one of these dimers, see Figs. D.5, D.7. A square lattice rotated by 45 degrees with lattice constant $b/\sqrt{2}$ is formed by the centers of the bonds. Its $2N$ sites shall for convenience also be labelled by (ij) and it will be clear from the context if the original

lattice or that of the bonds is parametrized. The reduced energy of one such complete covering D of $N/2$ dimers is defined by

$$\tilde{H}_d = H_d/T_d = \sum_{(ij)\in D} \epsilon_{ij}/T_d \tag{3.44}$$

where the sum is over all dimers of D. The bond energies ϵ_{ij} are independent random variables drawn from a Gaussian distribution with zero mean and unit variance $\overline{\epsilon_{ij}\epsilon_{kl}} = \delta_{ij,kl}$. T_d is the dimensionless dimer temperature and equivalent to the inverse strength of disorder as will be discussed in detail below. In the following, the subscript 'd' stands for quantities of the dimer model, while line lattice quantities are denoted by the subscript 'l'. The implementation of the polynomial algorithm [EKLP92] (with exponent $\simeq 2$) on a 32-processor cluster by Zeng and collaborators allows to compute thermodynamic quantities numerically exact – as opposed to, e.g., Monte Carlo sampling – for sizes up to $L = 512$ at typically 6000 disorder configurations for a range of dimer temperatures within days. Merely the measurement of the specific heat in Section 3.2.4 is not covered by the polynomial algorithm. Thermal fluctuations have to be computed from explicitly sampling over a representative set out of the $\exp[NG/\pi]$ [Kas61] possible dimer coverings, again for up to 6000 disorder configurations. This gives, however, also reliable results for sizes up to $L = 256$. The typical accuracy of the data for moments of disorder averaged quantities at the given number of disorder samples is $\simeq 10^{-5}$.

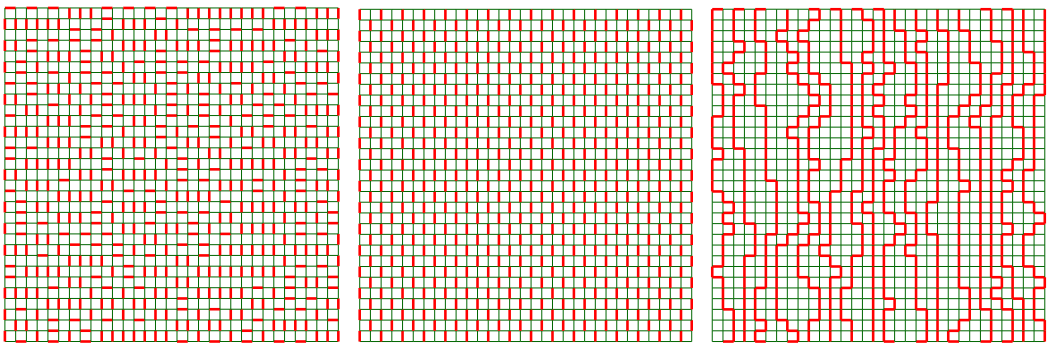

Fig. D.5: Mapping of a dimer (left) to a line configuration (right) via XOR-addition of the reference state (middle).

3.1.3 Relation

The two apparently diverse models are closely related. The random bond dimer model can be mapped onto an array of lines that interact via a hard core repulsion, preventing any line crossing. In Fig. D.6 the mapping with intermediate steps is sketched. From the dimer model (A) on top the discrete line model (C) can be reached directly and via the intermediate random solid on solid (SOS) model (B). Both the SOS model and the discrete lines have their continuous counterparts – in the bottom line of the sketch – that can be treated analytically: The random-field XY model (D) and the continuum (1+1)-dimensional line lattice (E). Below we will explain how to move between these models and we will be able to relate quantities of the isotropic dimer model and its version with a height profile (SOS) to quantities of the anisotropic vortex line lattice. As the starting point for a detailed tour

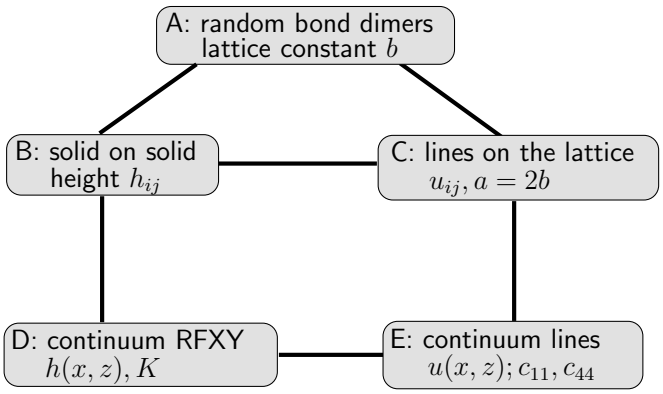

Fig. D.6: The relation of the dimer model to the (1+1)-dimensional vortex lattice. *Top*: discrete models; *bottom*: continuous models ; *left*: isotropic, *right*: anisotropic.

through the mapping table Fig. D.6 the dimer model (A) with the dimer temperature T_d being the only parameter is chosen. The line lattice can be reached very quickly via

(AC) Add the dimer pattern and a reference lattice as given in the middle of Figs. D.5, D.7 with an 'exclusive or' (XOR) operation. It means that only if a given bond is covered by either the dimer pattern or the reference pattern, it is covered in the resulting configuration, which will be noncrossing lines at *average* density $\rho = 1/(2b)$, which becomes sharply defined only for large systems. The ensemble of dimer configurations thus corresponds to a grand canonical vortex line ensemble with a chemical potential such that the average density is fixed. For the energies on the bonds that are covered in the respective configurations

$$H_{\rm lines}(\{\epsilon'_{ij}\}) = H_d(\{\epsilon_{ij}\}) + H_{\rm ref}(\{\epsilon'_{ij}\}). \tag{3.45}$$

is implied. Here $\{\epsilon_{ij}\}$ stands for a given distribution of energies on all of the bonds and the random energies ϵ' for the line lattice are defined as $\epsilon'_{ij} = -\epsilon_{ij}$ on the occupied bonds of the reference lattice and $\epsilon'_{ij} = \epsilon_{ij}$ elsewhere. If the dimer random bond energies $\{\epsilon_{ij}\}$ are distributed symmetrically with zero mean so are the line bond energies $\{\epsilon'_{ij}\}$.

(AB) A height profile $\{h_{ij}\}$ can be assigned to every plaquette in the following way [Hen97]: Every bond is given a sign ± 1 such that going through rows or columns of plaquettes the sign of the crossed bonds alternates. Starting at a given plaquette with arbitrary height, one moves to the neighbouring plaquettes and adds to the height '+3 times bond sign' if the crossed bond is covered by a dimer, or '-1 times bond sign' if it is not. The resulting numbers define a path-independent height profile h_{ij}.

(BC) Subtract the reference height profile and get

$$H_{ij} := h_{ij} - h_{ij}^{\rm ref} \tag{3.46}$$

on each plaquette with row index i and column index j, as illustrated by the numbers in Fig. D.7. H_{ij} is quantised in steps of width 4, sites with constant H form directed domains

of average width $2b$ that may be labelled by k; introduce displacements $u_k(i)$ of the domain wall k from its perfectly aligned position {i=1..n,j=2k}; the directed domain walls are the discretised lines; it holds (see Figs. D.7, D.8)

$$u_k(i) = \frac{H_{i,2k} + H_{i,2k+1}}{4} + 2k. \tag{3.47}$$

Note that the mapping to a displacement field makes sense only in an ensemble with a fixed number of lines, i.e., fixed density. For the grand canonical ensemble induced by the sum over dimer configurations, $u_k(i)$ is a good degree of freedom only for the average configurations, which, however, carry the dominant weight in the thermodynamic limit.

(CE) Sending the grid spacing to zero gives lines in a disorder environment with average spacing $a = 2b$. The individual lines wander freely under the sole restriction that they may not cross. Therefore the model corresponds to the continuum model of Section 3.1.1 with a hardcore repulsion only.

(BD) The continuum limit of the SOS model is the RFXY model with reduced stiffness K

$$\begin{aligned} \tilde{H}_{\mathrm{RFXY}} = & \frac{K}{2} \int d^2r (\nabla h)^2 \\ & + \frac{V}{T} \int d^2r \cos[Qh(\mathbf{r}) + \alpha(\mathbf{r})]. \end{aligned} \tag{3.48}$$

$\alpha(\mathbf{r})$ is a random phase, V a constant coupling strength and $Q = 2\pi/4$. Only going the way ACED in order to reach model D justifies the special form of the disorder coupling with the given value for Q.

(DE) Rescale $z \to z' = z\sqrt{c_{44}/c_{11}}$, define displacements

$$u(\mathbf{r}) := bh(\mathbf{r})/2 \tag{3.49}$$

and set

$$K := \frac{b^2\sqrt{c_{11}c_{44}}}{4T} = \frac{a^2\sqrt{c_{11}c_{44}}}{16T} \tag{3.50}$$

in order to get the elastic Hamiltonian for interacting lines

$$\begin{aligned} H_{\mathrm{el}} = & \frac{1}{2} \int d^2r \left\{ c_{11}(\partial_x u)^2 + c_{44}(\partial_z u)^2 \right\} \\ & + V' \int d^2r \cos[\frac{2\pi}{a} u(\mathbf{r}) + \alpha(\mathbf{r})] \end{aligned} \tag{3.51}$$

with an effective compression modulus c_{11} describing the line interaction in elastic approximation and with tilt modulus $c_{44} = g/a$.

The relation (3.49) between the line displacements and the dimer height profile is the continuum version of Eq. (3.47) which can be seen by use of Eq. (3.46) and the observation that $h_{ij}^{\mathrm{ref}} \simeq 2j$ upon coarse graining. This relation is in hindsight, knowing that the lines have a mean distance of $a = 2b$, the reason for the choice of $Q = 2\pi/4$ in model D, Eq. (3.48). These numbers are important below when the models are compared quantitatively. Also note that

the system size A is changed by going from the isotropic model (d for dimer) with stiffness K to the anisotropic line model (l for lines) according to

$$A_d/A_l = \sqrt{\frac{c_{11}}{c_{44}}} = K\frac{8T}{bg}. \tag{3.52}$$

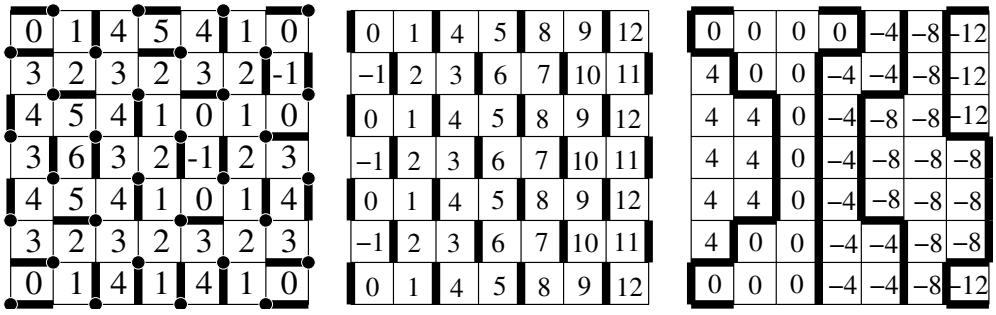

Fig. D.7: Dimer covering (left), reference state (middle) and line configuration (right), with height profiles h_{ij} (left and middle) and H_{ij} (right).

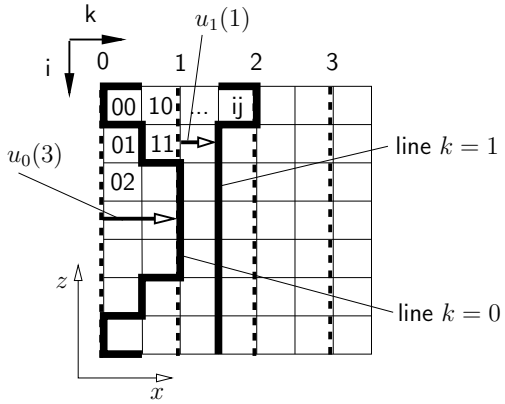

Fig. D.8: Illustration of displacements $u_k(j)$ in the discrete model, the dashed lines stand for the regular undisplaced line lattice. Eq. (3.47) can be checked in this sketch with the numbers for H_{ij} in Fig. D.7, right.

We now need to discuss quantitatively the relation of the three continuum model parameters, (i) line stiffness g, (ii) disorder strength Δ and (iii) temperature T, to the dimer model. In order to relate the two dimensionless parameters Δ/T^2 and ga/T of the continuum model to *two* dimer parameters, we want to modify and thus the generalise the dimer model slightly. Disorder strength will be determined by $1/T_d$, i.e., the dimer temperature will in the line picture not act as a temperature but rather as inverse disorder strength, see below, while for the mapping of the single line stiffness we introduce a second dimer parameter $\tilde{\epsilon}_h$. Instead of giving all bonds a random energy ϵ_{ij} drawn from the same distribution with zero mean, the horizontal bonds (denoted by $ij \in h$) are assigned the constant nonrandom energy

$$\frac{\epsilon_{ij\in h}}{T_d} = \tilde{\epsilon}_h > 0 \tag{3.53}$$

that penalises excursions of a line and thus increases the tilt modulus $c_{44} = g/a$ of the vortex array. The random energy on the vertical bonds remains unchanged and so does relation Eq. (3.45). Note that by fixing rather the reduced energy than the energy on the horizontal bonds, we have fixed the statistical weight of these bonds irrespective of the value of the dimer temperature T_d. By changing $\tilde{\epsilon}_h$, we can tune the ratio of the *average* numbers of occupied vertical ($\#_v$) and horizontal bonds ($\#_h$). Let us consider the pure limit of a vanishing disorder variance, i.e., $T_d = \infty$ or zero energy on the vertical bonds. As we assume g not to be renormalised by disorder in analogy to the continuum model, this limiting case suffices to determine the single line stiffness even in the presence of disorder. The partition function now is

$$Z_d = \sum_{\{D\}} \exp[-\#_h \tilde{\epsilon}_h],$$

from which the average number of occupied horizontal bonds can be obtained by taking the derivative with respect to[9] $z_h := \exp[-\tilde{\epsilon}_h]$

$$\langle \#_h \rangle = z_h \frac{\partial}{\partial z_h} \ln Z_d.$$

Kasteleyn calculates Z with the method of Pfaffians as a function of z_h, z_v [Kas61], here we have $z_v = 1$ and

$$\ln Z(z_h, z_v = 1) = N \frac{1}{2\pi i} \{L[iz_h] - L[-iz_h]\}$$

where $L[x] = -\int_0^x \frac{du}{u} \ln(1-u)$. One obtains the exact expression

$$\langle \#_h \rangle = N \frac{\arctan z_h}{\pi}.$$

As the total number of occupied bonds is fixed to $N_{\text{bonds}} = N/2$ this implies $\langle \#_v \rangle = N(1/2 - \arctan[z_h]/\pi)$. The numbers of occupied bonds in the dimer model translate to the numbers of horizontal and vertical segments in the discrete line model. The 'XOR'-addition of the dimer pattern and the reference pattern gives immediately $\langle \#_{h,\text{lines}} \rangle = \langle \#_h \rangle$, as the reference pattern contains only vertical bonds. Vertical segments in the line model come from (i) bonds that are occupied in the dimer pattern and not in the reference pattern and (ii) from the inverse. Out of the $N = L^2$ bonds of the lattice $N/2$ are not occupied in the reference pattern. The probability for any given bond out of these to be occupied in the dimer pattern is $\langle \#_v \rangle / N_{\text{bonds}} = 1 - 2\arctan[z_h]/\pi$, giving a contribution to $\langle \#_{v,\text{lines}} \rangle$ of $N/2(1 - 2\arctan[z_h]/\pi)$. With the analogous treatment of the reverse case one gets

$$\langle \#_{v,\text{lines}} \rangle = \frac{L^2}{2}.$$

The results must hold, of course, since on average there will be $L/2$ lines with L vertical segments each.

We now look at the fluctuations of a given line in the discrete model, again with $T_d = \infty$, under the constraints imposed by the dimer model. Let a given line make M steps in z-direction. After each vertical step it may either make a step left ($x_i = -1$) or right ($x_i = +1$) or no horizontal step ($x_i = 0$). The associated probabilities are uncorrelated and can be derived from the average total numbers of horizontal and vertical steps. Per line (on average $L/2$ in total) there are $\frac{L^2 \arctan z_h/\pi}{L/2}$ horizontal segments, i.e. $p_{+1} = p_{-1} = \arctan[z_h]/\pi$, and hence $p_0 = 1 - 2\arctan[z_h]/\pi$. We can

[9] The minus here is unusual and makes z the inverse fugacity rather than the fugacity; we keep the minus, however, in order to remain in contact to the notation in Ref. [Kas61].

now calculate the fluctuations of the horizontal wandering $X := \sum_i x_i$ of this given line of length $z = Mb$ as

$$\langle X^2 \rangle = \sum_{i=1}^{M=z/b} \langle x_i^2 \rangle = 2b \frac{\arctan z_h}{\pi} z.$$

A continuum Hamiltonian $H = \frac{g}{2} \int dz (\partial_z X)^2$ in comparison yields $\langle X^2(z) \rangle = \frac{T}{g} z$ and allows to read off

$$\frac{g}{T} = \frac{\pi}{2b \arctan z_h}, \tag{3.54}$$

which is plotted in Fig. D.9 as a function of $\tilde{\epsilon}_h$. The original pure isotropic dimer model corresponds to the case $\frac{g}{T}(\tilde{\epsilon}_h = 0) = 2/b$. Nonrandom positive energy on the horizontal bonds penalises excursions and stiffens the lines, reflected by $\lim_{\tilde{\epsilon}_h \to \infty} g/T = \infty$. The above line of argument – with resort to

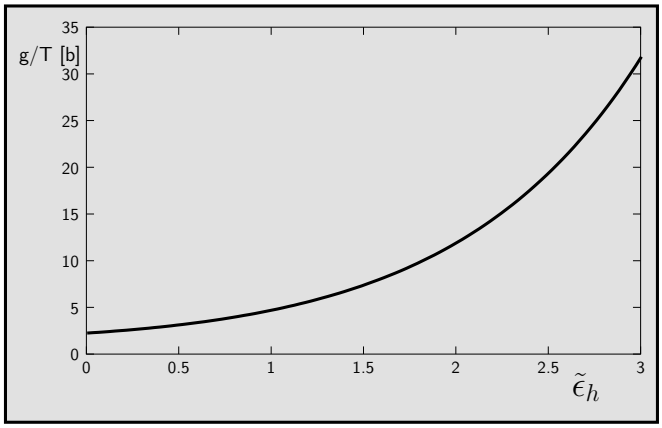

Fig. D.9: Plot of g/T in units of the dimer lattice constant b for varying $\tilde{\epsilon}_h$; note the limit $g/T \to 2$ for vanishing $\tilde{\epsilon}_h$ and the exponential increase.

overall average numbers of occupation – suggests an entropic rather than microscopic or energetic origin of part of the stiffness. In the case of disorder, i.e., finite T_d, c onsider the case of zero mean energy on both horizontal and vertical bonds. Then locally nothing will prevent a line from excursions that best benefit from nearby disorder, as long as in total and on average the numbers of vertical and horizontal segments equal $L^2/2$ and $L^2/4$, respectively. A given line may thus 'borrow' horizontal steps from the ensemble of lines – intuition says this will be locally of vanishing cost. A finite value of the single line stiffness arises only on larger length scales and saturates at $gb/T = 2$. This stiffness we will call 'entropic' as its origin lies in the constraint on the overall average number of possible configurations.

Quite differently, a finite value of $\tilde{\epsilon}_h$ imposes a *local energetic* cost on horizontal excursions, thus generating a finite short scale (s.sc.) stiffness. This may be determined tentatively by subtracting the $\tilde{\epsilon}_h = 0$-entropic contribution from the asymptotic large scale (l.sc.) value for general $\tilde{\epsilon}_h$, as given by Eq. (3.54)

$$\frac{g_{\text{s.sc.}}}{T} = \frac{g_{\text{l.sc.}}}{T} - \frac{2}{b} = \frac{\pi}{2b \arctan z_h} - \frac{2}{b}, \quad g_{\text{s.sc.}}(\tilde{\epsilon}_h = 0) = 0.$$

The following consideration supports this simple addition of microscopic and entropic stiffness without interference. Consider the partition function for the line system. The line configurations are in one-

to-one correspondence to dimer configurations. It is plausible that the finite energy on the horizontal bonds can be accounted for in terms of line degrees of freedom $u_i(z)$ by an elastic energy term $H_{0,\mathrm{s.sc.}}$. The origin of the entropic elastic term can be seen in the change of summation measure when going over from the summation over dimer coverings to the integration over line degrees of freedom. The above arguments showed that on large scales the line conformations carry a harmonic Boltzmann weight with entropic (entr.) stiffness $g_{\mathrm{entr}}b/T = 2$. In formulae this is represented as

$$\begin{aligned} Z_l &= \sum_{\{D\}} \exp[-(H_{0,\mathrm{s.sc.}}[D] + H_{\mathrm{dis}}[D])/T] \\ &= \int \mathcal{D}[\{x_i\}] \exp[-H_{0,\mathrm{entr.}}[x_i]/T] \exp[-(H_{0,\mathrm{s.sc.}}[x_i] + H_{\mathrm{dis+i.a.}}[x_i])/T] \\ &= \int \mathcal{D}[\{x_i\}] \exp[-(H_{0,\mathrm{entr.}}[x_i] + H_{0,\mathrm{s.sc.}}[x_i])/T] \exp[-H_{\mathrm{dis+i.a.}}[x_i]/T] \\ &= \int \mathcal{D}[\{x_i\}] \exp[-H_{0,\mathrm{l.sc.}}/T] \exp[-H_{\mathrm{dis+i.a.}}/T] \end{aligned}$$

and additivity of small scale and entropic stiffness seems at least very plausible. $H_{\mathrm{dis.+i.a.}}$ stands here for the disorder coupling of the lines and the line-line interactions.

Next we come to disorder strength. In the continuum theory it is measured by the disorder variance Δ, see Eq. (3.43). What is the corresponding quantity in dimer language? Noting the fact that $1/T_d^2$ is the variance of the reduced random bond energies in the dimer model, a first guess would identify the dimensionless strength of the continuum disorder potential $\sqrt{\Delta}/T$ with the dimensionless inverse dimer temperature $1/T_d$. Allowing for the disorder correlation length ξ_d, which acts as a cutoff in the continuum model, to differ slightly from the cutoff b in the discrete dimer model, we have

$$\frac{\Delta}{T^2} = \frac{\xi_d}{b}\frac{1}{T_d^2}. \tag{3.55}$$

A closer look at the models, however, suggests a modification to this mapping in the isotropic case with random energy on both horizontal and vertical bonds. In the dimer model the random energy collected by a given line is clearly proportional to its number of segments, i.e., the line length. In the continuum model, this is not the case. Disorder energy is written as the coupling of the line lattice density $\rho(x,z) = \sum_i \delta(x - x_i(z))$ to the disorder potential

$$H_{\mathrm{dis}} = \int dx dz\, V(x,z)\rho(x,z) = \sum_i \int dz\, V(x_i(z),z).$$

The disorder energy is not an integral over the arclength of the lines but over the z-coordinate. Therefore, disorder energy is proportional to the length projected onto the z-direction and not to the actual length and, as a consequence, a given dimer disorder corresponds to larger continuum disorder than assumed by Eq. (3.55). Fortunately, with the annealed disorder average of the free energy there is a quantity – the only one we can think of – that can be calculated analytically in both models. It may be used for the calibration of disorder strength. The calculation for the continuum model is straightforward whereas in the dimer model it is more involved but viable in the isotropic case. The details are given in Appendix 5 and one finds by comparison

$$\frac{\Delta}{T^2} = \frac{\xi_d}{b}\frac{2}{T_d^2}\Big\{1 - \frac{2GT_d^2}{\pi} + \frac{2T_d^2}{\pi}\int_0^{e^{-1/(2T_d^2)}} dx\, \frac{\arctan x}{x}\Big\} \tag{3.56}$$

model	density	stiffness	disorder	system size
vortex lattice	$\rho = 1/a$	g/T	Δ/T^2	L_x, L_z
isotropic dimer model	$1/(2b)$	$2/b$	$2\xi_d/T_d^2$	$\sqrt{N}b = L_x = L_z \frac{16KT}{ag}$
dimer model, horiz. energies $\tilde{\epsilon}_h = 0$	"	$2/b$	ξ_d/T_d^2	"
dimer model, $\tilde{\epsilon}_h > 0$, nonrandom	"	$\frac{\pi}{2b \arctan[e^{-\tilde{\epsilon}_h}]}$	"	"

Table D.2: Relation between parameters of the vortex lattice and the dimer model with random, zero or finite nonrandom horizontal bond energies.

with Catalan's constant $G = 1 - 1/3^2 + 1/5^2 - 1/7^2 + \cdots \simeq 0.915966$. Note the overall factor of two as compared to the first guess of Eq. (3.55) in agreement with the above argument concerning arclength vs. projected length. The contribution of the latter two terms in the bracket crosses over at $T_d \simeq 1$ from zero at small T_d to $\simeq 0.25$ at large T_d. This exact relation has been derived for one special observable and it should not be expected to hold likewise strictly for other physical quantities under consideration. Rather, to every observable in each of the models the modes around the short-scale cutoff, in which the model descriptions differ, contribute with different weight. The one free parameter ξ_d/b relating a continuum model to a discrete model will therefore be considered as an observable-dependent fitting parameter. It should, however, not turn out to vary dramatically around its expected value of order unity.

Below, simulations of both the isotropic dimer model and the dimer model with no energies on the horizontal bonds ($\tilde{\epsilon}_h = 0$) will be compared to theory. For the former, Eq. (3.56) will be used as disorder strength mapping (occasionally without the small correction terms) while for the latter Eq. (3.55) proves to fit very well, as here random energy in both models is collected only on vertical segments of a line.

The manipulation of the line stiffness and possible generation of a microscopic g via finite nonrandom horizontal bond energies $\tilde{\epsilon}_h > 0$ promises to be very interesting in many respects as is argued below. It has, however, not yet been simulated. For an analysis of these effects we have to refer the reader to a future joint publication with Zeng and collaborators, which is in preparation.

3.2 Thermodynamics

3.2.1 Large scale equivalence

In the dimer model the correlations of the height profile h_{ij} of model B can be determined very accurately. The quantity $\delta h(\mathbf{r}) = h(\mathbf{r}) - \langle h(\mathbf{0})\rangle$ measures the height relative to its thermal average, which may be nonzero in a disorder dominated pinned phase. Renormalisation group predicts (for a review see Ref. [NS00]) for the disorder averaged correlation function

$$C(\mathbf{r}) = \overline{\langle(\delta h(\mathbf{r}) - \delta h(\mathbf{0}))^2\rangle} = \frac{1}{2\pi K} \ln(|\mathbf{r}|/b),$$

i.e. logarithmic growth on large scales, irrespective of the value of $\langle h(\mathbf{0})\rangle$. A possible transition from a glassy low temperature phase with $\langle h(\mathbf{0})\rangle > 0$ to a free thermal phase with $\langle h(\mathbf{0})\rangle = 0$ therefore is

not reflected directly in this correlation function. However, the prefactor $1/(2\pi K)$ will be of interest. The stiffness K here is the *large scale* stiffness, renormalised by entropic contributions from thermal and disorder fluctuations on smaller scales. It can be calculated exactly from the RBA free energy Eq. (2.32). First one uses the thermodynamic definition of the compression modulus Eq. (2.23)

$$c_{11} = a\frac{\partial^2}{\partial a^2}\big(a\ f(a)\big) \tag{3.57}$$

and then relates this quantity via the mapping given in Eq. (3.50) to the isotropic stiffness K

$$K = \frac{\pi}{16}\left(1 + \frac{ag\Delta}{\pi^2 T^3}\right)^{1/2}.$$

Note that due to the linear dependency of the single line free energy on the density $\rho = 1/a$ only the interaction terms in the free energy Eq. (2.32) contribute. The comparison of the numerical data to the above predicted functional form are shown in Fig. D.11 for the original dimer model, and in Fig. D.12 for the model with $\tilde{\epsilon}_h = 0$. Disorder mappings are chosen respectively as explained above. The agreement is very good over orders of magnitude, while the full disorder relation from the comparison of annealed averages seems to fit better than the simple version. We emphasise that the validity of the replica Bethe Ansatz calculation with its analytical continuation to $n = 0$ is strongly confirmed by the excellent agreement. Interestingly no deviation is found in the large disorder, i.e., low T_d limit. The condition for the validity of the Bethe Ansatz calculation, Eq. (2.35), translates for $g/T = 2/b$ and $\Delta/T^2 = 2\xi_d/T_d^2$ (ξ is henceforth always measured in units of b) to

$$T_d \gtrsim T_d^* = \xi_d\sqrt{2\frac{gb}{T}} = 2\xi_d. \tag{3.58}$$

Thus, below $T_d \simeq 2$ one would have expected the comparison not to work out well as there the assumptions in the Bethe Ansatz cease to be valid. An explanation for the excellent fit even in this region is that the true T_d^* for the dimer problem with no nonrandom energy om the horizontal bonds is, in fact, vanishing due to a vanishing *microscopic* stiffness $g_{\mathrm{s.sc.}}$, see the considerations in Section 3.1.3, that should be used in Eq. (3.58). This argument is consistent with the comparison of the free energy, where the agreement is excellent if the microscopic stiffness in the single line free energy is set zero. A check of the conjecture should be possible with simulations for horizontal dimer energies $\tilde{\epsilon}_h > 0$.

In the pure limit $T_d \to \infty$, the stiffness approaches the value $K = \pi/16$ in agreement with the exact calculation for the nonrandom dimer model [Hen97] and the free fermion mapping for noncrossing lines. Hence, the dimer model obviously simulates a system of noncrossing lines most accurately. The value $K = \pi/16$ is of physical significance as shown by the RG scaling dimension of disorder for the RFXY model[10] Eq. (3.48),

$$\lambda_\Delta = 2(1 - \pi/16K^{-1}). \tag{3.59}$$

The limiting value of $K = \pi/16$ indicates that infinitesimal disorder is marginal and that the system is on the borderline between a glassy and a thermal free phase. As we have also seen above, any finite amount of disorder leads to an increase in K which in turn renders disorder a relevant perturbation leading to a glassy phase. It is therefore no surprise that only the low temperature glassy behaviour

[10] Note that the value $Q = 2\pi/4$ of model D is explicitly used here.

has been found in correlation functions that *do* depend qualitatively upon the phase [ZLH99]. The conclusion about the absence of the glass transition is confirmed although not the whole parameter space is tested by the isotropic dimer model with a fixed density of lines and a given line stiffness. If, however, one can tune the stiffness by the nonrandom energy on the horizontal bonds, a change in g/T and Δ/T^2 can be attributed to any change of two out of the three physical parameters g, Δ, T while we expect the limiting value of $K = \pi/16$ not to change with the modified stiffness (it drops out, see Eq. (3.57)). Hence one can convince oneself that the thermally free phase, which would require $K < \pi/16$ is not reached for g, Δ and especially no temperature T.

3.2.2 Free energy, internal energy and entropy

We now come to a direct comparison of fundamental thermodynamic quantities. We start with the disorder averaged free energy $\overline{F} = -T\overline{\ln Z}$. Due to the different meanings of temperature in the line and dimer context we will focus on the logarithm of the partition function $\overline{\ln Z}$. When relating the systems we have to keep in mind that for a fixed disorder configuration the dimer energy differs from that of the discrete line configuration which it is mapped onto by the random energy of the reference state, see Eq. (3.45). Therefore, we expect the quantities

$$\ln Z_d + E_{\mathrm{ref}}/T_d \leftrightarrow \ln Z_l = -A_{\mathrm{lines}} f_l/T \tag{3.60}$$

to correspond, i.e., to obey the same disorder distribution in the thermodynamic limit. In the disorder average $\overline{\ln Z_d + E_{\mathrm{ref}}/T_d}$ the reference energy does not contribute as the bond energies are drawn from a Gaussian distribution with zero mean. Higher moments, however, contain contributions of the E_{ref}-term in the above relation.
Volumes of the discrete and the continuous model are related according to Eq. (3.52)

$$A_d = (Lb)^2 = A_l \frac{16K}{a}\frac{T}{g} = L_x L_z \frac{\pi}{a}\frac{T}{g}\left(1 + \frac{ag\Delta}{\pi^2 T^3}\right)^{1/2}$$

and the line free energy density $\overline{f_l}$ is given by Eqs. (2.32), (2.33). The energetics and configurations of individual lines in the two models differ heavily on small scales. We thus cannot expect the disorder independent part in the single line free energy to be reproduced in the numerics, therefore the disorder independent contributions in $\overline{f_l}$ are combined such that in the pure limit the exact dimer result is matched. In this pure limit, the partition functions of the dimer model just counts the complete dimer coverings of the square lattice. This is a complex combinatorial problem as any flip of one dimer may necessitate a cascade of flips throughout the system. Nevertheless, the result is exactly known to be

$$L^{-2} \ln Z_d\Big|_{T_d=\infty} = \frac{G}{\pi}$$

in the thermodynamic limit [Kas61] with $G = 1 - 1/3^2 + 1/5^2 - 1/7^2 + \cdots \simeq 0.915966$ is Catalan's constant. The continuum line model parameters are translated to the dimer model along Table D.2 and for the model with no random energy on the horizontal bonds we get

$$\overline{\ln Z_d} = L^2\Big(\pi^2 + \frac{gb}{T}\frac{2\xi_d}{T_d^2}\Big)^{-1/2}\left(G + \frac{1}{T_d^2}(1 - \frac{\xi_d}{2}) - \frac{gb}{T}\frac{\xi_d^2}{12T_d^4}\right). \tag{3.61}$$

Here the disorder parameter relation $\xi_d/T_d^2 = \Delta/T^2$ has been used, which should be chosen if the anisotropic dimer model with random energy only on the vertical bonds is simulated. If the

vertical and the horizontal bonds carry random energy but no constant energy one should replace $1/T_d^2 \to 2/T_d^2$ (modulo correction terms of Eq. (3.56)), as explained above. The square root factor of Eq. (3.61) stems from the volume rescaling and the T_d^{-2} term in the second parenthesis comes from terms proportional to disorder in both the single line free energy and the interaction part. The last term $\propto T_d^{-4}$ comes from the term $\propto \Delta^2$ in the single line free energy Eq. (2.33).
We compare the formula to numerical data for the case $\tilde{\epsilon}_h = 0$, i.e. $gb/T = 2$, and find that it does not fit the data at all. However, dropping the T_d^{-4}-term, we get the plot Figs. D.13 and the plots Figs. D.14, D.15 for the isotropic dimer model. Only the large-T_d limit was fixed, yet the agreement is excellent over orders of magnitude down to small dimer temperatures.
Where is the Δ^2-term? In Eq. (3.61) we had not immediately replaced the line stiffness with a value on purpose. Given a scale dependent stiffness, the two occurences of g in the above formula in fact differ. In the square root, the stiffness must be the large scale effective stiffness $gb/T = 2$ as it comes from the rescaling of the sample *volumes*. The single line free energy, however, which accounts for the second occurence of g, is calculated in a quantum mechanical framework where g corresponds to a mass m, see Table D.1. This mass must surely be defined on microscopic time scales, as the quantum mechanical time evolution is determined from it. Now, in the simulations presented here – the isotropic model and the one with random energies only on the vertical bonds and no energy on the horizontal ones – no microscopic stiffness is generated, i.e., $g_{s.sc.} = 0$ as argued in Section 3.1.3. Hence the T_d^{-4}-term drops out of Eq. (3.61). This explanation is consistent with the very good agreement between RBA formulas and dimer simulations down to $T_d = 0$ with no indication of a finite $T_d^* = \xi_d\sqrt{2gb/T}$ below which the quantum mechanical RBA calculation should become invalid. Here again the vanishing microscopic stiffness enters.
In order to confirm these considerations unambiguously, it would be very interesting to study the case of finite nonrandom energies $\tilde{\epsilon}_h > 0$ on the horizontal dimer bonds. One could then check for a crossover at a then finite T_d^* and the effect of the single-line T_d^{-4}-term, which becomes of the order of the T_d^{-2}-term at T_d^*. Moreover, at low dimer temperatures the dimer free energy $-T_d \ln Z_d$ for a given disorder configuration would not simply approach a ground state energy that is independent of T_d and thus trivially account for $\overline{\ln Z_d} \sim T_d^{-1}$. Rather a new compromise between the T_d-independent reduced elastic energy and the disorder energy would have to be found at every value of T_d which, we recall, acts as disorder strength. The resultant scaling of $\overline{\ln Z_d} \propto T_d^{-\alpha}$ with unknown exponent α could be compared to the prediction $\alpha = 4/3$ implied by the replica symmetry breaking solution by Korshunov and Dotsenko [KD98].

Other thermodynamic potentials like the entropy and the internal energy of the dimer model

$$\begin{aligned} \overline{S_d} &= -\frac{\partial}{\partial T_d}\overline{F_d} = \frac{\partial}{\partial T_d}\left(T_d\overline{\ln Z_d}\right) \\ \overline{U_d} &= \overline{F_d} + T_d\overline{S_d} \end{aligned}$$

are easily calculated from the RBA solution. In the simulations, the internal energy $\overline{U_d} = \overline{\sum_D p(ij)\epsilon_{ij}}$ with the disorder-configuration-dependent occupation probability $p(ij)$ of bond (ij) can be obtained quite easily since the polynomial algorithm allows to calculate the probabilities $p(ij)$. The entropy is obtained by subtraction. A comparison of the numerical internal energy and entropy with the analytical formulae is given in Figs. D.16, D.17. Again, we use as only fit parameter the ratio between disorder correlation lengths in the two models ξ_d/b and find excellent agreement for $\xi_d/b \simeq 1$. The

slope of $\overline{S_d}$ at $T_d = 0$ is calculated from Eq. (3.61) to be

$$L^{-2}\frac{\partial}{\partial T_d}\overline{S_d}\Big|_{T_d=0} = \frac{G}{\xi_d^{1/2}} - \frac{\pi^2}{8\xi_d^{3/2}}(1-\frac{\xi_d}{2}), \tag{3.62}$$

and matches the simulation very well.

Summarising, the quantitative agreement between theory and simulations is very satisfying and for the thermodynamic potentials it is even more surprising than for the large scale stiffness. The latter is expected to show universality in the sense that it does not depend on microscopic details of the model while the former get contributions from all scales. A priori, the modes around the cutoff which is implemented, of course, differently in the continuum theory and the lattice model might have been expected to dominate and lead to incompatible results. This is not he case. Rather, the model differences on small scales can be accounted for by the *single* dimensionless fit parameter ξ_d/b.

3.2.3 Higher moments

Only the linear coefficient in n, i.e. the average free energy, of the solution to the Bethe Ansatz equations (2.31a), (2.31d) is known exactly. Higher cumulants describe sample to sample fluctuations in experimental setups of mesoscopic dimensions while for macroscopic systems their scaling will give information on the selfaveraging behaviour. The cumulants can be given analytically only in the strong disorder or dilute limit $l_d\rho = \rho/c \ll 1$, $c = \Delta g/T^3$ in a double expansion in small $(n, l_d\rho)$ [EK01]

$$\begin{aligned}\ln\overline{Z^n} &= \sum_j \frac{(-n)^j}{j!}\frac{\overline{F^j}_c}{T^j} = -\frac{L_xL_z}{2}\Big(\frac{\Delta}{T^2}\Big)^3\Big(\frac{g}{T}\Big)^2\Big\{\frac{n}{12}(1-n^2)l_d\rho + n(l_d\rho)^2 \\ &\quad -\frac{4}{3\pi}n^2(l_d\rho)^{3/2} + \left(\frac{1}{6}-\frac{1}{\pi^2}\right)n^3 l_d\rho + h.o.t.\Big\}. \end{aligned}\tag{3.63}$$

The disorder independent part of the single line free energy is dropped in the last equation as it cannot be calculated unambiguously in the path integral description. The first term in the parenthesis of Eq. (3.63) $\sim \rho$ describes the disorder contribution to the single line free energy cumulants while the following terms stem from interactions. They contain disorder dependent and independent parts, i.e., steric and entropic terms. In order to compare the RBA results for the cumulants (or moments) to the dimer model ones over the whole range of disorder strength, we look for the solution $\rho(k)$ of the RBA Equations (2.31a), (2.31d) numerically. From $\rho(k)$ the ground state energy of the quantum problem is calculated with Eq. (2.31c)

$$E_0 = \frac{T^2L_xc^2\rho}{24g}n(1-n^2) + \frac{nT^2L_x}{2g}\int_{-K}^{K} dk\; k^2\rho(k)$$

which immediately gives us the generating functional for the cumulants Eq. (2.30)

$$\ln\overline{Z^n} = -\frac{E_0(n)L_z}{T} + n\frac{L_x}{a}\ln Z_0.$$

Our approach is straightforward: Ultimately, we are interested in the coefficients of $E_0(n)$ written as a power series in the replica index n with disorder strength $c = g\Delta/T^3$ as a parameter. The comparison with the dimer model will consist in a comparison of these coefficient under variation

of disorder. We thus have to solve the coupled equations (2.31a), (2.31d) for $\rho(k)$ at fixed c and calculate $E_0(n)$ according to Eq. (2.31c). What we can do is write Eq. (2.31a) in the form

$$y = \frac{1}{n}\int_{-1}^{1} dy'\; g_n[\frac{K}{c}(y-y')]\tilde{\rho}(y') \tag{3.64}$$

with $y := k/K$, $\tilde{\rho}(y) := \rho(Ky)$ and $g_n[x] = 2\sum_{m\geq 0}\arctan[nx/(m^2+nm+x^2)]$. At fixed K/c, the dimensionless function $\tilde{\rho}(y)$ is computed by the inversion of the discretised integral equation. This inversion is quite delicate since the present kind of inverse problem is extremely badly conditioned. On the details of the numerical inversion, see below. With the solution we can calculate

$$\frac{\rho}{K} = \int_{-1}^{1} dy\; \tilde{\rho}(y).$$

The dimer model density $\rho = 1/(2b)$ fixes K and we finally know which value of c had been implied by our initially chosen K/c. In this approach we cannot – due to the coupling of the BA equations – modify n and c independently. A modified n implies a modified K, which results in a different value of c. We ought to adjust the parameter K/c in Eq. (3.64) upon change of n such that c remains constant. In practice, this is realised by the simple but time-consuming method of nested intervals. The integral equation (3.64) falls into the class of inhomogeneous Fredholm equations of the first kind. Its numerical inversion is notoriously difficult [PFTV93]. The reason is simple: Integration with a regular kernel acts as a smoothing process. The integral over the well behaved solution will differ only slightly from the integral over a suitable heavily oscillation function. In any discretisation and numerical treatment unavoidable errors will lead to very large errors in the approximate solution. If

$$\mathbf{b} = \mathbf{A}\,\mathbf{a} \tag{3.65}$$

represents the discretised version of Eq. (3.64) with $\mathbf{a}$ the solution and $\mathbf{b}$ the known left hand side of the integral equation then the discrete version $\mathbf{A}$ of the integral kernel is a very badly conditioned matrix, i.e., many of its entries are of the same order of magnitude. Upon inversion errors are heavily amplified. In practice, inversion theory becomes an optimisation problem [PFTV93]. 'Smoothness' (or maybe some other a priori information on the solution) has to be traded off against exact agreement – 'sharpness' – with the left hand side. This may sound more arbitrary than it is in our case. Different from the problem of modelling a finite set of statistical data we can increase the number of discretisation points at will. Convergence of the solution with a finer grid allows us to find the *unique* solution. To become specific: The way we enforce smoothness of the approximate solution is the well known linear algebra method of singular value decomposition (SVD) [PFTV93]. Consider the set of linear equations 3.65. What SVD will do for us is find either (a) the solution $\mathbf{a}$ with minimum modulus $|\mathbf{a}| = \sum_i a_i$ if the solution is degenerate, or (b) the vector $\mathbf{a}$ which minimises $|\mathbf{b} - \mathbf{A}\,\mathbf{a}|$ if $\mathbf{A}$ cannot be inverted. We make use of case (a) and choose in the discretisation the dimension N of the left hand side vector $\mathbf{b}$ smaller than the dimension M of $\mathbf{a}$. For a good convergence of the resulting approximate solution, the numerics show that a factor of $M/N \simeq 2$ puts the appropriate weight on a small modulus, by which large oscillations are suppressed and smoothness of the solution is assured.

The kernel Eq. (2.31b)

$$g_n(x) = 2\sum_{m\geq 0}\arctan[\frac{nx}{m^2+nm+x^2}]$$

is antisymmetric. This implies $\rho(k) = \rho(-k)$ and allows to restrict the integral to positive values of k'

$$nk = \int_0^K dk'\ \rho(k')\left\{g_n[(k-k')/c] + g_n[(k+k')/c]\right\}.$$

A factor of 2 in computation time at a given discretisation level is gained.
The following properties of the kernel $g_n(k/c)$, plotted in Fig. D.10, are noteworthy:

- A jump at $k = 0$: $\lim_{x\to\pm 0} g_n(x) = \pm\pi$.
- In both limits $c \to 0$ and $n \to 1$, $g_n(k/c)/n \to \pi\,\mathrm{sgn}(k)$. This is of course the free fermion limit with $\rho(k) = 1/(2\pi)$, $K = k_F = \pi/a$ and $E_0 = \hbar^2 L_x \pi^2/(6ma^3)$. In these limits all of the terms in $g_n(x)$ contribute. Numerically, this has been accounted for by an extrapolation routine for the evaluation of the kernel at the discretisation points.
- In the limit $n \to 0$ only the first order in n of $g_n(x)$ contributes. The resulting integral equation has also been derived in the context of a single polymer in disorder which maps on 1D interacting bosons [Kar87] and can be solved analytically to give the average free energy of Eq. (2.32) [EK01, EB03].
- c stretches $g_n(k/c)/n$ along the abscissa, n does so along the ordinate. The change of the kernel $\Delta g_n(y)/n$ over a discrete step Δy increases with $1/(nc)$. In order to keep up a given level of accuracy, $\frac{1}{n}\Delta g_n(y)/\Delta y$ has to remain fixed. The number of discretisation points thus has to increase like $1/(nc)$. We are unfortunately interested in small n as we want to extract the Taylor coefficients of $E_0(n)$ at $n = 0$ and moreover in small c as the result for large c is known analytically.

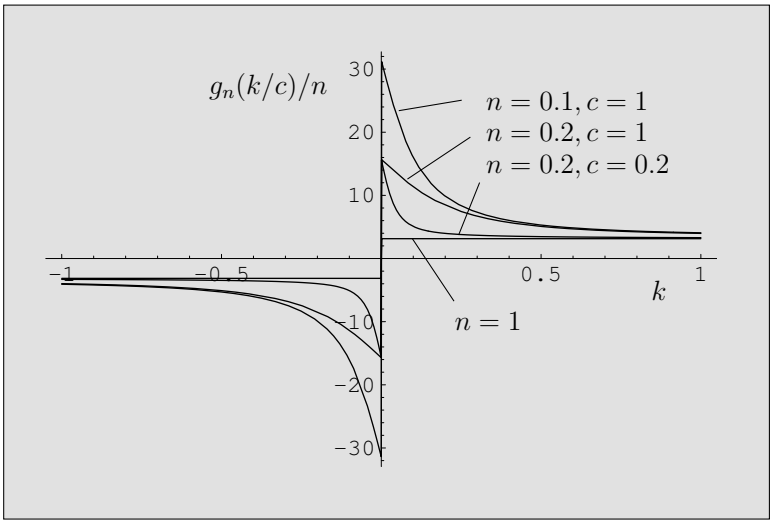

Fig. D.10: The kernel $g_n(k/c)/n$ of the BA integral equation; k, c in units of b^{-1}.

The above described solution scheme was implemented in the programming language C with the use of Numerical Recipe routines [PFTV93]. The data for the lowest disorder values, see Table D.3,

disorder c	$E_1^{\rm num}$ [$\pm 0.5\%$]	$E_1^{\rm exact}$	$E_2^{\rm num}$ [$\pm 5\%$]	$E_2^{\rm pert}$	$E_3^{\rm num}$ [$\pm 15\%$]	$E_3^{\rm pert}$
0.1	0.437	0.4364	-0.0279	-0.00479	0.0012	0.00033
0.5	0.537	0.5362	-0.137	-0.0531	0.011	0.0082
1	0.661	0.6612	-0.290	-0.1501	0.040	0.0327
1.5	0.786	0.7863	-0.448	-0.2756	–	–
2	0.911	0.911	-0.65	-0.424	0.16	0.131
3	1.16	1.161	-1.07	-0.780	0.35	0.294
5	1.65	1.661	-2.03	-1.678	0.86	0.817
7	2.16	2.161	-3.28	-2.779	1.92	1.60
10	2.91	2.911	-5.32	-4.745	3.7	3.27
12	3.40	3.411	-6.81	-6.24	4.9	4.70
20	5.41	5.411	-14.25	-13.42	14	13.1
25	6.65	6.661	-19.5	-18.76	23	20.4
30	7.89	7.911	-25.6	-24.66	32	29.4
40	10.39	10.411	-39.4	-37.96	61	52.3
50	12.90	12.911	-54.6	-53.05	95	81.7
75	19.14	19.161	-97.7	-97.46	187	183.8
100	25.35	25.411	-151.4	-150.05	357	327
200	50.34	50.411	-423	-424.41	1360	1307

Table D.3: Data for the determination of the free energy cumulants. Given are the coefficients of $\tilde{E}_0(n)$, see Eq. (3.67) as obtained by the numerical solution of the Bethe Ansatz equations (num.). The disorder parameter c is written in units of b^{-1}, the coefficients in units of b^{-3}. The superscript 'pert' stands for values from the perturbative solution Eq. (3.63). The errors given relate to the least accurate values at small c. For large c the errors decrease.

needed the highest discretisation level and consumed about 200h computation time on a 2GHz processor for the determination of the cumulants at fixed disorder c. A typical plot of $\tilde{\rho}(y)$ is given in Fig. D.18 and a plot of E_0 (in units of $2mb^3/(\hbar^2 nL_x)$) against n is given in Fig. D.19. The Taylor coefficients of $E_0(n)$ are obtained by repeated extrapolation to $n=0$, subtraction of this value from the finite-n ones and division over n. This straightforward procedure is the best we could think of but still very error-prone. While the desire for a small extrapolation error requires having points as close as possible to $n=0$, a simple calculation of error propagation shows that the error of a given data point at finite n goes as $n^{-2k}\Delta E_0$, where k stands for the order of the Taylor coefficient and ΔE_0 for the original error of the data. We therefore could extract reliable values only for cumulants as high as $k=2,3,4$. Moreover, the perturbative strong disorder solution for the cumulants Eq. (3.63) indicates that with increasing disorder c the Taylor coefficients decrease faster with the order. Their error will thus at small disorder be quickly of the size of the value itself. Again we find that the numerical computation for large c is easier just like the analytical calculation in this limit. The reliability of the numerics can be checked in limiting cases where analytical results are available. The limit of small c or $n \to 1$ should give the free fermion constant density $\rho(k) = 1/(2\pi)$. In Fig. D.20, a plot of the numerical solution in this case is shown, the agreement is very good. For $n \to 0$, the

density can be given perturbatively in K/c [EK01] as

$$\lim_{n\to 0}\rho(k)=\sqrt{1-\frac{k^2}{K^2}}\left\{\frac{1}{2\pi}\frac{K}{c}-\frac{\pi}{24}\left(\frac{K}{c}\right)^3+\mathcal{O}\left((K/c)^5\right)\right\}. \tag{3.66}$$

We compare the numerical solution for $n=0.001$ and $K/c=0.1$ with the above formula in Fig. D.21, again the result is satisfactory. We can also check against the exact results for the average free energy, i.e., the coefficient of the linear term, and the strong disorder limit of the cumulants, see Table D.3 and the plots below. In Table D.3 the coefficients $\{E_j\}$ of

$$\tilde{E}_0(n):=\int_{-K}^{K}dk\;k^2\rho(k)=K^3\int_{-1}^{1}dy\;y^2\tilde{\rho}(y)=\sum_{j\geq 0}E_{j+1}n^j \tag{3.67}$$

are given in units of $1/b^3$ for various values of c. Note that we have shifted the index in the series in order to point out that the p^{th} cumulant can be calculated from E_p.
For the comparison with the dimer model, we focus on the moments of the logarithm of the partition function rather than the free energy due to the different meaning of the temperatures in the two models. The cumulants

$$\overline{(\ln Z_l)_c^p}=\frac{\partial^p}{\partial n^p}\ln\overline{Z^n}\Big|_{n=0} \tag{3.68}$$

can be read off from the partition function of the replica problem, here given in terms of the coefficients of the numerical RBA solution

$$\ln\overline{Z^n}=\sum_{j\geq 1}\frac{(-n)^j}{j!}\frac{\overline{F^j}_c}{T^j}=-L_zL_x\frac{\rho g}{24T}\big(\frac{\Delta}{T^2}\big)^2n(1-n^2)-L_zL_x\frac{nT}{2g}\tilde{E}_0(n). \tag{3.69}$$

For the variance (2nd cumulant) and the skewness (3rd cumulant) we write the explicit formulas together with the expressions from the perturbative BA solution Eq. (3.63)

$$\overline{(\ln Z_l)_c^2}=\begin{cases}-A_l\dfrac{T}{g}E_2 & \text{full BA solution}\\ A_l\dfrac{4}{3\pi}\big(\dfrac{\Delta}{aT^2}\big)^{3/2}\big(\dfrac{g}{T}\big)^{1/2}\to A_l\dfrac{2}{3\pi}\dfrac{\xi_d^{3/2}}{T_d^3} & \text{perturbative}\end{cases} \tag{3.70}$$

$$\overline{(\ln Z_l)_c^3}=\begin{cases}6A_l\Big\{\big(\dfrac{\Delta}{T^2}\big)^2\dfrac{g}{T}\dfrac{1}{24a}-\dfrac{T}{2g}E_3\Big\} & \text{full BA solution}\\ 6A_l\big(\dfrac{\Delta}{T^2}\big)^2\dfrac{g}{T}\dfrac{1}{2a}\Big\{\dfrac{1}{12}-\big(\dfrac{1}{6}-\dfrac{1}{\pi^2}\big)\Big\}\to A_l\dfrac{3\xi_d^2}{T_d^4}\big(\dfrac{1}{\pi^2}-\dfrac{1}{12}\big) & \text{perturbative}\end{cases} \tag{3.71}$$

The parameter mapping for the case of no energy on the horizontal bonds $\tilde{\epsilon}_h=0$, $gb/T\to 2$, $\Delta/T^2\to\xi_d/T_d^2$, $a\to 2b$, has been applied to the perturbative solution. One more point should be kept in mind for the comparison, that is the rescaling of the volume Eq. (3.52)

$$A_l/A_d=\frac{ag}{\pi T}\big(1+\frac{ag\Delta}{\pi^2T^3}\big)^{-1/2}\to\frac{4}{\pi}\big(1+\frac{4\xi_d}{\pi^2T_d^2}\big)^{-1/2},$$

where the mapping again assumes the case $\tilde{\epsilon}_h=0$.
In the comparison below, we plot the quantity

$$\overline{(\ln Z_l)_c^p}/A_d=\overline{(\ln Z_l)_c^p}/A_l\times A_l/A_d=\overline{(\ln Z_d+E_{\text{ref}}/T_d)_c^p}/A_d.$$

It should be noted that for higher moments the energy relation Eq. (3.45) that brings in the reference energy in the above relation has to be remembered, while in the average free energy its contribution had been disorder-averaged to zero.

In replica theory the *cumulants* of random thermodynamic quantities appear naturally, while in simulations the *moments* are immediately accessible. The cumulants are polynomial combinations of the moments of the respective random variable. If the generating functional of the moments $\{m_p\}$ is

$$M(n) = 1 + nm_1 + n^2\frac{m_2}{2!} + n^3\frac{m_3}{3!} + \ldots,$$

then

$$K(n) := \ln M(n) = n\kappa_1 + n^2\frac{\kappa_2}{2!} + n^3\frac{\kappa_3}{3!} + \ldots$$

generates the cumulants $\{\kappa_p\}$. The lowest cumulants expressed in terms of moments are

$$\begin{aligned}
\kappa_1 &= m_1 \\
\kappa_2 &= m_2 - m_1^2 \\
\kappa_3 &= m_3 - 3m_1m_2 + 2m_1^3 \\
\kappa_4 &= m_4 - 4m_1m_3 - 3m_2^2 + 12m_1^2m_2 - 6m_1^4.
\end{aligned} \tag{3.72}$$

From the dependence of Eq. (3.69) on the system size $A_l = L_x \times L_z$ it follows immediately that all of the free energy cumulants scale linearly in A_l. Apart from the average free energy, the reduced cumulants $\kappa_p/\kappa_1^p = \overline{F_c^p}/\overline{F}^p$ hence vanish in the thermodynamic limit as $\overline{F_c^p}/\overline{F}^p \sim A^{1-p}$. This is nothing but the central limit theorem (CLT) at work: The distribution of the free energy becomes infinitely sharp in the limit of large systems. In other words, the vortex line array is self averaging which in light of the infinite correlation length reflected by logarithmic correlations had not been evident a priori. For the numerical determination of the cumulants the following problem is entailed. Immediately accessible in the simulations of the dimer model are the *moments* m_p of the free energy distribution. They scale with the system size like $m_p \sim A^p$. Looking at Eqs. (3.72), we see that the cumulant of order p has to be calculated as the sum of terms that grow by a factor A^{p-1} faster with the system size. Therefore, at a given accuracy of the dimer data, which primarily depends upon the number of disorder realisations, a limit is set to the system size up to where cumulants can be obtained in a reliable way. This maximum system size decreases with the order of the cumulant as the scaling A^p of the terms on the r.h.s. of Eq. (3.72) shows. On the other hand, finite size effects have to be minimised as well and, as a consequence, only the variance and the third cumulant can be obtained from the dimer data reasonably.

Figs. D.25 and D.26 are used to determine the maximum size L up to which the second moment should be compared. The data of the moments produced by the group at Washington have an accuracy of approximately 10^{-5}. Plot D.25 shows that only for sizes $L \lesssim 64$, the second cumulant of the free energy can be trusted for the range $T_d = 0.01..10$. Fig. D.26 demonstrates how the data for sizes $L = 128$ and $L = 256$ deviate at large T_d from the reliable data for $L = 16, 32, 64$. The overlap of the small sizes excludes the deviation of the large ones to be a finite size effect.

We therefore compare the variance of the free energy $\overline{(Z_l)_c^2}/L^2$ (where L^2 is the dimer volume) as obtained in the dimer model for $L = 64$ to the new numerical solution of the RBA equation in Figs. D.22, D.23. With the only fitting parameter $\xi_d \simeq 0.8$ the agreement is very good. Note the

very small but consistent deviation of both the dimer results and the numerical BA solution from a pure power law, which is a straight line in the logarithmic plot of the figures. In Fig. D.24 the data for the dimer system size $L = 256$ are plotted both against the numerical BA solution and the perturbative analytical solution of Eq. (3.63). The perturbative solution is good only for dimer temperatures $T_d \lesssim 1$, as expected. The misfit between the numerical BA solution and dimer data is due to the above described numerical errors in the simulation for the large system. Fig. D.27 serves as a demonstration of the negligible size of the cumulants with respect to the moments. The moments are fitted with the respective powers of the analytical expression for the first moment only, this amounts to setting all the cumulants apart from the average to zero. The misfit cannot be detected on the given scale.

The third cumulant – or skewness – of the partition function $\overline{(Z_l)_c^3}/L^2$ is compared in Fig. D.28. The dimer data are to be trusted only for the small system $L = 16$ and here only for $T_d \lesssim 1$, as demonstrated in Fig. D.29. In this range, no substantial deviations from the perturbative evaluation of the cumulant Eq. (3.71) is expected. Indeed, the agreement between theory and simulation is again very good, see Fig. D.28, with $xi_d = 0.8$. Although the data from the numerical solution of the full BA equation have an error of only $\sim 15\%$, they are of no use. The reason is the following. In Eq. (3.71), first line, the size of the second term with numerically determined values E_3 is throughout the parameter range about 85% of the first term. Since the terms are subtracted, the original error of 15% becomes an error of $\sim 100\%$ in the final expression for the third cumulant. For the moment, not much is lost since the perturbative solution could not have been improved considerably in the range $T_d \lesssim 1$ which is set by the dimer numerics at hand.
It must be noted that in order to fit the third cumulant, the term $\sim n^3$ from the term $\sim n/12(1-n^2)$ in Eq. (3.63) was essential, otherwise not even the sign of the cumulant would have matched. Now this term $\sim (g/T)(\Delta^2/T^4)n/12(1-n^2)$ in $\ln \overline{Z^n}$ is proportional to the density and essentially the single line result of Ref. [KN85]. The part $\sim n$ stemming from here we dropped in the discussion of the average free energy because we could not find the predicted power of disorder Δ^2 and we argued that this term is ineffective due to a vanishing microscopic stiffness $g_{s.sc.}/T = 0$. This argument seems a little debatable from the present perspective. Maybe even the relica solution for the single line problem has to be reconsidered.

3.2.4 Response functions

The disorder averaged specific heat of the *isotropic* dimer model with random energy on horizontal and vertical bonds

$$\overline{c_d} = L^{-2} T_d \frac{\partial}{\partial T_d} \overline{S_d} \tag{3.73}$$

$$= L^{-2} \frac{\partial}{\partial T_d} \overline{U_d} = L^{-2} T_d \frac{\partial^2}{\partial T_d^2} (T_d \overline{\ln Z_d}) \tag{3.74}$$

can be measured in the isotropic dimer model via the thermal fluctuations of the dimer energy

$$\overline{c_d} = L^{-2} \frac{\overline{\langle H_d^2 \rangle - \langle H_d \rangle^2}}{T_d^2}. \tag{3.75}$$

From the Bethe Ansatz free energy Eq. (2.32) (again without the Δ^2-term in the single line free energy) it is calculated easily by taking the derivatives after the mapping $\frac{\Delta}{T^2} = \frac{2\xi_d}{T_d^2}$

$$\overline{c_d} \quad = \quad 2T_d \frac{T_d^2\pi^2(2\pi^2 - \xi_d\pi^2 - 4\xi_d G) + 4\xi_d(\pi^2\xi_d + 16\xi_d G - 2\pi^2)}{(\pi^2 T_d^2 + 8\xi_d)^{5/2}}. \tag{3.76}$$

This formula compares very well to the simulations, see Fig. D.31 where the value of $\xi_d = 0.98$ is chosen.

If the agreement was only due to to special values of fitting parameters and not based on the identity of the models one would need a parameter for each of the following, at least: the position and height of the maximum, the slope for small T_d, the position and value of the turning point beyond the maximum. There is, however, only one fitting parameter ξ_d in Fig. D.31. Also note that the dimer specific heat probes for the agreement of the two models predominantly in the region around $T_d \simeq 1$ – the drop to zero for small and large T_d being generic rather than specific –, so it can be considered complementary to the free energy, which tested for amplitude and exponent at small T_d while the large T_d (or pure) limit was fixed by hand to the exactly known result, see Section 3.2.2.

The linear low temperature behaviour of the specific is typical of random systems and can easily be understood by looking at the lowest-lying excitations on a given scale ℓ. On each scale, for a given disorder environment the groundstate (with zero energy) and the lowest excitation (with energy E) form a two level system (TLS), whose specific heat is

$$c_{\ell,E} = \frac{\partial}{\partial T}\frac{Ee^{-E/T}}{e^{-E/T}+1}.$$

The excitation energies obey now a disorder distribution $p_\ell(E)$ and the contribution to the average specific heat from each scale is

$$\Delta\overline{c}_\ell \; L^2 = \int_0^\infty dE \; p_\ell(E) c_{\ell,E}.$$

For a finite density of excitations at small energies, $\lim_{E\to 0} p_\ell(E) > 0$, the specific heat as a superposition of exponential laws from each scale will be *linear* at $T = 0$, which is the famous insight of Anderson *et al.* [AHV72]. Integration over all lengthscales with the density of excitation (not distinguishing energies) $p(\ell)$ allows to write the specific heat as

$$\overline{c} = \int_0^L d\ell \; p(\ell) \; \Delta\overline{c}_\ell,$$

which becomes exact in the limit $T \to 0$. Now the low lying excitations, or secondary minima, are the central quantity of droplet theory – originally developed in the field of spin glasses [FH87, FH88] – namely the droplets. For their disorder distribution function, a scaling ansatz

$$p_\ell(E) \simeq \frac{1}{\gamma\ell^\Theta}\tilde{p}\big(\frac{E}{\gamma\ell^\Theta}\big)$$

with γ a constant and $\Theta = d - 2 + 2\zeta$, ζ being the roughness exponent of the problem under consideration, has repeatedly been suggested [FH88, NS00]. In our case of the dimer model, $d = 2$ and $\zeta = 0$, see the logarithmic roughness in the line array, and one expects logarithmic corrections to the scaling ansatz.

From the finite size scaling of the specific heat one can hope to obtain information on the droplet distribution as with growing size larger droplets will fit into the system. However, these bulk droplets seem to be dominated by the system boundaries. The number of the secondary minima on the boundaries scales like the linear size L giving a $1/L$-decay (instead of growth from bulk droplets) in the specific heat. Low-lying excitations on the boundary can be easily identified. Consider a bond on the boundary that is occupied in the groundstate. A configuration that does not cover this very bond may remain unchanged on all the other bonds since simulations are done with open boundary conditions. The missing energy on the bond is the excitation energy, whose probability distribution, however, is nontrivial. It is the probability $p_{\mathrm{occ}}(E)$ that a boundary bond carries energy E under the condition that it is occupied. This conditional probability can be related to the conditional probability that a bond is occupied given its energy $p_E(\mathrm{occ}) = p_{\mathrm{occ}}(E)p(E)/p(\mathrm{occ})$, with $p(\mathrm{occ}), p(E)$ being unconditional probabilities for the occupation and energy $\epsilon_{ij} = E$ of a bond, respectively. The latter conditional probability is just the probability $p(ij)$ mentioned above in the measurement of the internal energy $p(ij) = p_E(\mathrm{occ})$. It can be obtained rather easily from the dimer algorithm and would allow to compute the prefactor of the $1/L$-decay in the scaling of the $T_d = 0$-slope of the specific heat, see Fig. D.30. The smallest excitation in the bulk is likewise easily identified as the rotation of a plaquette that consists of two opposite dimers. The probability distribution for the energy difference of the two configurations is, however, not easily obtained. It is complicated by the condition that the two dimers before the flip must be part of the groundstate configuration. In the simulations, it should be stressed, statistics of droplet energies can in principle be measured systematically in the following straightforward procedure. For a given disorder configuration the groundstate dimer covering is determined. Then the energy of one arbitrary *occupied* bond in the bulk is set to infinity and the new groundstate is determined. It will not contain the bond with infinite energy and hence have higher energy than the original groundstate. The energy difference E together with the diameter l of the nonoverlapping region of the two groundstates is stored. The statistics of these pairs of values for many disorder realisations gives the droplet distribution $p_l(E)$. Quantitative support of the scaling prediction of droplet theory is in reach considering the orders of magnitude over which the dimer model can be simulated.

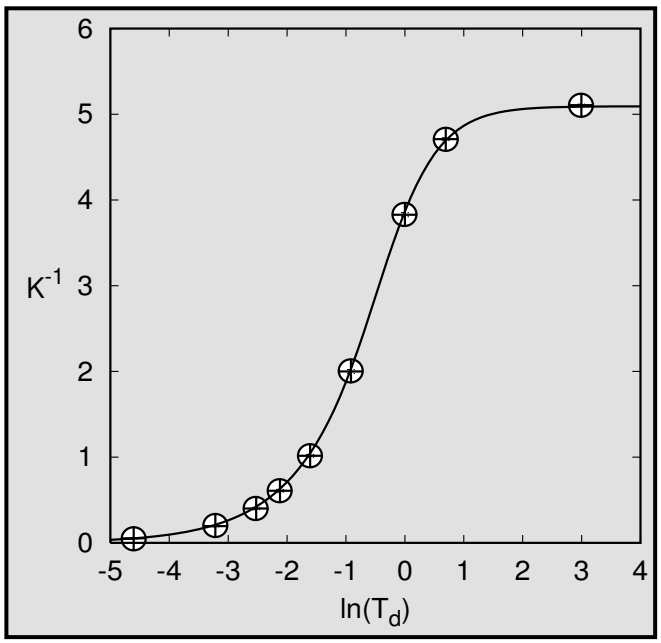

Fig. D.11: Plot of K as a function of the dimer temperature T_d. The line is the analytical result, the crosses are from simulations of the original isotropic dimer model; $\xi_d = 1.15$.

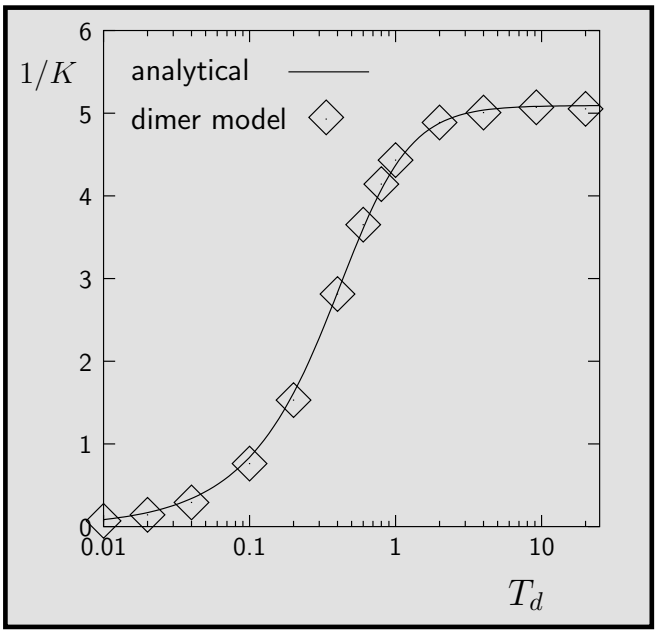

Fig. D.12: Plot of K as a function of the dimer temperature T_d; $\tilde{\epsilon}_h = 0$, $\xi_d = 0.83$.

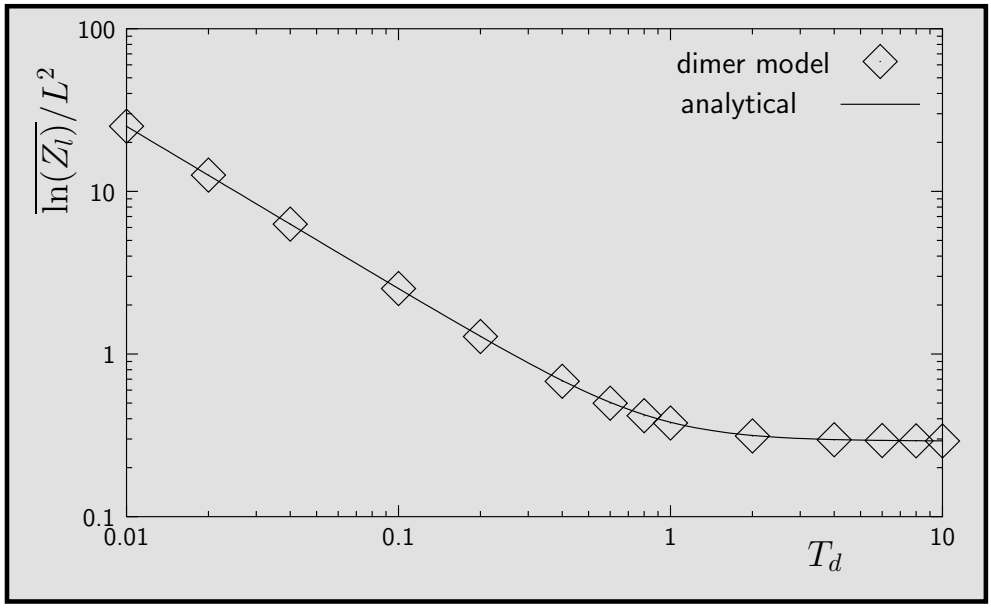

Fig. D.13: Comparison of the disorder averaged free energy for $\tilde{\epsilon}_h = 0$, $L = 256$, $\xi_d = 1.00$; dimer temperature $T_d \sim 1/\sqrt{\Delta}$ is inverse measure of disorder strength in the vortex problem.

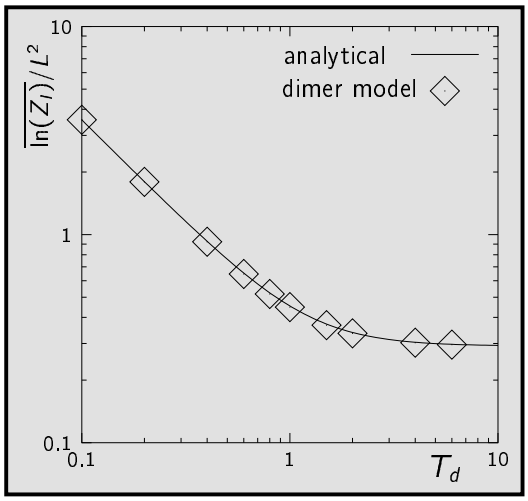

Fig. D.14: Comparison of the disorder averaged free energy; isotropic dimer model, $L = 512$, $\xi_d = 0.96$.

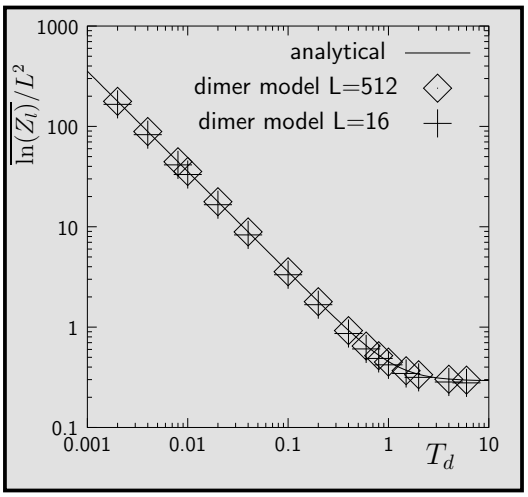

Fig. D.15: Size dependence of the numerical free energy density; data for $L = 16, 512$ compared to analytical result for the t.d. limit; isotropic dimer model, $\xi_d = 0.96$.

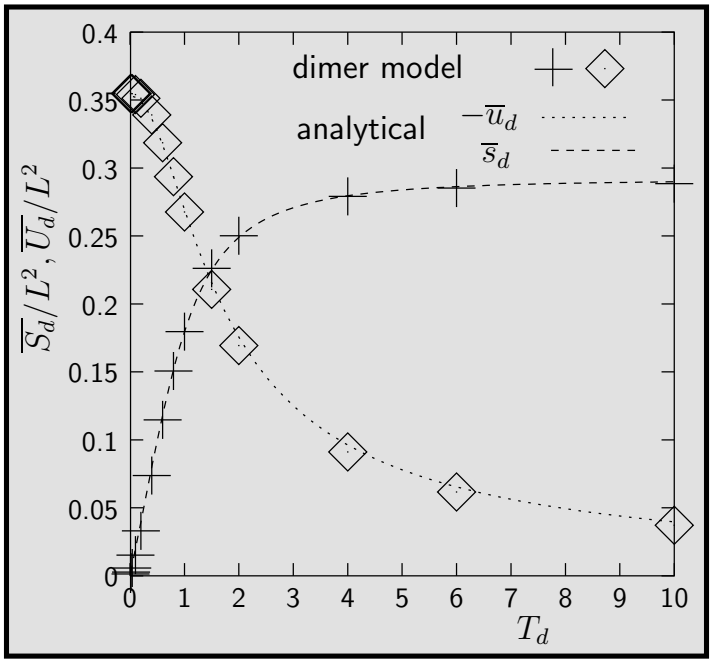

Fig. D.16: Comparison of average dimer model entropy $\overline{s_d}$ and internal energy $\overline{u_d}$ with only fitting parameter $\xi_d = 0.98$ (entropy) and $\xi_d = 1.00$ (internal energy); $L = 256$, $\tilde{\epsilon}_h = 0$.

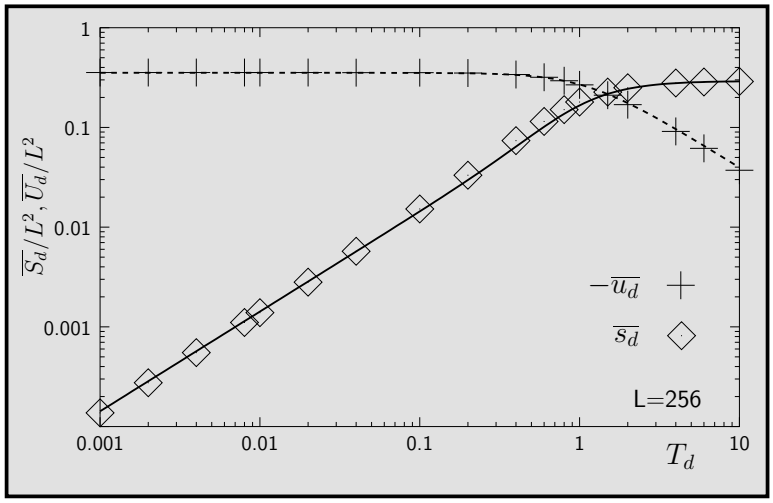

Fig. D.17: Entropy and internal energy in logarithmic plot. The lines are analytical curves with $\xi_d = 0.92$ for the entropy and $\xi_d = 0.99$ for the internal energy; $\tilde{\epsilon}_h = 0$, $L = 256$.

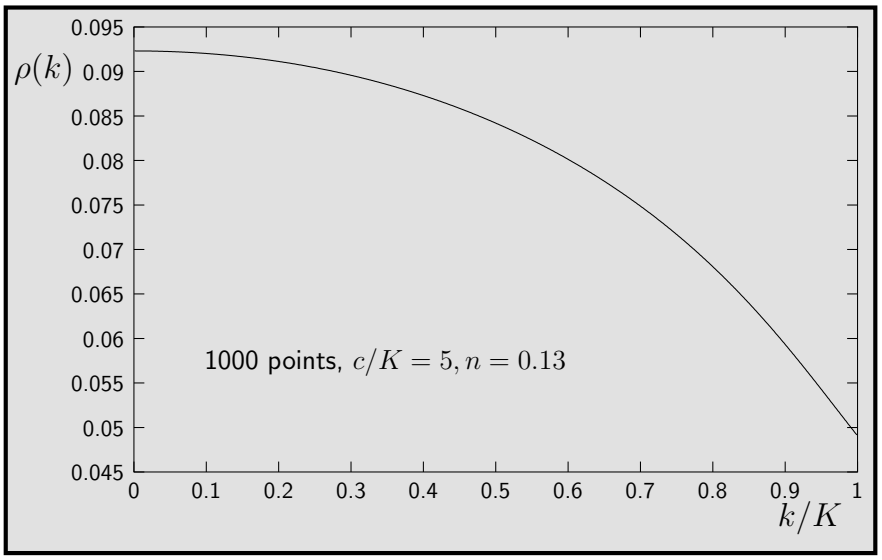

Fig. D.18: Typical Bethe Ansatz equation solution $\rho(k)$ at 1000 discretisation steps; takes approx. 1h.

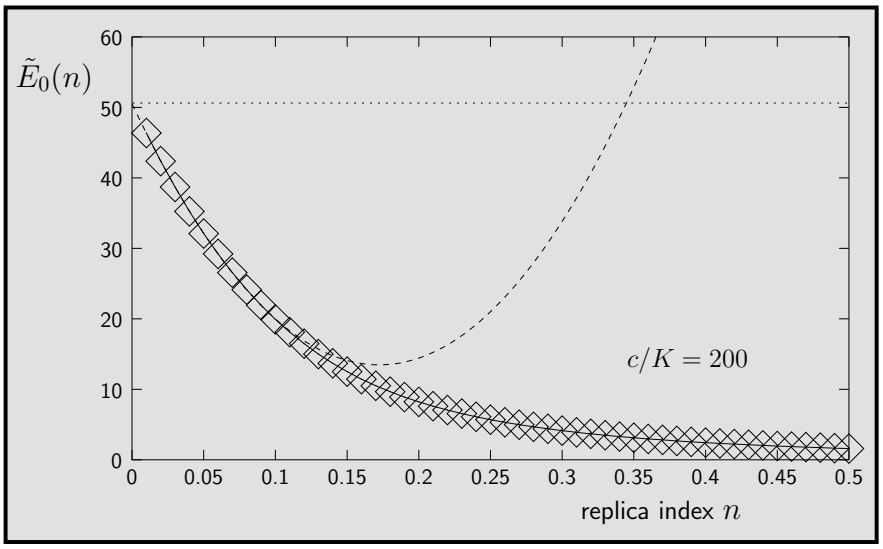

Fig. D.19: Typical plot of the SU(n) fermion groundstate energy $\tilde{E}_0$ as a function of the replica index n. The dotted line is the exactly known limit for $n \to 0$, the dashed line is a polynomial fit for small n. The Taylor coefficients at $n = 0$ give the free energy cumulants of the vortex line problem.

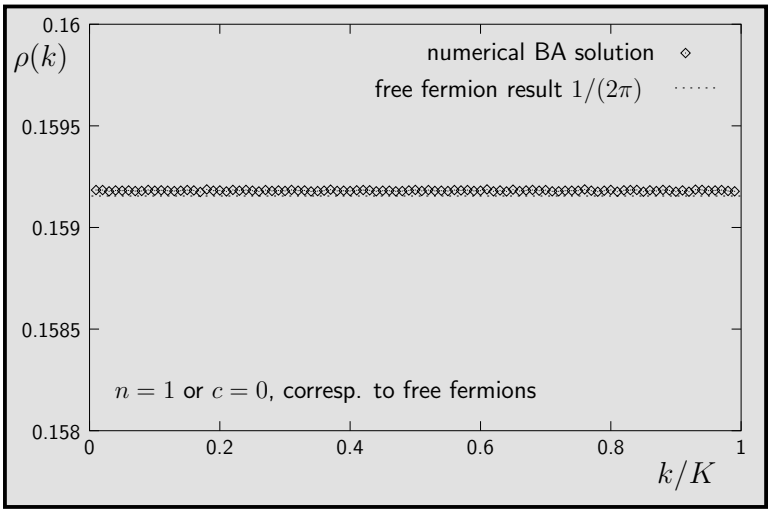

Fig. D.20: $\rho(k)$ in the limit $c/K \to 0$. Comparison to the free fermion value $\rho = 1/(2\pi)$ serves as check of numerics.

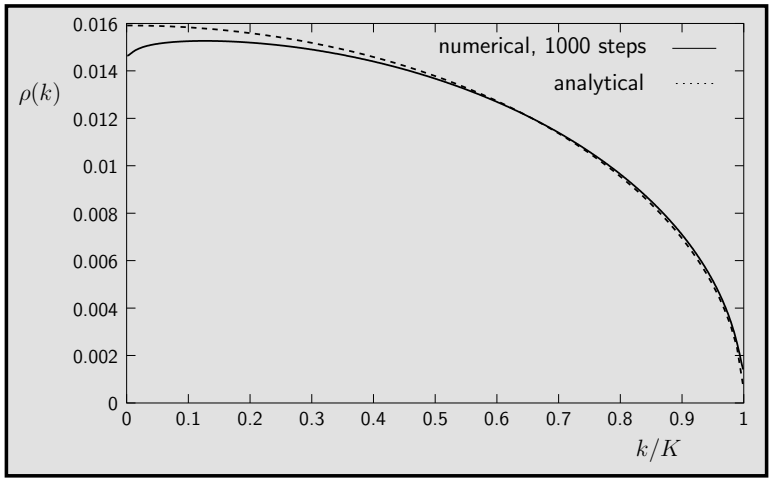

Fig. D.21: $\rho(k)$ in the limit $c/K \to \infty$. Comparison of data for $n = 0.001$, $c/K = 10$, 1000 steps, to the analytical expression Eq. (3.66) as check of numerics. Mismatch at $k/K \simeq 1$ due to finite n, mismatch at $k/K \simeq 0$ vanishes with increasing number of discretisation steps. Small n requires high discretisation level, the region around $k/K \simeq 0$ contributes, however, only weakly to the groundstate energy. For the extraction of cumulants, higher values of n are used where the mismatch vanishes.

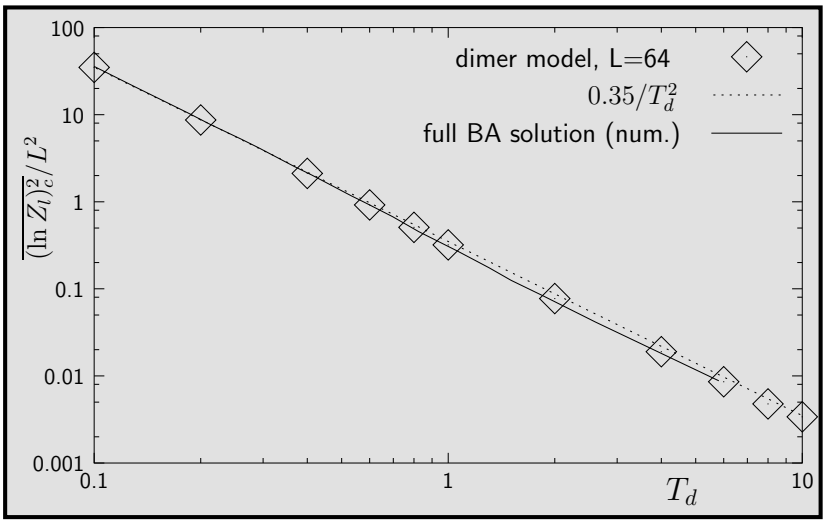

Fig. D.22: Free energy fluctuations $\overline{(\ln Z_l)_c^2}/L^2$. Dimer data ($L = 64$) and numerical solution of full BA equation are compared. The dotted line is a pure power law as a guide to the eye only. Dimer temperature $T_d \sim 1/\sqrt{\Delta}$ measures inverse disorder strength; $\tilde{\epsilon}_h = 0$, $\xi_d = 0.8$.

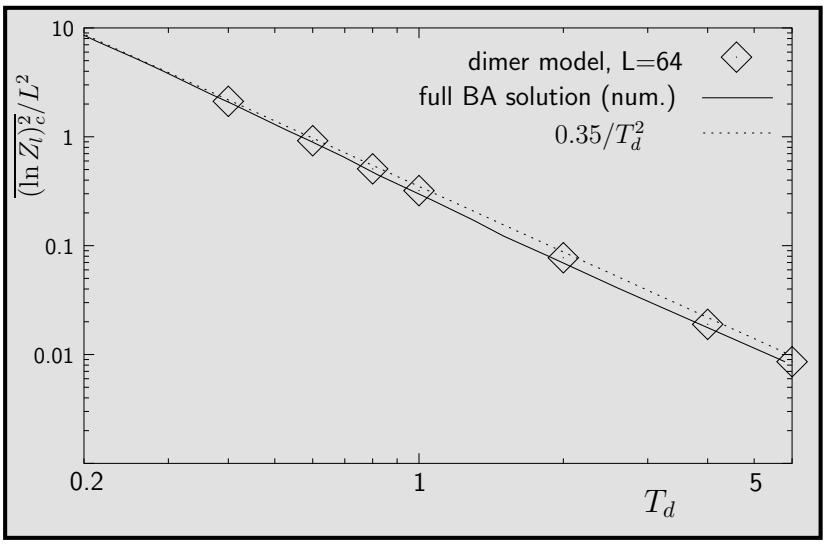

Fig. D.23: Same as Fig. D.22, smaller range of T_d, shows consistent deviation of dimer data and numerical BA solution from a pure powerlaw at large T_d.

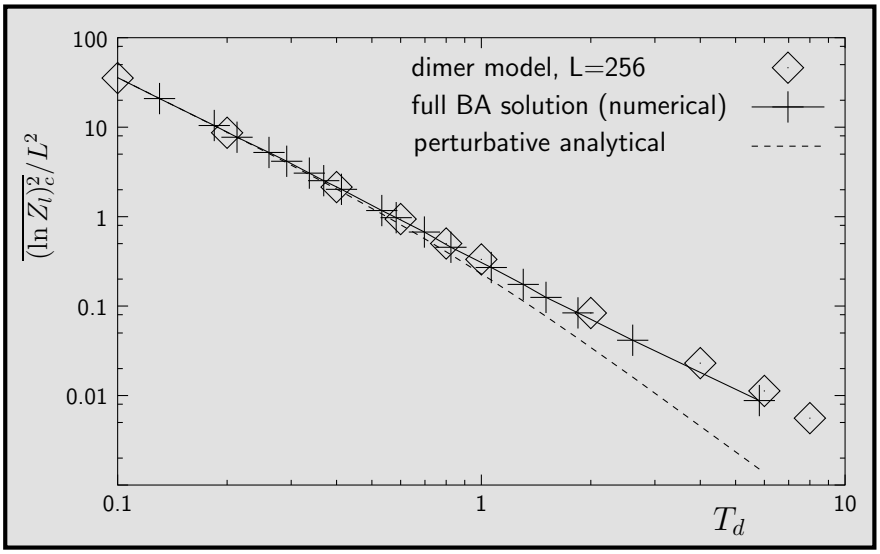

Fig. D.24: Comparison of numerical BA solution for free energy fluctuations (crosses and solid line) to perturbative analytical solution (dashed line). Diamonds are dimer results which are not reliable for $T_d \gtrsim 2$, see Fig. D.25; $\tilde{\epsilon}_h = 0$, $L = 256$, $\xi_d = 0.8$.

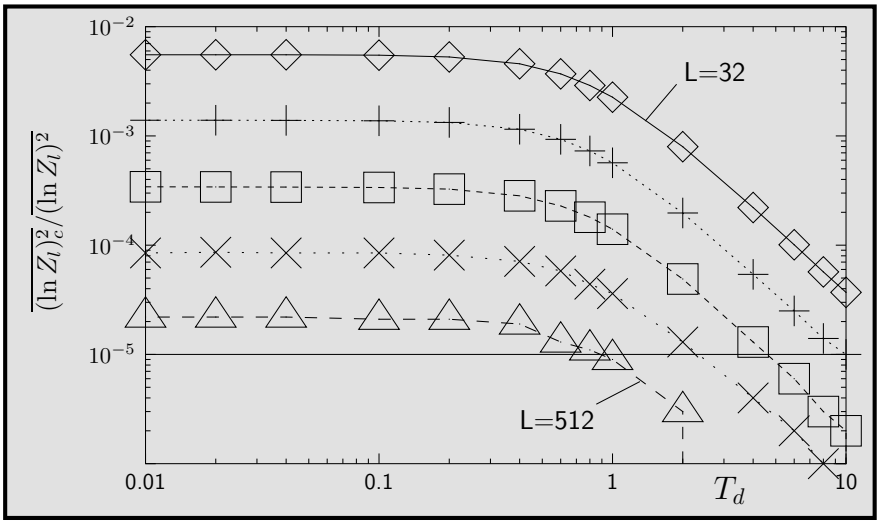

Fig. D.25: Second free energy cumulant over second moment for sizes $L = 32, 64, 128, 256, 512$ as measured in the dimer model, no analytical curves. Accuracy of dimer numerics is $\simeq 10^{-5}$, for $L > 64$ the accuracy is not sufficient for the determination of a reliable free energy variance at $T_d \lesssim 10$.

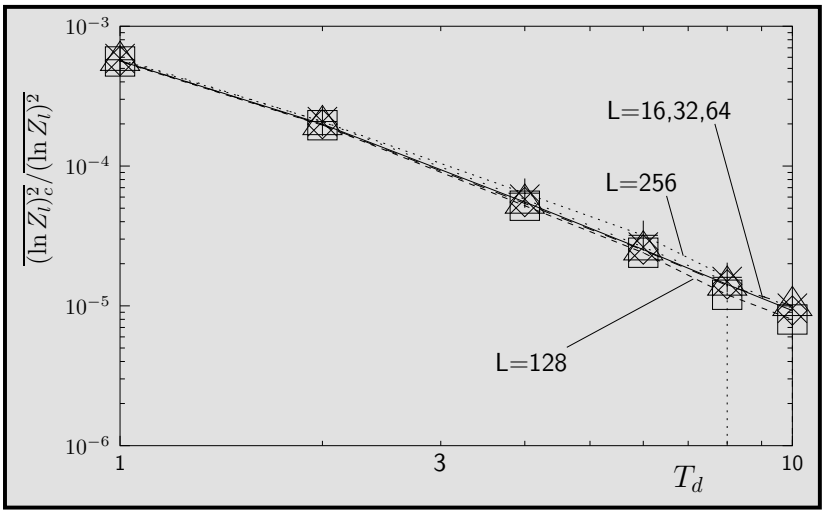

Fig. D.26: Second free energy cumulant over second moment, normalised to comparison with $L = 64$; convergence of data for $L \leq 64$, data for $L = 128$ and $L = 256$ deviate for large T_d due to accuracy limitations in the measured moments.

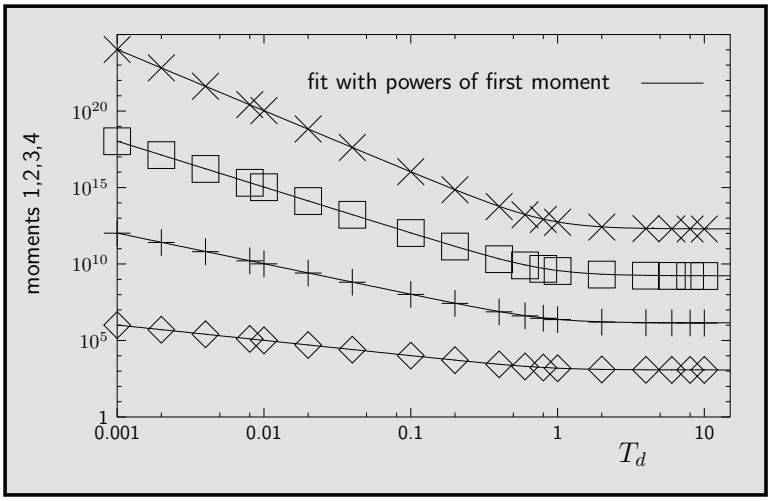

Fig. D.27: Fit of moments $p = 1 \ldots 4$ of the disorder distributed free energy $\overline{(\ln Z_d)^p}$ with powers of the analytical expression for the first moment; $\tilde{\epsilon}_h = 0$, $L = 256$. The mismatch between fit and curve (not visible at given scale) is proportional to size of cumulants. The relative vanishing of cumulants as expected from CLT is demonstrated.

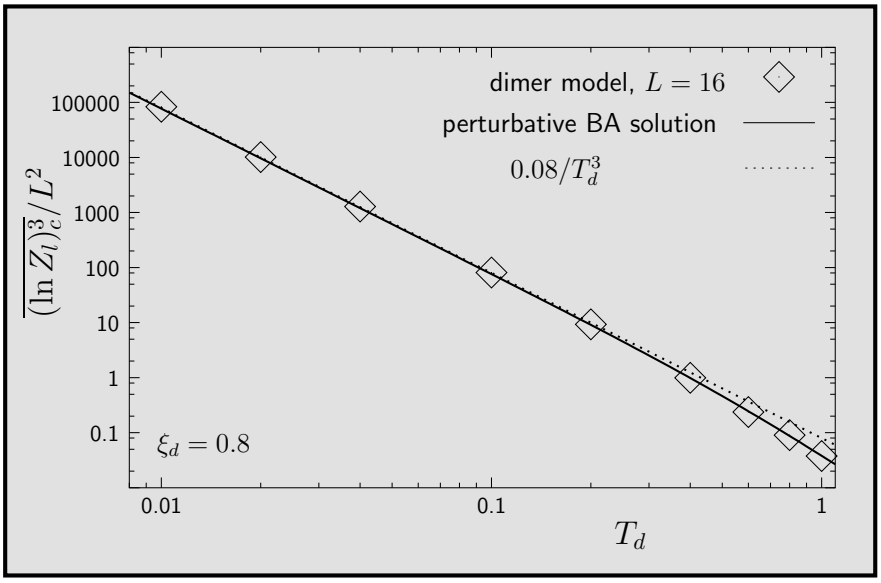

Fig. D.28: Third cumulant of free energy $\overline{(\ln Z_l)_c^3}/L^2$, comparison of dimer model (diamonds) to analytical perturbative results (full line); dimer data are not reliable for $T_d \gtrsim 1$, see Fig. D.29; the dotted line is a powerlaw as a guide to the eye only; $\tilde{\epsilon}_h = 0$, $\xi_d = 0.8$, $L = 16$.

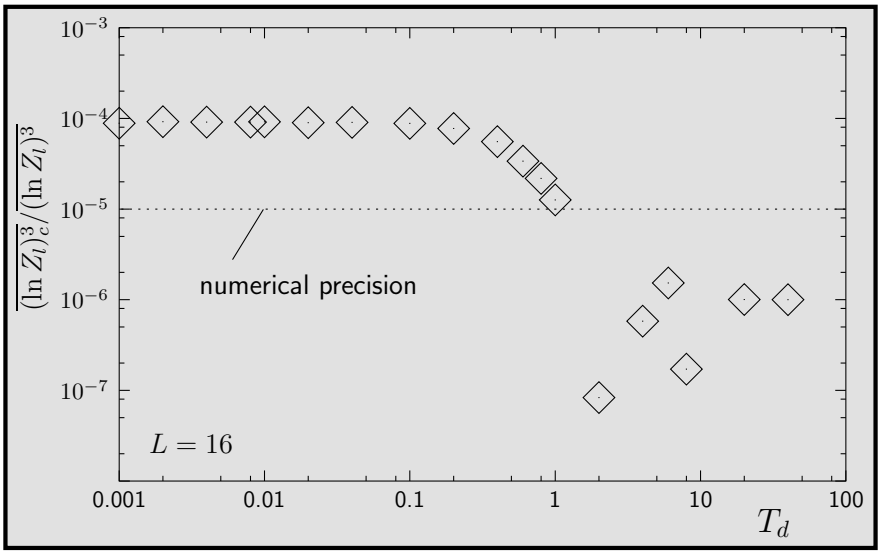

Fig. D.29: Third free energy cumulant over third moment as measured in the dimer model; accuracy of measured moments insufficient for $T_d \gtrsim 1$ at $L = 16$; for $L \geq 32$, the accuracy is insufficient for $T_d \gtrsim 0.001$. The dotted line gives the numerical accuracy of the third moment.

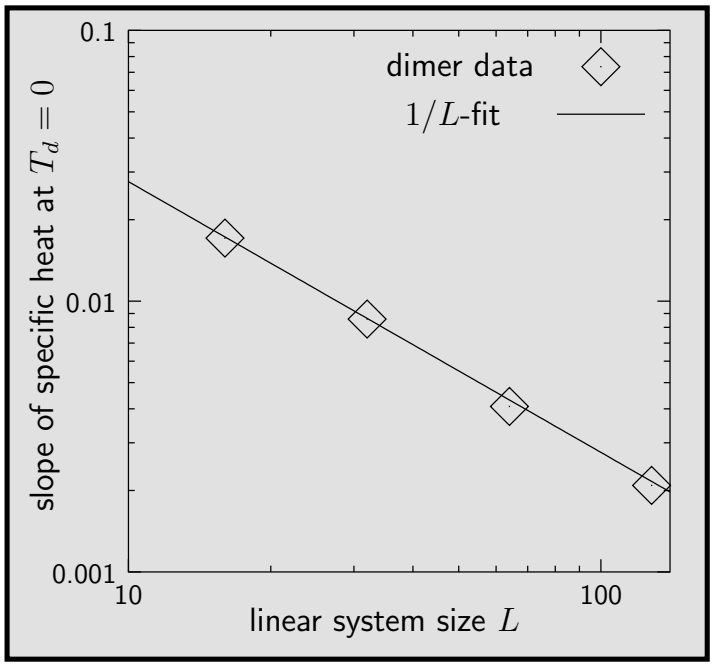

Fig. D.30: Slope of dimer specific heat $\overline{c_d}$ at $T_d = 0$ vs linear system size; boundary contributions with dependency $1/L$ dominate over bulk droplets of size L and produce $1/L$-saturation of the specific heat.

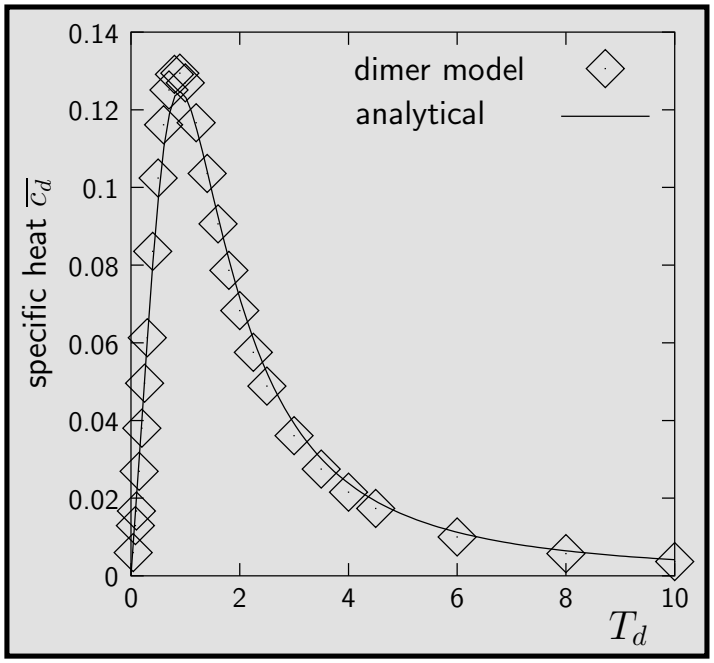

Fig. D.31: Comparison of dimer specific heat $\overline{c_d}$ of the isotropic model; analytical curve with $\xi_d = 0.98$; dimer data for $L = 256$.

4 Conclusion

The planar vortex glass (VG) had been well established and thoroughly investigated before. What is new about our approach and what can be learned? The answer is twofold. First, the exact calculation of the free energy for the noncrossing line array by a Replica Bethe Ansatz (RBA) [EK01] allows to address anew the long-disputed question about the existence of a thermally depinned phase above the VG. We can show that the transition is absent for the given special vortex interaction *and* argue that this result holds so much the more for a generalised finite-range repulsive interaction. The latter conclusion had been under debate and is here reached conclusively for the first time. We also show that a finite persistence length of the vortices – as opposed to a random-walk-like modelling – opens a small window for the thermally free phase sharply below the superconducting transition.

Second, the recently discovered mapping of noncrossing lines to the dimer tiling problem of combinatorial statistics *and* a new polynomial algorithm for the latter allow to compare RBA theory and numerically exact simulations. The details of the mapping to the simulated dimer model had to be clarified before high-precision numerical data were generated by the collaborating group of C. Zeng. Huge systems of linear size $L \leq 512$ can be treated within days, as compared to most advanced Monte Carlo simulation sizes $L \lesssim 64$. The agreement between theory and simulations is not only qualitatively but also quantitatively excellent for a wide range of observables: the large scale lattice stiffness; the average free energy, internal energy, entropy; moments of the disorder distributed free energy; specific heat. For all these, the only fitting parameter ξ_d varied in agreement with the expected value of $\simeq 1$ in the interval $(0.8..1.15)$.

The RBA calculation with the subtleties inherent to replica theory is on the one hand confirmed most clearly. On the other hand, simulation results gain weight in questions out of analytical reach. The new interplay between most recent qualitative advances in analytical and numerical approaches renders the planar disordered vortex system exceptional since, though being a genuine glass, it is still 'solvable' in many aspects and may serve as a model glass system. In view of the wide range of links between condensed matter systems and dimer tiling problems, e.g., between the Ising model on a square lattice and dimers on an associated lattice [Fis66], the exact solution of a *random* dimer model which is at hand with the RBA results might prove useful in other contexts.

E. Notes on the Bragg glass

1 List of extensions on formerly published work

In his diploma thesis, the author examined the triangular weakly disordered Abrikosov lattice with its quasi-long-range ordered Bragg glass phase. The main results had been published as a Letter under the title "Nonuniversal Quasi-Long-Range Order in the Glassy Phase of Impure Superconductors" [EBN99]. An extended and detailed version was worked out during the first few months of the doctoral programme. It is published as "Nonuniversal correlations and crossover effects in the Bragg-glass phase of impure superconductors" [BEN01] and contains the following main extensions:

- The symmetries of the problem are discussed in detail.
- The size of the basin of attraction of the fixed point is characterised.
- Results about finite scale crossover regimes are stressed.
- The details of the calculations (flow equation, numerical solution, correlations) are given.
- The discussion of order parameters is extended. The positional glass correlation function and the Ginzburg-Landau order parameter correlation function are included of which a short summary is given in the next section.

When in 2002 new experimental data on the Bragg glass became available, it was interpreted with no recurrence to several standard publications on the subject [KJB$^+$01]. In a note [BENS], we pointed at this fact and suggested the consideration of the nonuniversal large scale behaviour, which could even improve the agreement between theory and experiment.

In this context the possibility was examined whether the 'smallness' of the nonuniversal contribution to the Bragg glass exponent might be due to the technicality of the expansion around $D = 4$. The rationale lies in the analogy to nonuniversal melting in a pure $D = 2$ system. In our case, the exponent is also nonuniversal with respect to changes of microscopic parameters related to the $D = 2$ degrees of freedom perpendicular to the magnetic field, i.e., the elastic moduli c_{11} and c_{66}. Any extra dimension parallel to the magnetic field might 'dampen' this non-universality. Physically this extra dimension is one, of course, while in large parts of the calculation it is set to the value two, in order to be consistent in the expansion in $\epsilon = 4 - D$. We reviewed the calculations of [BEN01] and tried to calculate in $D = 3$ wherever possible, even if this might mean a slight mixing of orders of ϵ. The integrals (BEN01, 3.7) become more complicated but still are practicable. The Fourier transformation (BEN01, 4.1) can be done easily in three dimensions in the case $c_{44} = c_{11}$ (or $c_{44} = c_{66}$) and give a modified dependency in the microscopic elastic constants. Different from

$D = 4$, however, the result also depends inversely on the short-scale cutoff. The cutoff is anisotropic, in fact it is proportional to the inverse Larkin length scale in the plane and out of the plane. The Larkin lengths thus bring in another new dependency on the microscopic elastic constants. Putting this all together very carefully, we did not find a qualitatively more pronounced nonuniversality.

2 Correlation functions from the RG results

From the RG flow of the effective disorder strength, correlation functions shall be calculated. We first study the translational order parameter

$$\Psi_{\mathbf{G}}(\mathbf{r}) \equiv e^{i\mathbf{G}\mathbf{u}(\mathbf{r})} \tag{2.1}$$

The pair correlation function

$$C_{\mathbf{G}}(\mathbf{r}) = \overline{\langle \Psi_{\mathbf{G}}(\mathbf{r})\Psi^*_{\mathbf{G}}(\mathbf{0})\rangle} = \overline{\langle e^{i\mathbf{G}(\mathbf{u}(\mathbf{r})-\mathbf{u}(\mathbf{0}))}\rangle}.$$

is a measure for the translational order in the system. It is often called translational order correlation function and its scaling behaviour determines the intensity of the reflection pattern obtained in neutron scattering, $C_{\mathbf{G}}(\mathbf{r})$ is often referred to as translational order correlation or simply 'translational order'. Being exact to order ϵ, the average can be raised to the exponent as if $\mathbf{u}(\mathbf{r})$ was Gaussian distributed [Emi98]. We thus can obtain from the displacement correlations Eq. (4.8) in [BEN01] the result for the asymptotic scaling regime,

$$\begin{aligned} C_{\mathbf{G}}(\mathbf{r}) \quad &\propto \quad g_{\mathbf{G}} L_a^{\eta_{\mathbf{G}}(\kappa)} (\mathbf{x}^2 + z_t^2)^{-\frac{\eta_{\mathbf{G}}(\kappa)}{2(1+\kappa)}} \\ &\quad \times (\mathbf{x}^2 + z_l^2)^{-\frac{\eta_{\mathbf{G}}(\kappa)}{2(1+1/\kappa)}} \end{aligned} \tag{2.2}$$

with exponent

$$\eta_{\mathbf{G}}(\kappa) = \tilde{\Delta}^*(\kappa)(aG)^2$$

and the geometrical factor

$$\begin{aligned} g_{\mathbf{G}} \quad &= \quad \exp\left[\frac{\tilde{\Delta}^*(\kappa)(aG)^2}{1+\kappa} \left((\hat{\mathbf{x}}\hat{\mathbf{G}})^2 - \frac{1}{2} \right) \right. \\ &\quad \left. \times \left\{ \left(1 - h\left(\frac{|\mathbf{x}|}{z_t} \right) \right) - \kappa \left(1 - h\left(\frac{|\mathbf{x}|}{z_l} \right) \right) \right\} \right]. \end{aligned}$$

Our main result on the translational order of the flux line lattice consists in the decay of order with a *nonuniversal* exponent $\eta_{\mathbf{G}}(\kappa)$. Its dependency on κ, as obtained by the solution to the flow equation for $\tilde{\Delta}$ is shown in Fig. E.1 for one of the smallest reciprocal lattice vectors $\mathbf{G} = \mathbf{G}_0$ with $|\mathbf{G}_0| = 4\pi/(a\sqrt{3})$. The full decay exponent in Eq. (2.2) is modified by additional κ-dependent factors due to the anisotropic elasticity leading to different contributions from transversal and longitudinal modes.

Two limiting cases shall be considered: For $z \to 0$ the result simplifies to

$$\begin{aligned} C_{\mathbf{G}}(\mathbf{x}) \quad &\propto \quad (|\mathbf{x}|/L_a)^{-\eta_{\mathbf{G}}(\kappa)} \\ &\times \quad \exp\left\{ \tilde{\Delta}^*(\kappa)(aG)^2 \frac{1-\kappa}{1+\kappa} \left((\hat{\mathbf{x}}\hat{\mathbf{G}})^2 - \frac{1}{2} \right) \right\}. \end{aligned}$$

For $\kappa = 1$, the translational order decay is isotropic according to

$$C_{\mathbf{G}}(\mathbf{r}') \propto L_a^{\eta_{\mathbf{G}}(1)} |\mathbf{r}'|^{-\eta_{\mathbf{G}}(1)}$$

with the rescaled coordinate $\mathbf{r}'$ defined above. This isotropic limit can be used to demonstrate clearly that the triangular flux line lattice considered here and the scalar model – describing the square lattice geometry – do not belong to the same universality class. Whereas we obtain $\eta_{\mathbf{G}}(1) = 1.14\epsilon$ for the triangular lattice, the result in the RG approach for the scalar model is $\eta_{\mathbf{G}}(1) = \pi^2/9\epsilon = 1.10\epsilon$.

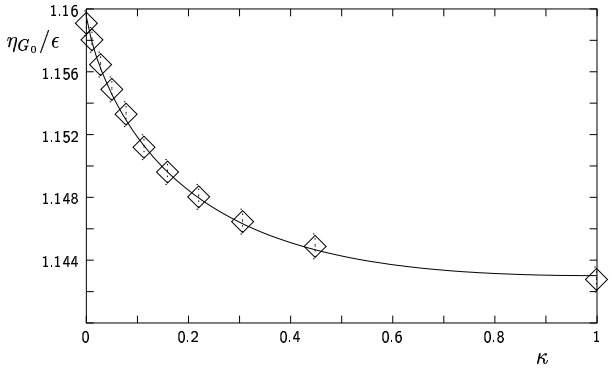

Fig. E.1: Dependency of the exponent $\eta_{\mathbf{G}_0}$ on the ratio $\kappa = c_{66}/c_{11}$ of elastic constants.

Another correlation function that can be constructed from the translational order parameter Eq. (2.1) is the *positional glass* correlation function suggested by spin glass theory [BY86]

$$S_{PG}(\mathbf{G}, \mathbf{r}) = \overline{|\langle \Psi_{\mathbf{G}}(\mathbf{r}) \Psi^*_{\mathbf{G}}(\mathbf{0}) \rangle|^2}.$$

It measures the thermal fluctuations of the flux lines around their disordered ground state. We calculate $S_{PG}(\mathbf{G}, \mathbf{r})$ within our framework from the Hamiltonian renormalised up to scale $|\mathbf{r}| = \Lambda^{-1} e^l$. First order perturbation theory in the pinning energy gives the corrections to the mere thermal result to first order in ϵ. We get

$$S_{PG}(\mathbf{G}, \mathbf{r}) \backsimeq S^0_{PG}(\mathbf{G}, \mathbf{r}) \left\{ 1 + \epsilon \sum_{m \geq 1} c_m \left(\frac{T}{r^2} \right)^{2m} \right\},$$

where $S^0_{PG}(\mathbf{G}, \mathbf{r})$ denotes the correlation function for the pure system with thermal fluctuations only and c_m are numerical coefficients. $S^0_{PG}(\mathbf{G}, \mathbf{r})$ is finite for $r \to \infty$ and reduced with respect to unity merely by the standard Debye-Waller factor. Since the order ϵ corrections decay, they can surely not compensate the leading constant term and make up for a more than powerlaw decay of the whole correlation function. This provides signature of a positional glass to order ϵ.

Heavily discussed, however not definitely answered, is the question if there exists a *phase coherent vortex glass* state in impure type-II superconductors. A finite asymptotic value of the correlation function

$$C_{VG}(\mathbf{r}) = \overline{|\langle \Psi(\mathbf{r}) \Psi^*(\mathbf{0}) \rangle|^2} \tag{2.3}$$

of the Ginzburg-Landau complex order parameter $\Psi(\mathbf{r})$ is proposed to identify such a phase coherent vortex glass [Fis89, FH91]. The order parameter can be decomposed in amplitude and phase factor,

$\Psi = |\Psi| e^{i[\phi_0 + \delta\phi]}$, with groundstate phase ϕ_0 and phase fluctuations $\delta\phi$. In the London limit the amplitude is constant and finite outside the vortices and C_{VG} becomes

$$C_{VG}(\mathbf{r}) = |\Psi|^2 \overline{|\langle e^{i[\delta\phi(\mathbf{r}) - \delta\phi(\mathbf{0})]}\rangle|^2}.$$

Phase fluctuations and vortex displacements are related by [Moo92]

$$\nabla^2 \delta\phi(\mathbf{r}) = \frac{2\pi}{a} \left(\nabla_\perp \times \mathbf{u}(\mathbf{r})\right).$$

This allows for the calculation of $C_{VG}(\mathbf{r})$ in the framework of the elastic description of the flux line lattice. We use perturbation theory for $\mathcal{H}_{dis}$ with fluctuations on scales below $|\mathbf{r}|$ having renormalised this perturbation. Then corrections to the thermal average term $(e^{-\langle[\delta\phi(\mathbf{r}) - \delta\phi(\mathbf{0})]^2\rangle_0})$ are given to first order in ϵ by

$$\begin{aligned} C_{VG}(\mathbf{r}) &= e^{-\langle[\delta\phi(\mathbf{r}) - \delta\phi(\mathbf{0})]^2\rangle_0} \times \Big\{ 1 \\ &+ \frac{1}{T^2} \sum_{\mathbf{G}} \hat{R}^*_{\mathbf{G}} \int_{\bar{\mathbf{r}}} \left[\cosh(2F(\mathbf{r}, \bar{\mathbf{r}})) - 4\cosh(F(\mathbf{r}, \bar{\mathbf{r}}))\right] \Big\}. \end{aligned} \tag{2.4}$$

Here $\hat{R}^*_{\mathbf{G}} = R^*_{\mathbf{G}} \exp(-G_\alpha G_\beta \langle u_\alpha(\mathbf{0}) u_\beta(\mathbf{0})\rangle_0) \sim \epsilon$ are the reduced Fourier coefficients of the random energy correlator, see Eq. (2.12) in [BEN01]. We have abbreviated $F(\mathbf{r}, \bar{\mathbf{r}}) = \Gamma(\mathbf{r} - \bar{\mathbf{r}}) - \Gamma(-\bar{\mathbf{r}})$ with $\Gamma(\mathbf{r}) = \langle \mathbf{G}\mathbf{u}(\mathbf{r}) \delta\phi(\mathbf{0})\rangle_0$. The exponential factor of $\hat{R}^*_{\mathbf{G}}$ is finite in $d > 2$. For the disorder induced correction in Eq. (2.4), we focus on the isotropic limit with $c_{44} = c_{66}$ and get

$$\Gamma(\mathbf{r}) = \frac{T}{4\pi a^2 c_{44}} \frac{G_y x - G_x y}{r^2} \left(1 - \frac{2}{\Lambda r} J_1(\Lambda r)\right),$$

where $J_1(x)$ is the Bessel function of first kind. Upon expansion of the $\cosh$-terms, a careful investigation of the behaviour for large $|\mathbf{r}|$ of the remaining integrals gives to order ϵ

$$\begin{aligned} C_{VG}(\mathbf{r}) &\simeq e^{-\langle[\delta\phi(\mathbf{r}) - \delta\phi(\mathbf{0})]^2\rangle_0} \\ &\times \left\{ 1 + \epsilon \left[d_1 T^2 \ln(r\Lambda) + d_2 + \sum_{m \geq 0} c_m T^2 \left(\frac{T}{r}\right)^{2m} \right] \right\}. \end{aligned}$$

The constants d_i, c_i are again numerical coefficients, yet different from the ones in Eq. (2). The exponential factor of Eq. (2.4) merely represents the effect of thermal fluctuations and reads

$$\begin{aligned} &\langle[\delta\phi(\mathbf{r}) - \delta\phi(\mathbf{0})]^2\rangle_0 \\ &\qquad = \frac{8\pi^2}{a^4} T \int_{\mathbf{q}} \frac{q_\perp^2}{q^4} \mathcal{G}^T(\mathbf{q}) [1 - \cos(\mathbf{q}\mathbf{r})] \sim \frac{1}{\epsilon} |\mathbf{r}|^\epsilon. \end{aligned}$$

Corrections to order ϵ can hence not compete against the exponential decay of $C_{VG}(\mathbf{r})$ that originates from strong thermal fluctuations. Thus we conclude that to order ϵ there is no phase coherent vortex glass. Whether this result is valid to higher orders in ϵ and thus in $D = 3$ remains, however, unclear within the present analysis. Dorsey et al. [DHF92] indeed found a vortex glass transition in $6 - \epsilon$ dimensions starting from a Ginzburg-Landau Hamiltonian. If this transition exists down to three dimensions cannot be clarified here unambiguously. In the analysis of the translational order correlation function the field $\mathbf{u}(\mathbf{r})$ was treated as if Gaussian distributed. This is certainly wrong, even to order ϵ, for the more complex correlation functions $S_{PG}(\mathbf{G}, \mathbf{r})$, $C_{VG}(\mathbf{r})$. The use of the present renormalisation group scheme in the context of correlation functions therefore remains debatable.

F. Appendix

1 Bosonisation

In this appendix we sketch the method of 'bosonisation' of one-dimensional interacting fermion systems. Fermi-liquid theory of quasiparticles does not apply to dimension one, however, the lowlying degrees of freedom are well described by collective density fluctuations with bosonic statistics. The reparametrisation of the configurational space can even be extended to a one-to-one correspondence on the basic operator level. The generic algebraic behaviour both of correlation functions and the density of states is easily obtained in bosonised language as well as phase diagrams in the presence of various instabilities. Spin charge separation is another characteristic feature of dimension one and a natural consequence in the reparametrisation procedure. The method is also of great use in the field of spin chains that can be mapped to Fermi system by a Jordan-Wigner transformation [Hal80]. Below, in very broad steps the bosonisation of an interacting Fermi system is reviewed starting with the spinless case before giving the modifications by spin degrees of freedom. Out of the considerable amount of pedagogical literature on the subject the review by Voit Ref. [Voi95] and the tutorial by Schulz Ref. [Sch95] were most helpful to the present author. The historical credit for the development of the field goes largely to Haldane [Hal81a, Hal81b] who built on early work by Mattis and Lieb [ML65] and Luttinger [Lut63].

Basic assumptions of Fermi-liquid theory break down in one dimension. The one-particle Green's function $\mathcal{G}(\omega, k)$ does not have a single pole by which the quasiparticle energies $\omega(k)$ can be defined and the quasiparticle amplitude $Z = \langle \hat{\Psi}^{N+1} | c^\dagger | \hat{\Psi}^N \rangle$ vanishes. Adiabatic continuity with respect to a slow switching on of interactions is not given. While in three dimensions the Fermi liquid is unstable towards the superconducting state for attractive interactions, in one dimension the additional mean field instability to charge density wave formation for repulsive interactions indicates the inadequacy of single-particle states for the description of the interacting system. A better and concerning the ease of calculations even ideal set of states can, however, be identified.

Consider the low energy sector of interacting fermions in one dimension. Spin is neglected for the moment. The dispersion is linearised around the two Fermi points over momentum windows $k_\mathrm{F} \pm k_0, -k_\mathrm{F} \mp k_0$. The kinetic energy then reads

$$\hat{H}_0 = v_\mathrm{F} \sum_k \{(k - k_\mathrm{F}) \hat{a}_k^\dagger \hat{a}_k + (-k - k_\mathrm{F}) \hat{b}_k^\dagger \hat{b}_k\}, \tag{1.1}$$

with $\{\hat{a}^\dagger\}$ ($\{\hat{b}^\dagger\}$) free-particle Fermi operators $\hat{c}^\dagger$ at the right (left) Fermi point, which create right- (left-) moving momentum eigenstates.

A density-density interaction via a potential $U(x)$ reads in second quantisation

$$\hat{H}_{\rm int} = \sum_{q,k,k'} \tilde{U}(q)\hat{c}^\dagger_{k-q}\hat{c}^\dagger_{k'+q}\hat{c}_{k'}\hat{c}_k.$$

The confinement of the operators to the momentum windows around the Fermi points allows for three distinct scattering processes:
(i) $(k_{\rm F};k_{\rm F}) \to (k_{\rm F};k_{\rm F})$, $(-k_{\rm F};-k_{\rm F}) \to (-k_{\rm F};-k_{\rm F})$, momentum transfer $q \simeq 0$, forward scattering,
(ii) $(-k_{\rm F};k_{\rm F}) \to (-k_{\rm F};k_{\rm F})$, $(k_{\rm F};-k_{\rm F}) \to (k_{\rm F};-k_{\rm F})$, $q \simeq 0$ and
(iii) $(-k_{\rm F};k_{\rm F}) \to (k_{\rm F};-k_{\rm F})$, $(k_{\rm F};-k_{\rm F}) \to (-k_{\rm F};k_{\rm F})$, $q \simeq 2k_{\rm F}$, backward scattering , see Fig. F.2. Without spin to possibly distinguish fermions, process (iii) can be combined with (ii). One assumes slowly varying $\tilde{U}(q)$ over the momentum window and parametrises the scattering (ii)+(iii) by $g_2 = \tilde{U}(0) - \tilde{U}(2k_{\rm F})$ and (i) by $g_4 = \tilde{U}(0)$. The interaction energy then is

$$H_{\rm int} = \sum_{k,k';q} \left\{ g_2\ \hat{a}^\dagger_{k+q}\hat{b}^\dagger_{k'-q}\hat{b}_{k'}\hat{a}_k + g_4\ \hat{a}^\dagger_{k+q}\hat{a}^\dagger_{k'-q}\hat{a}_{k'}\hat{a}_k \right\} + (\{\hat{a}\} \leftrightarrow \{\hat{b}\})$$

With the momentum cutoff k_0 sent to infinity, the exactly solvable Luttinger model is obtained. The choice of constant scattering amplitudes g_i requires some cutoff function $\exp(-\alpha q)$ in momentum integrals. Results should be finite if α is sent to zero at the very end.

We now introduce the right- and leftmover density operators

$$\hat{\rho}_+(q) = \sum_k \hat{a}^\dagger_{k+q}\hat{a}_k \quad , \quad \hat{\rho}_-(q) = \sum_k \hat{b}^\dagger_{k+q}\hat{b}_k$$

with bosonic commutation relations

$$[\hat{\rho}_\pm(-q), \hat{\rho}_\pm(q')]_- = \delta_{qq'}\frac{qL}{2\pi}\ ,\ [\hat{\rho}_+(-q), \hat{\rho}_-(q')]_- = 0.$$

The finite commutator for $q = q'$ is one point where the infinite Fermi sea of the Luttinger model is essential. This subtlety, however, does not touch the applicability of the results to the physical finite Fermi sea system.

The basic observation about the density operators now is that the state create by such a density operator is a superposition of particle-hole excitations that all have – due to the linear dispersion relation – energy $v_{\rm F}q$. This superposition is hence an eigenstate of the kinetic energy operator Eq. (1.1). Basic quantum mechanics allow to write H_0 as a *bilinear* form in the bosonic density operators

$$\hat{H}_0 = \frac{2\pi v_{\rm F}}{L}\sum_{q>0}\left\{\hat{\rho}_+(q)\hat{\rho}_+(-q) + \hat{\rho}_-(q)\hat{\rho}_-(-q)\right\},$$

just like the interacting part

$$\hat{H}_{\rm int} = \frac{1}{2L}\sum_q \{2g_2\hat{\rho}_+(q)\hat{\rho}_-(-q) + g_4[\hat{\rho}_+(q)\hat{\rho}_+(-q) + \hat{\rho}_-(q)\hat{\rho}_-(-q)]\}.$$

The bilinear Hamiltonian can be diagonalised easily with eigenvalues

$$\omega(q) = |q|[(v_{\rm F} + g_4/(2\pi))^2 - (g_2)/(2\pi)^2]^{1/2}.$$

Bosonisation has thus been achieved not by treating the interaction but rather by writing the non-interacting part of the energy in the new density degrees of freedom, that readily diagonalise the

interaction. Both the simple form of the kinetic energy in terms of the density operators and the fact that these form a basis of the relevant Hilbert space derive from the linear one-dimensional dispersion relation. Fig. F.1 illustrates why the eignestates of the above density operators are a promising candidate for the important low-lying excitations only in one dimension. The spectrum of particle-hole excitations (excitons) is pictured on the right. From the excitons at small q with the (approximately) linear dispersion the new 'particles' are built. Now in one dimension, there are no low-lying excitations at higher $q < 2kF$, that could be the decay products of those superpositions. In higher dimensions, the missing states are filled in and the density states no longer cover the low-energy sector of the Hilbert space. Hence, bosonisation can be ultimately traced back to the restricted phase space special to one dimension. Bosonic field operators can be introduced on

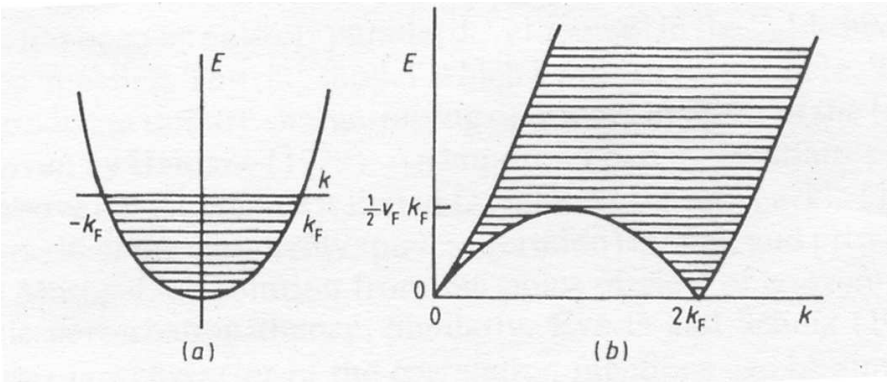

Fig. F.1: (a) Single particle spectrum of the free Fermi gas in 1D; (b) Particle-hole pair spectrum has no low-frequency excitations with $0 \leq |q| \leq 2k_{\mathrm{F}}$, unlike in higher dimensions where these states are filled in. Figure taken from [Hal81a]

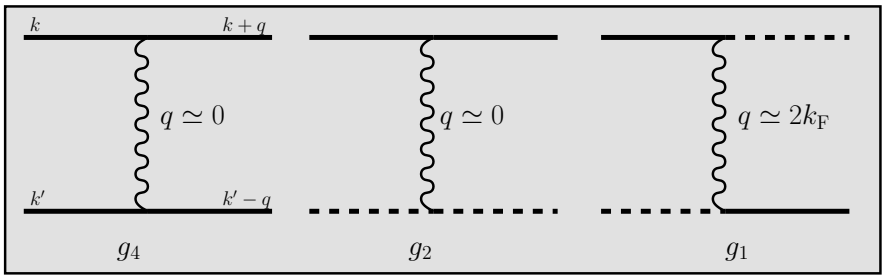

Fig. F.2: "g-ology": forward scattering (left and middle) and backward scattering (right). Legs with a filled line represent leftmovers, dashed legs rightmovers.

the way to a boson representation of the Fermi field operator

$$\hat{\Phi}(x) = -\frac{i\pi}{L}\sum_{q\neq 0} e^{-\alpha|q|/2-iqx}[\hat{\rho}_+(q)+\hat{\rho}_-(q)] + \hat{N}\pi x/L$$

$$\hat{\Pi}(x) = \frac{1}{L}\sum_{q\neq 0} e^{-\alpha|q|/2-iqx}[\hat{\rho}_+(q)-\hat{\rho}_-(q)] + \hat{J}/L$$

$$\hat{N} = \hat{N}_+ + \hat{N}_- \quad , \quad \hat{J} = \hat{N}_+ - \hat{N}_-$$

$\hat{N}_\pm$ counts the number of particles above the ground state on the right- and left-moving branch. $\hat{\Pi}$ is the canonically conjugate operator to $\hat{\Phi}$

$$[\hat{\Phi}(x), \hat{\Pi}(x')]_- = i\delta(x - x').$$

The famous inversion of the above relations is

$$\begin{aligned} \hat{\Psi}^\dagger_\pm(x) &= \lim_{\alpha\to 0} (2\pi\alpha)^{-1/2} \hat{U}^\dagger_\pm \exp[\pm i\hat{\Phi}(x) - i\hat{\Theta}(x)] \\ \hat{\Psi}^\dagger(x) &= \hat{\Psi}^\dagger_+(x)\exp(-ik_{\mathrm{F}}x) + \hat{\Psi}^\dagger_-(x)\exp(ik_{\mathrm{F}}x), \end{aligned}$$

with $\frac{\partial\hat{\Theta}}{\partial x} := \pi\hat{\Pi}$. $\hat{U}^\dagger_\pm$ increases the particle number on the respective branch by one. Bosonisation is now complete, any operator can be written in terms of the bosonic field operators $\hat{\Phi}, \hat{\Pi}$.

The interacting Hamiltonian takes the simple form of an elastic quantum string Hamiltonian

$$\begin{aligned} \hat{H} &= \frac{1}{2}\int dx \{ v_N \left(\pi\hat{\Pi}\right)^2 + v_J \Big(\frac{\partial\hat{\Phi}}{\partial x}\Big)^2 \} \\ v_N &= v_{\mathrm{F}} + (g_4 + g_2)/(2\pi) \\ v_J &= v_{\mathrm{F}} + (g_4 - g_2)/(2\pi). \end{aligned}$$

In the path integral formulation, $\hat{\Phi}, \hat{\Pi}$ lose their operator character and the coupling term $-2i\frac{\partial\Phi}{\partial x}\frac{\partial\Theta}{\partial\tau}$ appears in the action. Φ and Θ are dual classical fields then.

The density operator is expressed in terms of the bosonic fields as

$$\hat{\rho}(x) - \rho_0 = -\frac{1}{\pi}\frac{\partial\hat{\Phi}}{\partial x} + \frac{1}{\sqrt{2}\pi\alpha}\cos[2k_{\mathrm{F}}x - \sqrt{2}\hat{\Phi}].$$

From the continuity equation $\partial_t\hat{\rho} + \partial_x\hat{j} = 0$ the slowly varying part of the current operator follows directly

$$\hat{j}(x) = v_J\hat{\Pi} \to \frac{i}{\pi}\frac{\partial\Phi}{\partial\tau}.$$

The above expressions of the fermion field operator are rigorous results for the Luttinger model, for the derivation see Ref. [Hal81a] and the very detailed review Ref. [vDS98]. A more heuristic, physically motivated derivation of the bosonisation formula was given by Haldane in Ref. [Hal81b], *later* than the rigorous publication Ref. [Hal81a]. There, higher order harmonic terms in k_{F} appear via the field operator in the expression for the density. These terms are frequently given a physical interpretation, e.g. in Ref. [Sch93], and are of considerable effect in certain situations. In what sense they are a manifestation of the nonlinear corrections to the free particle dispersion in a rigorous treatment, as sometimes asserted[1] remains unclear to the author.

The modifications of a spin-$1/2$ degree of freedom carried by the fermions to the above results are mainly twofold.

(i) The back scattering between fermions of opposite spin cannot be rewritten as a contribution of

[1] T. Giamarchi in private communication; this possibility is also mentioned in [Sch95]; One of the authors of [vDS98], H. Schoeller, showed in private communication awareness of the problem, but neither him could resolve it, nor M. P. A. Fisher when asked by him.

g_2-forward scattering. Written in the bosonic field operators, this interaction is anharmonic.
(ii) For each spin projection $\uparrow, \downarrow$ a set of bosonic field operators is introduced. The Hamiltonian decouples in the rotated basis $\hat{\Phi}_{c,s} = (\hat{\Phi}_\uparrow \pm \hat{\Phi}_\downarrow)/\sqrt{2}$, $\hat{\Pi}_{c,s} = (\hat{\Pi}_\uparrow \pm \hat{\Pi}_\downarrow)/\sqrt{2}$

$$\hat{H} = \hat{H}_c + \hat{H}_s + \hat{H}_{g_1}.$$

$\hat{H}_{c/s}$ are formally identical to the spinless bosonised Hamiltonian with parameters v_N, v_J and fields now carrying the index c, s. The anharmonic backscattering is a function of the s-field only

$$\hat{H}_{g_1} = \frac{2g_1}{(2\pi\alpha)^2} \int dx \cos(\sqrt{8}\hat{\Phi}_s).$$

The charge and spin density operators demonstrate that with c, s charge and spin degrees of freedom have been identified

$$\begin{aligned} \hat{\rho}(x) - \rho_0 &= -\frac{\sqrt{2}}{\pi}\frac{\partial\hat{\Phi}_c}{\partial x} + \frac{\rho_0}{\pi}\left\{e^{i2k_{\rm F}x - i\sqrt{2}\hat{\Phi}_c}\cos(\sqrt{2}\hat{\Phi}_s) + h.c.\right\} \\ \hat{\sigma}_z(x) &= -\frac{\sqrt{2}}{\pi}\frac{\partial\hat{\Phi}_s}{\partial x} + \frac{i\rho_0}{\pi}\left\{e^{-i2k_{\rm F}x + i\sqrt{2}\hat{\Phi}_c}\sin(\sqrt{2}\hat{\Phi}_s) + h.c.\right\}. \end{aligned}$$

The decoupling of the Hamiltonian together with the – in general – distinct parameters for the charge and spin sector

$$\begin{aligned} v_{N,c} = v_{\rm F} + (g_4 + g_2 - g_1/2)/\pi \quad ; \quad v_{J,c} = v_{\rm F} + (g_4 - g_2 + g_1/2)/\pi \\ v_{N,s} = -g_1/(2\pi) \quad ; \quad v_{J,s} = g_1/(2\pi) \end{aligned}$$

manifests spin charge separation in one-dimensional electron systems. Other than above in the spinless case, none of the back scattering has been included in the parameter g_2. A spin independent density-density interaction has been assumed and hence $g_2 = g_4 = \tilde{U}(0), g_1 = \tilde{U}(2k_{\rm F})$.

For repulsive interactions $g_1 > 0$ the backward scattering term is irrelevant in the RG sense. On large scales, correlation functions thus show the algebraic behaviour of a harmonic two dimensional theory. This is the remarkable 'Luttinger liquid': All the exponents of large scale correlation functions and transport characteristics are determined by the parameters of the underlying bosonic model, which is harmonic even for *strong* coupling.

2 A technical problem: real- vs momentum-space renormalisation for dual fields

The flow equations for coupled Luttinger liquids with disorder Eqs. (C.3.19) were derived in a momentum-shell renormalisation scheme, however with an ad hoc modification. The modification could only be justified by comparison of the results to the real-space RG for a single Luttinger liquid with disorder as, e.g., in Refs. [GS88, GS89].
What did we do? Undoubtedly, disorder stiffens on larger scales the Φ-field in imaginary time τ-direction by the generation of a 'gamma'-term $\frac{1}{2\pi}\int_{x,\tau}\gamma\left(\partial_\tau\Phi\right)^2$, even in the phase where disorder eventually is irrelevant. In the scheme above, this disorder feedback was compared to the harmonic action *after* integration over the Θ-field in order to read off the renormalisation of the LL parameters. The renormalised parameters were then used on large scales both in the correlators of the Φ- and

Θ-fields, although the latter had before been integrated out. In the analysis of any anharmonicities in the Φ-fields, there is nothing wrong about this procedure. However, thinking straightforwardly, we would proceed differently if we wanted to analyse, e.g., the Josephson coupling, which is written in the Θ-fields. One would then not integrate out the Θ-field at all but instead the Φ-field *after* disorder has created its feedback.

Let us look at what happens in the straightforward approach in the simpler case of a single Luttinger liquid. We are in the phase where disorder is irrelevant and where it has left behind the above γ-term. One then arives for the correlator in the Θ-sector as the equivalent of Eq. (C.2.11b)

$$\langle \Theta^a_{\mathbf{q}} \Theta^b_{-\mathbf{q}} \rangle \quad = \quad \frac{\pi \delta^{ab}}{v_J q^2 + \omega^2 (1 + \gamma v_J)/v_N} \left(1 + \frac{\gamma}{v_N} \frac{\omega^2}{q^2} \right). \tag{2.3}$$

The dependence on ω of the γ-term implies the divergence of the correlations $\langle [\Theta(x,0) - \Theta(0,0)]^2 \rangle$, if no UV cutoff in ω is assumed. With a cutoff Λ_ω, the correlations are proportional to $\Lambda_\omega x$. As one consequence, the superconducting order parameter correlations are no longer quasi-long-ranged but short-ranged with a correlation length $\propto \Lambda_\omega^{-1}$. Similar consequences result for any observable that is written after bosonisation in the Θ-fields only.
In physical terms the implications are drastic. Superconducting order in a one-dimensional electron gas (1DEG) with any finite amount of impurities would under no circumstances represent an instability of the system in contradiction to the literature, e.g., Ref. [GS89]. Josephson coupling between 1DEGes would be irrelevant. More seriously, the situation seems to be analogous for anharmonicities of the sine-Gordon type. T. Giamarchi has drawn our attention to the following scenario. Consider the bosonised XXY-spin chain, which has a cosine-anharmonicity in the Φ-field. The relevance of this term indicates the Ising transition, but we focus here on the parameter range where it is irrelevant. The correlations of the spin raising and lowering operators become in bosonised language

$$\langle \hat{S}^+(x) \hat{S}^-(0) \rangle = \langle \exp[i(\Theta(x,0) - \Theta(0,0))] \rangle. \tag{2.4}$$

A straightforward momentum-shell RG would render these correlations short-ranged, in contradiction to exact Bethe ansatz results [KBI93]. Even worse for the isotropic XXX-chain. The cosine-term is marginally irrelevant, enough in the momentum-shell reasoning to generate a finite yet small γ and again give short-ranged correlations of $\hat{S}^+, \hat{S}^-$, while the correlations of $\hat{S}_z$ which are written in the Φ-field decay algebraically. Spin rotation invariance for the XXX-chain requires, however, not only the same qualitative behaviour but even the same exponents in the power law.
This is very unsatisfactory, even alarming. What has gone wrong? We will try to trace back the problem. To this end we go below through the steps of both the momentum-shell (this one very briefly) and the real-space RG.

2.1 Action and free correlations

Let us first for convenience define again the problem of a single spinless 1DEG with impurity backward scattering in its most simple form. We neglect impurity forward scattering and write the action as a

free harmonic part plus the disorder anharmonicity

$$S = S_0 + S_D \tag{2.5a}$$

$$S_0 = \frac{1}{2\pi}\int_{x\tau}\left\{uK\left(\partial_x\Theta\right)^2 + u/K(\partial_x\Phi)^2 - 2i\partial_x\Theta\partial_\tau\Phi\right\} \tag{2.5b}$$

$$S_D = -\mathcal{D}\int_{x,\tau,\tau'}\cos[\sqrt{2}(\Phi_{x,\tau}-\Phi_{x,\tau'})]. \tag{2.5c}$$

A short-scale cutoff $\alpha \simeq \pi\Lambda^{-1}$ in the position coordinate is implicit whereas the imaginary time integration is unrestricted and replica indices are suppressed. The free correlators are

$$\mathcal{G}^0_{\Phi\Phi} = \frac{\pi K}{uq^2+\omega^2/u} = \frac{\pi}{v_N q^2+\omega^2/v_J} \tag{2.6a}$$

$$\mathcal{G}^0_{\Theta\Theta} = \frac{\pi/K}{uq^2+\omega^2/u} = \frac{\pi}{v_J q^2+\omega^2/v_N} \tag{2.6b}$$

$$\mathcal{G}^0_{\Theta\Phi} = \frac{-\pi i\omega/q}{u^2q^2+\omega^2} = \frac{-\pi i\omega/q}{v_Jv_Nq^2+\omega^2}, \tag{2.6c}$$

$$K = \sqrt{v_J/v_N} \tag{2.6d}$$

$$u = \sqrt{v_Jv_N}. \tag{2.6e}$$

This gives the real-space correlation functions

$$\begin{aligned}\langle\Theta\Phi\rangle_0(x,\tau) &:= \langle\Theta(x,\tau)\Phi(0,0)\rangle_0 = \\ &= \frac{1}{(2\pi)^2}\int d\omega\int dq\, e^{iqx+i\omega\tau}\frac{\omega}{q}\frac{-i\pi}{u^2q^2+\omega^2} \\ &= -\frac{i^2}{4}\,\mathrm{sign}[\tau]\int\frac{dq}{q}e^{-q\alpha}e^{iqx-qu|\tau|} \\ &= \frac{i}{2}\,\mathrm{sign}(\tau)\arctan[\frac{x}{|u\tau|+\alpha}]\end{aligned} \tag{2.7a}$$

$$\langle\Phi\Phi\rangle_0(x,\tau) = -\frac{K}{4}\ln[\frac{x^2+(u|\tau|+\alpha)^2}{\alpha^2}] + \langle\Phi^2\rangle_0 \tag{2.7b}$$

$$\begin{aligned}F(x,\tau) &:= \langle[\Phi(x,\tau)-\Phi(0,0)]^2\rangle_0 \\ &= \frac{2}{(2\pi)^2}\int d\omega\int dq\,(1-e^{iqx+i\omega\tau})\frac{\pi}{v_Nq^2+\omega^2/v_J} \\ &= K\int\frac{dq}{q}e^{-q\alpha}(1-e^{iqx-qu|\tau|}) \\ &= \frac{K}{2}\ln[\frac{x^2+(u|\tau|+\alpha)^2}{\alpha^2}]\end{aligned} \tag{2.7c}$$

$$G(x,\tau) := \langle[\Theta(x,\tau)-\Theta(0,0)]^2\rangle_0 = \frac{1}{2K}\ln[\frac{x^2+(u|\tau|+\alpha)^2}{\alpha^2}] \tag{2.7d}$$

$$\langle\Phi^2\rangle_0 := \langle\Phi(x,\tau)^2\rangle_0 = \frac{K}{2}\ln[L/\alpha]. \tag{2.7e}$$

The correlation functions obey the relations

$$\partial_\tau\langle\Phi\Phi\rangle_0(x,\tau) = iuK\partial_x\langle\Theta\Phi\rangle_0(x,\tau) \tag{2.8a}$$

$$\partial_\tau\langle\Theta\Phi\rangle_0(x,\tau) = \frac{iu}{K}\partial_x\langle\Phi\Phi\rangle_0(x,\tau) + i\delta(\tau)\arctan[\frac{x}{\alpha}]., \tag{2.8b}$$

These can be derived either within the path-integral approach by a comparison of the correlators or by use of the canonic commutation relations between $\hat{\Phi}$ and $\partial_x\hat{\Theta} = \pi\hat{\Pi}_\Phi$.

2.2 Flow equations in momentum-shell RG

The equations of flow (EoF) in momentum-shell RG – derived in analogy to the procedure of Chapter C – with cutoff $\Lambda \simeq \pi/\alpha$ are

$$\frac{d}{dl}\mathcal{D} = (3-K)\mathcal{D} \tag{2.9a}$$

$$\frac{d}{dl}v_N = v_J = 0 \tag{2.9b}$$

$$\frac{d}{dl}\gamma = \frac{8\pi}{v_J v_N^2 \Lambda^3}\mathcal{D}. \tag{2.9c}$$

The generation of a constant γ may be included in a – rather curiously – dispersive v_N

$$\frac{d}{dl}v_N = \frac{8\pi}{v_J v_N^2 \Lambda^3}\frac{\omega^2}{q^2}\mathcal{D} \tag{2.10a}$$

$$\frac{d}{dl}v_J = 0. \tag{2.10b}$$

The prefactor of $\omega^2/q^2\mathcal{D}$ in the above equations is not expected to be universal, other than the general structure and the dispersion. In the nonlocalised phase, we obtain the asymptotic correlators

$$\langle \Phi^a_{\mathbf{q}}\Phi^b_{-\mathbf{q}}\rangle = \frac{\pi\delta^{ab}}{v_N q^2 + \omega^2(1/v_J+\gamma)} \tag{2.11a}$$

$$\langle \Theta^a_{\mathbf{q}}\Theta^b_{-\mathbf{q}}\rangle = \frac{\pi\delta^{ab}}{v_J q^2 + \omega^2(1+\gamma v_J)/v_N}\left(1+\frac{\gamma}{v_N}\frac{\omega^2}{q^2}\right). \tag{2.11b}$$

As described above, these correlators imply quasi-long-ranged correlations of $e^{i\sqrt{2}\Phi}$ but only short-ranged correlations for $e^{i\sqrt{2}\Theta}$ over a length $\xi_\Theta \propto \Lambda_\omega^{-1}$.

2.3 Real-space RG

The focus is on the spatial behaviour of correlation functions. We want to see, if the above momentum-space results are reproduced if one considers renormalisation of correlation functions rather than of the Hamiltonian. The method used by Giamarchi and Schulz (GS in the following) [GS88, GS89] is explained in detail. It is largely analogous to methods that are used to treat the Kosterlitz-Thouless transition in the two-dimensional XY model.
Starting point is a perturbative expansion of the correlation function under the assumption of small disorder

$$\begin{aligned} R_\Phi(\mathbf{r}_1-\mathbf{r}_2) &\equiv e^{-F_{12}^{\text{eff}}} \equiv \langle e^{i\sqrt{2}[\Phi_1-\Phi_2]}\rangle \\ &= \frac{Z_0}{Z}\langle e^{i\sqrt{2}[\Phi_1-\Phi_2]}e^{-S_D}\rangle_0 \\ &= (1+\langle S_D\rangle_0)\langle e^{i\sqrt{2}[\Phi_1-\Phi_2]}(1-S_D)\rangle_0 + \mathcal{O}(\mathcal{D}^2) \\ &= e^{-F_{12}} + \langle S_D\rangle_0 e^{-F_{12}} - \langle e^{i\sqrt{2}[\Phi_1-\Phi_2]}S_D\rangle_0 \\ &= \dots \end{aligned}$$

With $\Phi_i = \Phi(x_i, \tau_i), \mathbf{r}_i = (x_i, u\tau_i), x_3 = x_4 = x, \tau_3 = \tau, \tau_4 = \tau'$ and

$$
\begin{aligned}
&-\langle e^{i\sqrt{2}[\Phi_1-\Phi_2]} S_D\rangle_0 = \\
&= \frac{\mathcal{D}}{2}\int_{\tau\tau' x}\left\{e^{\langle[(\Phi_1-\Phi_2)+(\Phi_3-\Phi_4)]^2\rangle_0} + e^{\langle[(\Phi_1-\Phi_2)-(\Phi_3-\Phi_4)]^2\rangle_0}\right\} \\
&= e^{-F_{12}}\frac{\mathcal{D}}{2}\int_{\tau\tau' x} e^{-\langle[\Phi_3-\Phi_4]^2\rangle_0}\left\{e^{\langle(\Phi_1-\Phi_2)(\Phi_3-\Phi_4)\rangle_0} + e^{-\langle(\Phi_1-\Phi_2)(\Phi_3-\Phi_4)\rangle_0}\right\} \\
&= e^{-F_{12}}\frac{\mathcal{D}}{2}\int_{\tau\tau' x} e^{-\langle[\Phi_3-\Phi_4]^2\rangle_0}\left\{e^{\langle(\Phi_1-\Phi_2)(\Phi_3-\Phi_4)\rangle_0} + e^{-\langle(\Phi_1-\Phi_2)(\Phi_3-\Phi_4)\rangle_0} - 2\right\} - \langle S_D\rangle_0 e^{-F_{12}} \\
&= e^{-F_{12}}\mathcal{D}\int_{\tau\tau' x} e^{-\langle[\Phi_3-\Phi_4]^2\rangle_0}\left\{\cosh\langle(\Phi_1-\Phi_2)(\Phi_3-\Phi_4)\rangle_0 - 1\right\} - \langle S_D\rangle_0 e^{-F_{12}},
\end{aligned}
$$

one has

$$
\begin{aligned}
\ldots &= e^{-F_{12}}\left\{1 + \mathcal{D}\int_{\tau\tau' x} e^{-\langle[\Phi_3-\Phi_4]^2\rangle_0}\left[\cosh\langle(\Phi_1-\Phi_2)(\Phi_3-\Phi_4)\rangle_0 - 1\right]\right\} \\
&\simeq e^{-F_{12}}\left\{1 + \frac{\mathcal{D}}{2}\int_{\tau\tau' x} e^{-\langle[\Phi_3-\Phi_4]^2\rangle_0}\left[\langle(\Phi_1-\Phi_2)(\Phi_3-\Phi_4)\rangle_0^2 + \mathcal{O}(\Delta\tau^4)\right]\right\} \qquad (2.12) \\
&= \ldots
\end{aligned}
$$

We have introduced $\Delta\tau = \tau' - \tau$ and below we will also use the centre of mass coordinate $\mathbf{R} = (x, u(\tau+\tau')/2) = (X, Y)$ of the internal points '3', '4'. In the following, terms of order $(\Delta\tau)^4$ under the integral are always neglected as the important contribution is expected to come from small $\Delta\tau$. We use

$$
\begin{aligned}
\langle(\Phi_1-\Phi_2)(\Phi_3-\Phi_4)\rangle_0 &= u\Delta\tau\left(\partial_y\langle\Phi_2\Phi_{\mathbf{R}}\rangle_0 - \partial_y\langle\Phi_1\Phi_{\mathbf{R}}\rangle_0\right) + \mathcal{O}(\Delta\tau^2) \\
&= \frac{K}{2}u\Delta\tau\left(\partial_y\ln[|\mathbf{r}_2-\mathbf{R}|\Lambda] - \partial_y\ln[|\mathbf{r}_1-\mathbf{R}|\Lambda]\right)
\end{aligned}
$$

to get

$$
\begin{aligned}
&\int_{\tau\tau' x} e^{-F_{34}}\langle(\Phi_1-\Phi_2)(\Phi_3-\Phi_4)\rangle_0^2 = \\
&= \frac{K^2 u}{4}\int_{\Delta\tau}\Delta\tau^2 e^{-F(\Delta\tau)}\int d^2R\left(\partial_y\ln[|\mathbf{r}_2-\mathbf{R}|\Lambda] - \partial_y\ln[|\mathbf{r}_1-\mathbf{R}|\Lambda]\right)^2 \\
&= \frac{K^2 u}{4}\int_{\Delta\tau}\Delta\tau^2 e^{-F(\Delta\tau)}\left(2\pi\ln[|\mathbf{r}_2-\mathbf{r}_1|\Lambda] - \pi\cos[2\phi]\right). \qquad (2.13)
\end{aligned}
$$

The angle ϕ is defined by $\tan\phi := u(\tau_2-\tau_1)/(x_2-x_1)$ and the integral over $\mathbf{R}$

$$
\begin{aligned}
&\int d^2R\left[\partial_Y\ln|\mathbf{a}-\mathbf{R}| - \partial_Y\ln|-\mathbf{R}|\right]^2 = \\
&= \int d^2R\left\{[\partial_Y\ln|\mathbf{a}-\mathbf{R}|]^2 + [\partial_Y\ln|-\mathbf{R}|]^2 - 2[\partial_Y\ln|\mathbf{a}-\mathbf{R}|][\partial_Y\ln|-\mathbf{R}|]\right\} \\
&= 2\int d^2R\left\{[\partial_Y\ln|\mathbf{R}|]^2 - [\partial_Y\ln|\mathbf{a}-\mathbf{R}|][\partial_Y\ln|-\mathbf{R}|]\right\} \\
&\equiv 2I_1 - 2I_2
\end{aligned}
$$

in the last step is evaluated with

$$\begin{aligned}
I_1 &= \int d^2R\,[\partial_Y \ln|\mathbf{R}|]^2 = \int d^2R\,\frac{R_y^2}{R^4} = \pi\int_{1/\Lambda}^{L}\frac{dR}{R} = \pi\ln(L\Lambda)\\
I_2 &= \int d^2R\,[\partial_Y \ln|\mathbf{a}-\mathbf{R}|][\partial_Y \ln|-\mathbf{R}|]\\
&= -\int d^2R\,\frac{(a_y-R_y)R_y}{(\mathbf{a}-\mathbf{R})^2R^2}\\
&= \int d^2R\,\frac{aR\sin\phi^2\cos\theta - R^2(\sin^2\phi\cos^2\theta+\sin^2\theta\cos^2\phi)}{(a^2+R^2-2aR\cos\theta)R^2}\\
&= -\sin^2\phi\int d\theta\int dx\frac{\cos\theta - x\cos\theta^2}{1+x^2-2x\cos\theta} - \cos^2\phi\int d\theta\int dx\frac{x\sin^2\theta}{1+x^2-2x\cos\theta}\\
&\underset{\text{maple}}{=} -(\sin^2\phi-\cos^2\phi)\int_0^1 dx\pi x + \pi\int_1^{|\mathbf{a}|}\frac{dx}{x}\\
&= \frac{\pi}{2}(-\sin^2\phi+\cos^2\phi) + \pi\int_1^{L/|\mathbf{a}|}\frac{dx}{x} = \frac{\pi}{2}\cos[2\phi] + \pi\int_1^{L/|\mathbf{a}|}\frac{dx}{x}\\
&= \frac{\pi}{2}\cos[2\phi] + \pi\ln[L/|\mathbf{a}|].
\end{aligned}$$

ϕ being the angle between the x-axis and $\mathbf{a}$ and θ the angle between $\mathbf{a}$ and $\mathbf{R}$ we substituted above

$$\begin{aligned}
R_x &= R\cos(\phi+\theta) = R(\cos\phi\cos\theta - \sin\phi\sin\theta)\\
R_x^2 &= R^2(\cos^2\phi\cos^2\theta + \sin^2\phi\sin^2\theta - 2\cos\phi\sin\phi\cos\theta\sin\theta)\\
R_y &= R\sin(\phi+\theta) = R(\sin\phi\cos\theta + \cos\phi\sin\theta)\\
R_y^2 &= R^2(\sin^2\phi\cos^2\theta + \sin^2\theta\cos^2\phi + 2\cos\phi\sin\phi\cos\theta\sin\theta).
\end{aligned}$$

The result Eq. (2.13) is inserted in the perturbative expansion of Eq. (2.12) and we re-exponentiate

$$\begin{aligned}
\ldots &= e^{-F_{12}^{\rm eff}} = e^{-F_{12}}\left\{1 + \frac{\mathcal{D}}{2}\frac{K^2u}{4}\int_{\Delta\tau}\Delta\tau^2 e^{-F(\Delta\tau)}\left(2\pi\ln[|\mathbf{r}_2-\mathbf{r}_1|\Lambda] - \pi\cos[2\phi]\right)\right\}\\
F_{12}^{\rm eff} &= F_{12} - \frac{\mathcal{D}}{8}\frac{K^2\alpha^3}{u^2}\int_{\Delta\tau u/\alpha}\left(\frac{\Delta\tau u}{\alpha}\right)^2 e^{-F(\Delta\tau)}\left(2\pi\ln[|\mathbf{r}_2-\mathbf{r}_1|\Lambda] - \pi\cos[2\phi]\right). \qquad (2.14)
\end{aligned}$$

Now the idea of the RG is to integrate out $\Delta\tau u/\alpha$ over dl at the lower cutoff (which here has to be introduced) iteratively and thus to renormalise in every step the parameters in F_{12}, see Eq. (2.7c); the rest of the integral is brought to the original form by 'pulling down' the cutoff back to $\alpha = 1/\Lambda$ and absorb the change in a renormalised $\mathcal{D}' = \mathcal{D} + \frac{d}{dl}\mathcal{D}dl$. The l.h.s. of Eq. (2.14) remains constant, it is the renormalised correlation function on largest scales, while on intermediate scales more and more of the effect of the integral is absorbed in the first term of the r.h.s. K is renormalised and a $\cos[2\phi]$-term generated in the correlations $F_{12}^{\rm eff}$, whose amplitude we denote for the moment with d

$$\begin{aligned}
\frac{d}{dl}K &= -\frac{\mathcal{D}K^2\alpha^3\pi}{2u^2} = -\frac{\mathcal{D}_{\rm GS}K^2}{4}\\
\frac{d}{dl}d &= \frac{\mathcal{D}\pi K^2\alpha^3}{4u^2}\\
\frac{d}{dl}\mathcal{D} &= (3-K)\mathcal{D}.
\end{aligned}$$

We have introduced $\mathcal{D}_{\rm GS} = 2\mathcal{D}\alpha^3\pi/u^2$ in order to make contact to the notation in Refs. [GS88, GS89].

The renormalisation of d can be rewritten in terms of a feedback to u, to this end we need

$$\begin{aligned}
\cos[2\phi] &= 1 - 2\sin^2\phi = 1 - \frac{2y^2}{y^2+x^2},\ y = u\tau, \\
\partial_u F_{12} &= \frac{K}{2u}\frac{y^2}{y^2+x^2}, \\
dF_{12} &= \partial_u F_{12} du + \partial_d F_{12} dd + \partial_K F_{12} dK \\
&= \frac{2y^2}{x^2+y^2}\left(\frac{K}{2u}du - dd\right) + \partial_K F_{12} dK + dd.
\end{aligned}$$

The effect of a finite $\frac{d}{dl}d$ is now attributed to a finite $\frac{d}{dl}u$ and $\frac{d}{dl}d$ is set to zero. This gives the equation of flow

$$\frac{d}{dl}u = -\frac{1}{4}uK\mathcal{D}_{\rm GS}.$$

The renormalisation of u, K rewritten in terms of v_N, v_J hence is

$$\frac{d}{dl}v_N = 0 \tag{2.15a}$$

$$\frac{d}{dl}v_J = -\frac{\pi\mathcal{D}\alpha^3 v_J^2}{u^3}. \tag{2.15b}$$

These are the EoF in GS, they give quasi-long range order both in the Φ- and the Θ-sector. Where is the reason for the discrepancy with respect to the momentum-shell result Eq. (2.10).? A hint comes from an alternative derivation of the RG relations. We rewrite Eq. (2.13) as

$$\begin{aligned}
&\int_{\tau\tau' x} e^{-F_{34}} \langle(\Phi_1 - \Phi_2)(\Phi_3 - \Phi_4)\rangle_0^2 = \\
&\quad = 2\int_{\Delta\tau} e^{-F(\Delta\tau)} \int_{\mathbf{Q}} \left(\mathcal{G}^0_{\Phi\Phi}\right)^2 4\sin^2\left[\frac{\omega\Delta\tau}{2}\right]\{1 - \cos\mathbf{Q}(\mathbf{r}_1 - \mathbf{r}_2)\} \\
&\quad = 2\int_{\Delta\tau} \Delta\tau^2 e^{-F(\Delta\tau)} \int_{\mathbf{Q}} \left(\mathcal{G}^0_{\Phi\Phi}\right)^2 \omega^2\{1 - \cos\mathbf{Q}(\mathbf{r}_1 - \mathbf{r}_2)\}.
\end{aligned}$$

Insertion in the expansion of the correlation function and re-exponentiation gives

$$F_{12}^{\rm eff} = F_{12} - \frac{\mathcal{D}2\alpha^3}{u^3}\int_{1/\Lambda}^{L}\frac{d(u\Delta\tau)}{\alpha}\left(\frac{u\Delta\tau}{\alpha}\right)^{2-K}\int_{\mathbf{Q}}\left(\mathcal{G}^0_{\Phi\Phi}\right)^2\omega^2\{1 - \cos\mathbf{Q}(\mathbf{r}_1 - \mathbf{r}_2)\}$$

and from here follows in the RG spirit

$$dF_{12} = -\frac{2\mathcal{D}\alpha^3 dl}{u^3}\int_{\mathbf{Q}}\left(\mathcal{G}^0_{\Phi\Phi}\right)^2\omega^2\{1 - \cos\mathbf{Q}(\mathbf{r}_1 - \mathbf{r}_2)\}.$$

In order to absorb the differential change in parameters of the free model, we now compare to the differential of F_{12} with respect to a change in v_N, v_J

$$dF_{12} \stackrel{!}{=} \frac{2}{\pi}\int_{\mathbf{Q}}\left(\mathcal{G}^0_{\Phi\Phi}\right)^2\{1 - \cos\mathbf{Q}(\mathbf{r}_1 - \mathbf{r}_2)\}\left(\frac{\omega^2}{v_J^2}dv_J - q^2 dv_N\right),$$

and get the renormalisation condition

$$\frac{\omega^2}{v_J^2}dv_J - q^2 dv_N = -\frac{\pi\mathcal{D}\alpha^3}{u^3}\omega^2 dl. \tag{2.16}$$

This equation is fulfilled by either of the sets of RG equations (2.9, 2.15)! One was led to the GS-set only by the implicit additional condition of a scale-independent renormalisation of v_N, v_J. In order to decide which set is correct, we need a second equation to supplement Eq. (2.16). This will be provided by the RG for the correlation function $e^{-G_{12}^{\rm eff}} \equiv \langle e^{i\sqrt{2}[\Theta_1-\Theta_2]}\rangle$. In close analogy to the Φ-correlations, we get

$$\begin{aligned} dG_{12} &= \frac{2\mathcal{D}\alpha^3 dl}{u^3}\int_{\mathbf{Q}}\{1-\cos\mathbf{Q}(\mathbf{r}_2-\mathbf{r}_1)\}\omega^2(\mathcal{G}^0_{\Theta\Phi})^2 \\ &= \frac{2\mathcal{D}\alpha^3 K^2 dl}{u^5}\int_{\mathbf{Q}}\{1-\cos\mathbf{Q}(\mathbf{r}_2-\mathbf{r}_1)\}\frac{\omega^4}{q^2}(\mathcal{G}^0_{\Theta\Theta})^2 \\ &= \frac{2\mathcal{D}\alpha^3 dl K^2}{u^5}\int_{\mathbf{Q}}\{1-\cos\mathbf{Q}(\mathbf{r}_2-\mathbf{r}_1)\}\Big(u^2 q\mathcal{G}^{\mathbf{Q}}_{\Theta\Theta}-\frac{\pi v_N}{q}\Big)^2, \end{aligned} \tag{2.17}$$

which is compared to the differential change of G_{12} by a small change in v_J, v_N

$$dG_{12} \stackrel{!}{=} \frac{2}{\pi}\int_{\mathbf{Q}}\left(\mathcal{G}^0_{\Theta\Theta}\right)^2\{1-\cos\mathbf{Q}(\mathbf{r}_1-\mathbf{r}_2)\}\left(\frac{\omega^2}{v_N^2}dv_N - q^2 dv_J\right).$$

The comparison gives

$$\frac{\omega^2}{v_N^2}dv_N - q^2 dv_J = \frac{\pi\mathcal{D}\alpha^3 K^2}{u^5}\frac{\omega^4}{q^2 v_N^2}dl \tag{2.18}$$

and the unique solution to the two equations (2.16,2.18) is the RG equations from the momentum-shell approach (modulo the non-universal prefactor). However, if in Eq. (2.17) the dubiously singular $\pi v_N/q$-term in the round brackets is dropped, the RG conditions are

$$\frac{\omega^2}{v_J^2}dv_J - q^2 dv_N = -\frac{\pi\mathcal{D}\alpha^3}{u^3}\omega^2 dl \tag{2.19a}$$

$$\frac{\omega^2}{v_N^2}dv_N - q^2 dv_J = \frac{\pi\mathcal{D}\alpha^3}{u}K^2 q^2 dl, \tag{2.19b}$$

which are solved by the GS-equations of flow. We remind of the relations $K^2 = v_J/v_N, u^2 = v_J v_N$.

2.4 Conclusion

The situation is still puzzling. Shall we retain the $\pi v_N/q$-term or not? What is its significance? It can be more clearly seen after Fourier transformation how singular the effect of this is term is. On the way to the flow equations we expanded in the small time difference $\Delta\tau = \tau_3 - \tau_4 = \tau - \tau'$. The $1/q$-term hence corresponds one-to-one to the second, delta-function term in Eq. (2.8b), which is ultra-local in time. Going back to the step before the expansion proves helpful. Consider the equivalent of Eq. (2.12) for the Θ-correlations

$$\langle e^{i\sqrt{2}(\Theta_1-\Theta_2)}\rangle = e^{\langle[\Theta_1-\Theta_2)]^2\rangle}\left\{1+\mathcal{D}\int_{\tau\tau' x} e^{-G_{12}}(\cosh\langle(\Theta_1-\Theta_2)(\Phi_3-\Phi_4)\rangle - 1)\right\} \tag{2.20}$$

and here the argument of the $\cosh$

$$\langle(\Theta_1-\Theta_2)(\Phi_3-\Phi_4)\rangle = \langle\Theta_1\Phi_3\rangle - \langle\Theta_1\Phi_4\rangle + \langle\Theta_2\Phi_4\rangle - \langle\Theta_2\Phi_3\rangle. \tag{2.21}$$

From Eq. (2.7a), we see that each of the four terms jumps by $\pi/2$ (in the limit $\alpha \to 0$) if the time coordinates of the respective Θ- and the Φ-field conincide generating the delta function in the relation for the derivatives. In an expansion of the $\cosh$-term the role of these jumps now has to be analysed carefully, hereby Fig. F.3 might be helpful. The two external points '1', '2' are fixed in the $x\tau$-plane while the internal points '3', '4' are characterised by their small distance $\Delta\tau$, which is integrated over iteratively at the lower cutoff, and their centre of mass coordinate $R = (X, Y)$, which is integrated over the whole plane. The expansion in the derivation above had assumed the argument of the $\cosh$ to be small. This is certainly justified whenever the two internal points are not separated by one of the lines $\tau = \tau_1$ or $\tau = \tau_2$. If they are so, however, the sign functions of the correlators between the internal points and the separating point give opposite signs, see Eq. (2.7a),and instead of being small, the limit of the argument of the $\cosh$ is

$$\lim_{\Delta\tau\to 0}\langle(\Theta_1 - \Theta_2)(\Phi_3 - \Phi_4)\rangle = i\arctan[\frac{x_1 - X}{|u\tau_1 - Y| + \alpha}] + \mathcal{O}(\Delta\tau) \tag{2.22}$$

with the coordinates (x_1, τ_1) of the separating point. One therefore has to expand in these situations the $\cosh$ not around zero but around $i\arctan[\frac{x_1-X}{|u\tau_1-Y|+\alpha}] \simeq i\frac{\pi}{2}$. The latter approximation comes from the fact that the present consideration is necessary only in corridors of small width $|u\tau_i - Y|$ around the external times $i - 1, 2$. With $\cosh[i\pi/2 + \mathcal{O}(\Delta\tau)] = -\sin[\mathcal{O}(\Delta\tau)] = \mathcal{O}(\Delta\tau)$ we have – as it seems to the author – the key to the question if to drop the $1/q$-term or not and consequently which set of RG equations to trust. Due to the linear dependency on the argument upon expansion in the corridors – rather than the quadratic dependency in the rest of the plane – configurations with inverted internal points such as (b), (c) in Fig. F.3 cancel in the integration of the centre of mass coordinate of the internal points. The jumps in the $\langle\Theta\Phi\rangle$-correlator make themselves felt only in the corridors, here their effect cancels due to symmetry. We can therefore drop them in the first place, i.e., trust the equations of flow (2.19). For reasons of completeness, we comment on the last term in the integrand of Eq. (2.20), the 1. Outside the corridors, it is combined with the $\cosh$ in order to give a contribution of order $\Delta\tau^2$. Inside the corridors, the $\cosh$ becomes by the shift in the argument a $\sin$. Here, the has to be considered separately and upon integration it renormalised the amplitude of the algebraically decaying correlations. This, however, can be absorbed in a renormalised cutoff.

The situation now seems clarified as far as the RG for the order parameter correlation function

$$R_\Theta(x, \tau) := \langle\exp[i\sqrt{2}(\Theta(x, \tau) - \Theta(0, 0))]\rangle.$$

is concerned, which is addressed directly by the real-space approach. But how can this be reconciled with the momentum-space RG that still seems inherently correct. Maybe the solution lies in the following direction. In momentum-space RG, the Hamiltonian is renormalised. In case of a Gaussian fixed point it allows to read off

$$B_\Theta(x, \tau) := \langle[\Theta(x, \tau) - \Theta(0, 0)]^2\rangle.$$

The naive use of $R_\Theta(x, \tau) = \exp[-B_\Theta(x, \tau)]$ might be spoiled by contributions to $R_\Theta(x, \tau)$ from finite scales, where the action is not Gaussian yet. This direction of search for a solution to the puzzle is sustained by two observations. First, going through the real-space RG for $B_\Theta(x, \tau)$, we start at the level after the expansion of the $\cosh$ around zero and thus cannot use the same argument as above

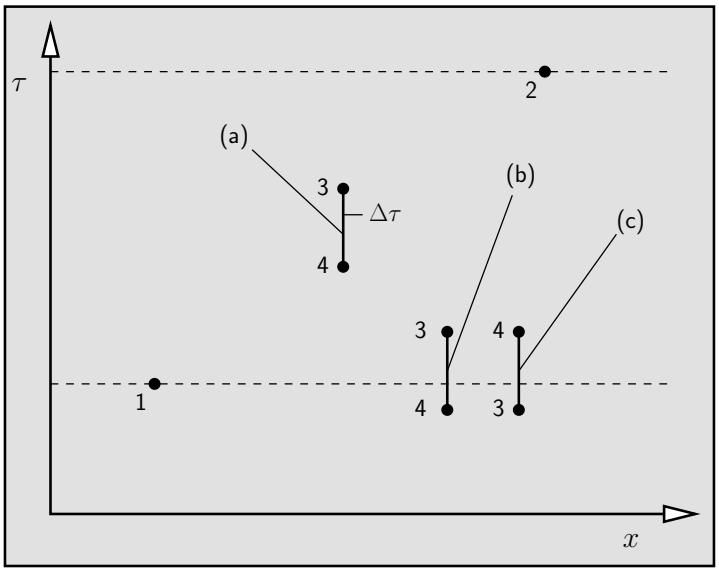

Fig. F.3: The external points '1', '2' and internal points '3', '4' of the first order expansion of $\langle e^{i\sqrt{2}(\Theta_1-\Theta_2)}\rangle$ in the space-time plane. For situations like (a), the $\cosh$ may be expandend around zero, for situations (b), (c) around $i\pi/2$. Contributions to the renormalised correlation function from configurations (b) and (c) cancel.

in order to discard the singular term in the correlator. We are therefore lead to the momentum-shell RG equations in this case.
Second, we consider a simplified scenario, the quantum mechanical harmonic oscillator $H = \frac{1}{2m}\hat{p}^2 + \frac{\kappa}{2}\hat{x}^2$ perturbed by the quartic anharmonicity $\lambda\hat{x}^4$. The momentum expectation value $\langle\hat{p}^2\rangle$ can be calculated via two routes. (i) by standard quantum mechanical perturbation theory on an operator level using the set of unperturbed harmonic oscillator states, and (ii) in the perturbative path-integral approach, where the classical field p plays the role of $\partial_x\Theta$ and x the role of $\partial_x\Phi$ of the bosonisation problem. Route (ii) is the very analogue to the perturbative momentum-shell RG that is so hard to interpret. Interestingly, in this zero-dimensional model case, the result can be checked against the operator calculation which is beyond doubt. The agreement is one-to-one. As for the bosonisation problem, we thus do not expect to obtain the wrong correlations $B_\Theta(x,\tau)$ in the momentum shell approach.

The proposed resolution might have physical implications. If some observable can be found that appears in bosonised form as $e^{ip\Theta}$, such that the shift due to the sign function, as described above, is not to a point where symmetry allows to neglect these singular terms, the momentum-shell RG equations should apply. $p = \sqrt{4}$ would be such a value for which as a consequence short-ranged correlations of $e^{ip\Theta}$ are expected. The author could not think of any such observable, maybe there are none that show this non-Luttinger liquid behaviour. This in turn would comply with the Luttinger liquid hypothesis, stating that *all* large scale correlations in the phase with no relevant instabilities are of algebraic form with exponents related to the coefficients at the Luttinger liquid fixed point.

3 Spin wave contribution to the RFXY free energy

The 'spin wave' part of the disorder free energy Eq. (D.2.11) is calculated as

$$\begin{aligned}
\ln\det(\mathcal{M}^{-1/2}) &= -\frac{1}{2}\ln\left[\Pi_i\lambda_i\right] \\
&= -\frac{1}{2}\ln\left[\Pi_{\mathbf{q}} q^{2n}(J-n\sigma\cos^2\theta)J^{n-1}T^{-n}\right] \\
&= -\frac{1}{2}\ln\left[\Pi_{\mathbf{q}}\left(q^2(1-n\frac{\sigma}{J}\cos^2\theta)^{1/n}J/T\right)^n\right] \\
&= n\sum_{\mathbf{q}}\ln\frac{1}{|q|} - n/2\ln(J/T)\sum_{\mathbf{q}} -n/2\sum_{\mathbf{q}}\ln(1-n\frac{\sigma}{J}\cos^2\theta)^{1/n} \\
\lim_{n\to 0}\frac{1}{n}\ln\det\mathcal{M}^{-1/2} &= c(J,T) - \frac{1}{2}\sum_{\mathbf{q}}(-\frac{\sigma}{J}\cos^2\theta) \\
&= c(J,T) + \frac{\tilde{A}}{\xi_x\xi_z}\frac{\sigma}{4J}.
\end{aligned}$$

4 Correlated random walk

Consider a random walk with correlations $\langle x_{i+n}x_i\rangle = \sigma^2 e^{-2n/n_c}$. Then straightforward calculation [Tay21] gives for $n_c \gg 1$

$$\frac{\langle X_n^2\rangle}{(n_c\sigma)^2} := \frac{\langle(\sum_{i=1}^n x_i)^2\rangle}{(n_c\sigma)^2} = \frac{n}{n_c} + (\frac{1}{2}e^{-n/n_c} - 1).$$

With $n_c = \xi/a$, $n = z/a$ and $X_n = \big(x(z) - x(0)\big)/a$ we have for $z \gg \xi$

$$\langle(x(z)-x(0))^2\rangle = \sigma^2\xi(z-\xi) = \frac{T}{g}(z-\xi). \tag{4.23}$$

Now a can be sent to zero to reach the continuum. The identification $\sigma^2\xi = T/g$ gives exactly the momentum space cutoff result 2.37 of Section 2.6. Note that in order to make contact between the continuum random walk and the discrete random walk in the uncorrelated case, one has to choose $\sigma^2 a = T/g$. With this choice, we would have a factor of $\xi/a > 1$ in the correlations. This shows that correlations are *enhanced* by an overall factor and *suppressed* by the shift $z \to z - \xi$. It can be shown that the overall effect is always an increase of the fluctuations, as one might have intuitively guessed. If however, after introducing correlations, the new prefactor is identified with the effective, measurable T/g the effect is a reduction of fluctuations due to the shift-term. To sum up: Turning on correlations is not so physical, rather the effective g is fixed and small modes are forbidden, as implemented by a momentum UV cutoff. Eq. 4.23 describes the measurable fluctuations in terms of measurable parameters. The result reproduces the expression obtained with a momentum UV cutoff.

5 Annealed average of dimer and vortex free energies

In this appendix the annealed averages of both the discrete line system of the random-bond dimer model and the continuum disordered line lattice are calculated. The results are used to gauge disorder strengths in the systems and yield Eq. (33.56).

The relation between the energies of the discrete line configuration (lines), dimer pattern (D) and reference pattern (R) is

$$H_{\rm lines}(\{\epsilon'_{ij}\}) = H_D(\{\epsilon_{ij}\}) + H_R(\{\epsilon'_{ij}\}).$$

Here, it holds for the bond energies $\epsilon'_{ij} = -\epsilon_{ij}$ on the reference pattern, $\epsilon'_{ij} = \epsilon_{ij}$ elsewhere. ϵ_{ij} is a symmetrically distributed random variable with mean $\overline{\epsilon_{ij}} = 0$ and variance $\overline{\epsilon_{ij}\epsilon_{kl}} = \delta_{ij,kl}$.
Consider the difference δF of the annealed average of free energy in the random line system and in the pure system

$$\delta F/T = \ln \frac{\overline{Z}_{\rm lines}}{Z_{\rm lines,0}}.$$

For the continuum, the calculation is straightforward and very short. It gives

$$\delta F_{\rm cont.}/T = \frac{\Delta\rho}{2T^2\xi_d} L_x L_y. \tag{5.24}$$

For the lattice model, the disorder average of the partition function with the discrete line energy is

$$\begin{aligned}
\overline{Z}_{\rm lines} &= \sum_{\{D\}} \overline{\exp\Big\{-\frac{1}{T}_d \Big(\sum_{ij\in D}\epsilon_{ij} + \sum_{ij\in R} -\epsilon_{ij}\Big)\Big\}} \\
&= \sum_{\{D\}} \exp\Big\{\frac{1}{2T_d^2}\overline{\Big(\sum_{ij\in D}\epsilon_{ij} - \sum_{ij\in R}\epsilon_{ij}\Big)^2}\Big\} \\
&= \sum_{\{D\}} \exp\Big\{\frac{1}{2T_d^2}\Big(\sum_{ij\in D}\overline{\epsilon_{ij}^2} + \sum_{ij\in R}\overline{\epsilon_{ij}^2} - 2\sum_{ij\in D}\sum_{kl\in R}\overline{\epsilon_{ij}\epsilon_{kl}}\Big)\Big\} \\
&= \exp\Big(\frac{L^2}{2T_d^2}\Big)\sum_{\{D\}}\exp\Big\{-\frac{1}{T_d^2}\sum_{ij\in D} I_{ij}\Big\},
\end{aligned}$$

with $I_{ij} = 1$ on the reference bonds and $I_{ij} = 0$ elsewhere. Note that the sum over the squares of the dimer energies is independent of the dimer configuration only in the case of the isotropic dimer model. In the case with random energies only on the vertical bonds it would not give a simple factor to the sum over dimer configurations.
The remaining sum over dimer configurations

$$Z_R := \sum_D \exp\left\{-\frac{1}{T_d^2}\sum_{ij\in D} I_{ij}\right\}$$

can be done exactly with the methods of Ref. [Kas61] in a variation of the calculation given there. It yields

$$\ln Z_R = \frac{N^2}{\pi}\int_0^{e^{-1/(2T_d^2)}} dx\,\frac{\arctan[x]}{x}$$

The partition function of the pure lattice model is easily obtained by taking the limit $T_d \to \infty$,

$$\ln Z_{\rm lines,0} = \frac{G}{\pi}$$

with Catalan's constant $G = 0.915966$. Thus we finally obtain for energy difference

$$\delta F_{\rm discr.}/T = L^2\left\{\frac{1}{2T_d^2} - \frac{G}{\pi} + \frac{1}{\pi}\int_0^{e^{-1/(2T_d^2)}} dx\,\frac{\arctan[x]}{x}\right\}.$$

The comparison with Eq. (5.24) at the line density $\rho = 1/(2b)$, b being the dimer lattice spacing, gives the desired relation

$$\frac{\Delta}{T^2} = \frac{\xi_d}{b}\frac{1}{T_d^2}\left\{2 - \frac{4GT_d^2}{\pi} + \frac{4T_d^2}{\pi}\int_0^{e^{-1/(2T_d^2)}} dx\,\frac{\arctan[x]}{x}\right\}.$$

Bibliography

[Abr64] A. A. Abrikosov. *Soviet Phys. JETP*, 19:988, 1964.

[AHV72] P. W. Anderson, B. I. Halperin, and C. M. Varma. *Phil. Mag.*, 8:1, 1972.

[AKM+01] N. Avraham, B. Khaykovich, Y. Myasoedov, M. Rappaprt, H. Shtrikman, D. E. Feldman, T. Tamegai, P. H. Kes, M. Li, M. Konczykowski, K. van der Beek, and E. Zeldov. *Nature (London)*, 411:451, 2001.

[ALS02] Y. Ando, A. N. Lavrov, and K. Segawa. *Phys. Rev. Lett.*, 88:137005, 2002.

[Ape82] W. Apel. *J. Phys. C*, 15:1973, 1982.

[AR82] W. Apel and T. M. Rice. *Phys. Rev. B*, 26:7063, 1982.

[AS74] M. Abramowitz and I. Stegun. *Handbook of Mathematical Functions*. Dover Publications, 1974.

[ASKL99] Y. Ando, K. Segawa, S. Komiya, and A. N. Lavrov. *Phys. Rev. Lett.*, 83:2813, 1999.

[Bak82] P. Bak. *Rep. Prog. Phys.*, 45:587, 1982.

[Bal93] L. Balents. *Europhys. Lett.*, 24:489, 1993.

[BAP+99] C. A. Bolle, V. Aksyuk, F. Pardo, P. L. Gammel, E. Zeldov, E. Bucher, R. Boie, D. J. Bishop, and D. R. Nelson. *Nature (London)*, 399:43, 1999.

[BC91] C. Bourbonnais and L. G. Caron. *Int. J. Mod. Phys. B*, 5:1033, 1991.

[BD87] E. Brunet and B. Derrida. *Phys. Rev. E*, 61:200, 1987.

[BEN01] S. Bogner, T. Emig, and T. Nattermann. *Phys. Rev. B*, 174501:63, 2001.

[BENS] S. Bogner, T. Emig, T. Nattermann, and S. Scheidl. comment; cond-mat/0110592.

[BH94] G. G. Batrouni and T. Hwa. *Phys. Rev. Lett.*, 72:4133, 1994.

[Bin83] K. Binder. *Z. Phys. B*, 50:343, 1983.

[BM86] J. G. Bednorz and K. A. Müller. *Z. Phys. B*, 64:189, 1986.

[BMS+01] F. Bouquet, C. Marcenat, E. Steep, R. Calemczuk, W. K. Kwok, U. Welp, G. W. Crabtree, R. A. Fisher, N. E. Phillips, and A. Schilling. *Nature (London)*, 411:448, 2001.

[BO90] J.-P. Bouchaud and H. Orland. *J. Stat. Phys.*, 61:877, 1990.

[Bra77] E. H. Brandt. *J. Low Temp. Phys.*, 26:735, 1977.

[BY86] K. Binder and A. Young. *Rev. Mod. Phys.*, 58:801, 1986.

[CAM+91] S-W. Cheong, G. Aeppli, T. E. Mason, H. Mook, S. M. Hayden, P. C. Canfield, Z. Fisk, K. N. Clausen, and J. L. Martinez. *Phys. Rev. Lett.*, 67:1791, 1991.

[CCC93] C. H. Chen, S-W. Cheong, and A. S. Cooper. *Phys. Rev. Lett.*, 71:2461, 1993.

[CFY+93] R. Cubitt, E. M. Forgan, G. Yang, S. L. Lee, D. M. Paul, H. A. Mook, M. Yethiraj, P. H. Kes, T. W. Li, A. A. Menovsky, Z. Tarnawski, and K. Mortensen. *Nature (London)*, 365:407, 1993.

[CHC+94] S-W. Cheong, H. Y. Hwang, C. H. Chen, B. Batlogg, L. W. Rupp, Jr, and S. A. Carter. *Phys. Rev. B*, 49:7088, 1994.

[CHM+91] M. K. Crawford, R. L. Harlow, E. M. McCarron, W. E. Farneth, J. D. Axe, H. Chou, and Q. Huang. *Phys. Rev. B*, 44:7749, 1991.

[CO82] J. L. Cardy and S. Ostlund. *Phys. Rev. B*, 25:6899, 1982.

[CS95] D. Cule and Y. Shapir. *Phys. Rev. Lett.*, 74:114, 1995.

[CS96] D. Cule and Y. Shapir. *Phys. Rev. E*, 53:1553, 1996.

[dG68] P. G. de Gennes. *J. Chem. Phys.*, 48:2257, 1968.

[DGS+00] C-H. Du, M. E. Ghazi, Y. Su, I. Pape, P. D. Hatton, S. D. Brown, W. G. Stirling, M. J. Cooper, and S-W. Cheong. *Phys. Rev. Lett.*, 84:3911, 2000.

[DHF92] A. T. Dorsey, M. Huang, and M. P. A. Fisher. *Phys. Rev. B*, 45:523, 1992.

[DMD98] P. Dai, H. A. Mook, and F. Dogan. *Phys. Rev. Lett.*, 80:1738, 1998.

[DMHD01] P. Dai, H. A. Mook, R. D. Hunt, and F. Dogan. *Phys. Rev. B*, 63:054525, 2001.

[EB03] T. Emig and S. Bogner. *Phys. Rev. Lett.*, 90:185701, 2003.

[EBN99] T. Emig, S. Bogner, and T. Nattermann. *Phys. Rev. Lett.*, 83:400, 1999.

[EFKL00] V. J. Emery, E. Fradkin, S. A. Kivelson, and T. C. Lubensky. *Phys. Rev. Lett.*, 85:2160, 2000.

[EK93] V. J. Emery and S. A. Kivelson. *Physica C*, 289:597, 1993.

[EK00] T. Emig and M. Kardar. *Phys. Rev. Lett.*, 85:2176, 2000.

[EK01] T. Emig and M. Kardar. *Nucl. Phys. B*, 604:479, 2001.

[EKL90] V. J. Emery, S. A. Kivelson, and H.-Q. Lin. *Phys. Rev. Lett.*, 64:475, 1990.

[EKLP92] N. Elkies, G. Kuperberg, M. Larsen, and J. Propp. *J. Algebr. Comb.*, 1:111+;219+, 1992.

[EKZ97] V. J. Emery, S. A. Kivelson, and O. Zachar. *Phys. Rev. B*, 56:6120, 1997.

[Emi98] T. Emig. *Disorder Driven Roughening Transitions of Elastic Manifolds and Periodic Media and on Surface Charging in High-T_c Superconductors*. PhD thesis, Universität zu Köln, 1998.

[EN97] T. Emig and T. Nattermann. *Phys. Rev. Lett.*, 79:5090, 1997.

[EN98] T. Emig and T. Nattermann. *Phys. Rev. Lett.*, 81:1469, 1998.

[EN99] T. Emig and T. Nattermann. *Eur. Phys. J. B*, 8:525, 1999.

[ER90] J. R. Engelbrecht and M. Randeria. *Phys. Rev. Lett.*, 65:1032, 1990.

[FH87] D. S. Fisher and D. A. Huse. *J. Phys. A*, 20L:1005, 1987.

[FH88] D. S. Fisher and D. A. Huse. *Phys. Rev. B*, 38:386, 1988.

[FH91] D. S. Fisher and M. P. A. Fisher D. A. Huse. *Phys. Rev. B*, 43:130, 1991.

[Fis61] M. E. Fisher. *Phys. Rev.*, 124:1664, 1961.

[Fis66] M. E. Fisher. *J. Math. Phys.*, 7:1776, 1966.

[Fis84] M. E. Fisher. *J. Stat. Phys.*, 34:667, 1984.

[Fis86] D. S. Fisher. *Phys. Rev. Lett.*, 56:1964, 1986.

[Fis89] M. P. A. Fisher. *Phys. Rev. Lett.*, 62:1415, 1989.

[FL81] D. S. Fisher and P. A. Lee. *Phys. Rev. B*, 23:6851, 1981.

[FL89] M. P. A. Fisher and D. H. Lee. *Phys. Rev. B*, 39:2756, 1989.

[GH82] Y. Y. Goldschmidt and A. Houghton. *Nucl. Phys. B*, 210:155, 1982.

[GL94] T. Giamarchi and P. Le Doussal. *Phys. Rev. Lett.*, 72:1530, 1994.

[GS88] T. Giamarchi and H. J. Schulz. *Phys. Rev. B*, 37:325, 1988.

[GS89] T. Giamarchi and H. J. Schulz. *Phys. Rev. B*, 39:4620, 1989.

[Hal80] F. D. M. Haldane. *Phys. Rev. Lett.*, 45:1358, 1980.

[Hal81a] F. D. M. Haldane. *J. Phys. C*, 14:2585, 1981.

[Hal81b] F. D. M. Haldane. *Phys. Rev. Lett.*, 47:1840, 1981.

[HEKK02] C. Howald, H. Eisaki, N. Kaneko, and A. Kapitulnik. 2002. preprint cond-mat/0201546.

[Hen97] C. L. Henley. *J. Stat. Phys.*, 89:483, 1997.

[HF94] T. Hwa and D. S. Fisher. *Phys. Rev. Lett.*, 72:2466, 1994.

[HHF85] D. A. Huse, C. L. Henley, and S. S. Fisher. *Phys. Rev. Lett.*, 55:2924, 1985.

[HLZ+92] S. M. Hayden, G. H. Lander, J. Zaretsky, P. J. Brown, C. Stassis, P. Metcalf, and J. M. Honig. *Phys. Rev. Lett.*, 68:1061, 1992.

[HML+02] J. E. Hoffmann, K. McElroy, D.-H. Lee, K. M. Lang, H. Eisaki, S. Uchida, and J. C. Davis. *Science*, 297:1148, 2002.

[HNMD99] N. Hasselmann, A. H. Castro Neto, C. Morais Smith, and Y. Dimashko. *Phys. Rev. Lett.*, 82:2135, 1999.

[HSI99] A. W. Hunt, P. M. Singer, and T. Imai. *Phys. Rev. Lett.*, 82:4300, 1999.

[IUT+00] N. Ichikawa, S. Uchida, J. M. Tranquada, T. Niemöller, P. M. Gehring, and J. R. Schneider. *Phys. Rev. Lett.*, 85:1738, 2000.

[Jer91] D. Jerome. *Science*, 252:1509, 1991.

[JKKN77] J. V. José, L. P. Kadanoff, S. Kirkpatrick, and D. R. Nelson. *Phys. Rev. B*, 16:1217, 1977.

[Kar87] M. Kardar. *Nucl. Phys. B*, 290:582, 1987.

[Kas61] P. W. Kasteleyn. *Physica (Utrecht)*, 27:1209, 1961.

[KBB+92] B. Keimer, N. Belk, R. J. Birgenau, A Cassanho, C. Y. Chen, M. Greven, M. A. Kastner, A. Aharony, Y. Endoh, R. W. Erwin, and G. Shirane. *Phys. Rev. B*, 46:14034, 1992.

[KBI93] V. E. Korepin, N. M. Bogoliubov, and A. G. Izergin. *Quantum Inverse Scattering Method and Correlation Functions*. Cambridge University Press, 1993.

[KD98] S. E. Korshunov and V. E. Dotsenko. *J. Phys. A*, 31:2591, 1998.

[KE96] S. A. Kivelson and V. J. Emery. *Synth. Met.*, 80:151, 1996.

[KFE98] S. A. Kivelson, E. Fradkin, and V. J. Emery. *Nature (London)*, 393:550, 1998.

[KG76] R. A. Klemm and H. Gutfreund. *Phys. Rev. B*, 14:1086, 1976.

[KHM+99] H. Kimura, K. Hirota, H. Matsushita, K. Yamada, Y. Endoh, S.-H. Lee, C. F. Majkrzak, R. Erwin, G. Shirane, M. Greven, Y. S. Lee, M. A. Kastner, and R. J. Birgenau. *Phys. Rev. B*, 59:6517, 1999.

[Kie93] J. Kierfeld, 1993. J. Kierfeld, Diploma Thesis, Universität zu Köln (1993).

[Kie98] J. Kierfeld. *Physica C*, 300:171, 1998.

[KJB+01] T. Klein, I. Journard, S. Blanchard, J. Marcus, R. Cubitt, T. Giamarchi, and P. Le Doussal. *Nature (London)*, 413:404, 2001.

[KN85] M. Kardar and D. R. Nelson. *Phys. Rev. Lett.*, 55:1157, 1985.

[Kos74] J. M. Kosterlitz. *J. Phys. C*, 7:1046, 1974.

[KT73] J. M. Kosterlitz and D. J. Thouless. *J. Phys. C*, 6:1181, 1973.

[KZ87] M. Kardar and Y.-C. Zhang. *Phys. Rev. Lett.*, 58:2807, 1987.

[Lan69] L. D. Landau. *Statistical Physics*. Pergamon Press, Oxford, 1969.

[LC97] S.-H. Lee and S-W. Cheong. *Phys. Rev. Lett.*, 79:2514, 1997.

[LG95] P. Le Doussal and T. Giamarchi. *Phys. Rev. Lett.*, 74:606, 1995.

[LG00] P. Le Doussal and T. Giamarchi. *Physica C*, 331:233, 2000.

[LL69] L. D. Landau and E. M. Lifshitz. *Elasticity Theory*. Pergamon Press, Oxford, 1969.

[LNP92] I. Lyuksyutov, A. G. Naumovets, and V. Pokrovsky. *Two-dimensional crystals*. Academic Press, San Diego, 1992.

[LRK77] P. A. Lee, T. M. Rice, and R. A. Klemm. *Phys. Rev. B*, 15:2984, 1977.

[Lut63] J. M. Luttinger. *J. Math. Phys.*, 4:1154, 1963.

[LWC02] P. Le Doussal, K. J. Wiese, and P. Chauve. *Phys. Rev. B*, 66:174201, 2002.

[Mac89] K. Machida. *Physica C*, 158:192, 1989.

[MAM92] T. E. Mason, G. Aeppli, and H. A. Mook. *Phys. Rev. Lett.*, 68:1414, 1992.

[MD99] H. A. Mook and F. Dŏgan. *Nature (London)*, 401:145, 1999.

[MDDH00] H. A. Mook, P. Dai, F. Dŏgan, and R S Hunt. *Nature (London)*, 404:729, 2000.

[MDHC98] C. Morais Smith, Y. Dimashko, N. Hasselmann, and A. O. Caldeira. *Phys. Rev. B*, 58:453, 1998.

[MFY+00] M. Matsuda, M. Fujita, K. Yamada, R. J. Birgeneau, M. A. Kastner, H. Hiraka, Y. Endoh, S. Wakimoto, and G. Shirane. *Phys. Rev. B*, 62:9148, 2000.

[MKL01] R. Mukhopadhyay, C. L. Kane, and T. C. Lubensky. *Phys. Rev. B*, 64:045120, 2001.

[ML65] D. C. Mattis and E. H. Lieb. *J. Math. Phys.*, 6:304, 1965.

[MMRL95] E. Marinari, R. Monasson, and J. J. Ruiz-Lorenzo. *J. Phys. A*, 28:3975, 1995.

[Moo92] M. Moore. *Phys. Rev. B*, 45:7736, 1992.

[MS64] W. W. Mullins and R. F. Sekerka. *J. Appl. Phys.*, 35:444, 1964.

[MS02] R. Moessner and S. L. Sondhi. *Prog. Theor. Phys. Supp.*, 145:37, 2002.

[MSFS88] A. R. Moodenbaugh, Y. Xu. M. Suenaga, T. J. Folkerts, and R. N. Shelton. *Phys. Rev. B*, 38:4596, 1988.

[Nat85] T. Nattermann. *Phys. Stat. Sol. (b)*, 132:125, 1985.

[Nel83] D. R. Nelson. In C. Domb and J. L. Lebowitz, editors, *Phase Transitions and Critical Phenomena Vol.7*. Academic Press, London, 1983.

[NEU99] T. Noda, H. Eisaki, and S. Uchida. *Science*, 286:265, 1999.

[NIF+99] T. Niemöller, N. Ichikawa, T. Frello, H. Hunnefeld, N. H. Andersen, S. Uchida, and J. R. Schneider. *Eur. Phys. J. B*, 12:509, 1999.

[NL91] T. Nattermann and H. Leschhorn. *Europhys. Lett.*, 14:603, 1991.

[NLS91] T. Nattermann, I. Lyuksyutov, and M. Schwartz. *Europhys. Lett.*, 16:295, 1991.

[Noz92] P. Nozières. Shape and growth of crystals. In C. Godrèche, editor, *Solids far from Equilibrium*. Cambridge Univ. Press, Cambridge, 1992.

[NS00] T. Nattermann and S. Scheidl. *Adv. Phys.*, 49:607, 2000.

[NU92] Y. Nakamura and S. Uchida. *Phys. Rev. Lett.*, 46:5841, 1992.

[NV92] D. R. Nelson and V. M. Vinokur. *Phys. Rev. Lett.*, 68:2398, 1992.

[NV93] D. R. Nelson and V. M. Vinokur. *Phys. Rev. B*, 48:13060, 1993.

[NW96] C. Nayak and F. Wilczek. *Int. J. Mod. Phys. B*, 10:2125, 1996.

[PFTV93] W.H. Press, B.P. Flanery, S.A. Teukolsky, and W.T. Velterling. *Numerical Recipes in C, 2nd ed.* Cambridge Univ. Press, 1993.

[PT79] V. L. Pokrovsky and A. L. Talapov. *Phys. Rev. Lett.*, 42:65, 1979.

[RGC+96] A P Ramirez, P L Gammel, S-W. Cheong, D J Bishop, and P Chandra. *Phys. Rev. Lett.*, 76:447, 1996.

[SBT+95] V. Sachan, D. J. Buttrey, J. M. Tranquada, J. E. Lorenzo, and G. Shirane. *Phys. Rev. B*, 51:12742, 1995.

[Sch89] H. J. Schulz. *J. Physique*, 50:2833, 1989.

[Sch93] H. J. Schulz. *Phys. Rev. Lett.*, 71:1864, 1993.

[Sch95] H. J. Schulz. In E. Akkermans *et al.*, editor, *Proceedings of Les Houches Summer School LXI*. World Scientific, 1995.

[SD00] S. Scheidl and Y. Dinçer. 2000. cond-mat/0006048.

[SMR+01] A. Soibel, Y. Myasoedov, M. L. Rappaport, T. Tamegai, S. S. Banerjee, and E. Zeldov. *Phys. Rev. Lett.*, 87:167001, 2001.

[SVBO88] U. Schulz, J. Villain, E. Brézin, and H. Orland. *J. Stat. Phys.*, 51:1, 1988.

[TAI+96] J. M. Tranquada, J. D. Axe, N Ichikawa, Y. Nakamura, S. Uchida, and B Nachumi. *Phys. Rev. B*, 54:7489, 1996.

[TAI+97] J. M. Tranquada, J. D. Axe, N Ichikawa, A R Moodebaugh, Y. Nakamura, and S. Uchida. *Phys. Rev. Lett.*, 78:338, 1997.

[Tay21] G. I. Taylor. *Proc. London Math. Soc.*, 20:196, 1921.

[TBSL94] J. M. Tranquada, D.J Buttrey, V. Sachan, and J. E. Lorenzo. *Phys. Rev. Lett.*, 73:1003, 1994.

[TIU99] J. M. Tranquada, N. Ichikawa, and S. Uchida. *Phys. Rev. B*, 59:14712, 1999.

[TP00] O. Tchernyshyov and L. P. Pryadko. *Phys. Rev. B*, 61:12503, 2000.

[TSA+95] J. M. Tranquada, B. J. Sternlieb, J. D. Axe, Y. Nakamura, and S. Uchida. *Nature (London)*, 375:561, 1995.

[VC01] A. Vishwanath and D. Carpentier. *Phys. Rev. Lett.*, 86:676, 2001.

[vDS98] J. v. Delft and H. Schoeller. *Annalen der Physik*, 7:225, 1998.

[VF84] J. Villain and J. F. Fernandez. *Z. Phys. B*, 54:139, 1984.

[vHS00] F. von Oppen, B. I. Halperin, and A. Stern. In R. F. Bishop, N. R. Walet, and Y. Xian, editors, *Advances in Quantum Many-Body Theory*, volume 3. World Scientific, 2000.

[Voi95] J. Voit. *Rep. Prog. Phys.*, 58:977, 1995.

[vVN+98] M. von Zimmermann, A. Vigliante, T. Niemöller, N. Ichikawa, T. Frello, J. Madsen, P. Wochner, S. Uchida, N. H. Andersen, J. M. Tranquada, D. Gibbs, and J. R. Schneider. *Europhys. Lett.*, 41:629, 1998.

[Wen90] X. G. Wen. *Phys. Rev. B*, 42:6623, 1990.

[WLK+97] B. O. Wells, Y. S. Lee, M. A. Kastner, R. J. Christianson, , R. J. Birgenau, K. Yamada, Y. Endoh, and G. Shirane. *Science*, 277:1067, 1997.

[WSE+00] S. Wakimoto, G. Shirane, Y. Endoh, K. Hirota, S. Ueki, K. Yamada, R. J. Birgenau, M. A. Kastner, Y. S. Lee, P. M. Gehring, and S. H. Lee. *Phys. Rev. B*, 60:R769, 2000.

[Wu03] F. Y. Wu. 2003. preprint cond-mat/0303251.

[YHC99] Y. Yoshinari, P. C. Hammel, and S-W. Cheong. *Phys. Rev. Lett.*, 82:3536, 1999.

[YLK+98] K. Yamada, C. H. Lee, K. Kurahashi, J. Wada, S. Wakimoto, S. Ueki, Y. Endoh, S. Hosoya, G. Shirane, R. J. Birgenau, M. Greven, M. A. Kastner, and Y. J. Kim. *Phys. Rev. B*, 57:6165, 1998.

[Zaa00] J. Zaanen. *Phys. Rev. Lett.*, 84:753, 2000.

[Zac00] O. Zachar. *Phys. Rev. B*, 62:13836, 2000.

[ZG89] J. Zaanen and O. Gunnarsson. *Phys. Rev. B*, 40:7391, 1989.

[ZHvS96] J. Zaanen, M. L. Horbach, and W. van Saarloos. *Phys. Rev. B*, 53:8671, 1996.

[ZKE98] O. Zachar, S. A. Kivelson, and V. J. Emery. *Phys. Rev. B*, 57:1422, 1998.

[ZLH99] C. Zeng, P. L. Leath, and T. Hwa. *Phys. Rev. Lett.*, 83:4860, 1999.

[ZMK+95] E. Zeldov, D. Majer, M. Konczykowski, V. B. Geshkenbein, V. M. Vinokur, and H. Shtrikman. *Nature (London)*, 375:373, 1995.

[ZMS96] C. Zeng, A. A. Middleton, and Y. Shapir. *Phys. Rev. Lett.*, 77:3204, 1996.

[ZOK+01] J. Zaanen, O. Y. Osman, H. V. Kruis, Z. Nussinov, and J. Tworzydlo. *Philos. Mag. B*, 10:1485, 2001.

Dank

mein Dank gilt:

- dem Betreuer der Arbeit, Thorsten Emig, für die große Unterstützung und seine kollegiale, produktive Anleitung;
- Stefan Scheidl, der in der Anfangszeit die Arbeit betreute und auf den Weg brachte und mir über Jahre ein wertvoller Lehrer war;
- Herrn Prof. T. Nattermann;
- den Kollegen in der Arbeitsgruppe, Bernd, Andreas, Frank, Rauno und Christoph;
- den Kollegen von der Fussballwiese;
- natürlich meinen Eltern;
- vor allem aber meiner Freundin Anja mit Sepp, ohne die nichts geht.

Zusammenfassung

Die vorliegende Arbeit untersucht den Einfluss von Unordnung auf planare periodische Strukturen in Supraleitern. Im ersten Teil stellen die vor etwa 10 Jahren entdeckten Streifenphasen in Hochtemperatursupraleitern diese periodische Überstruktur jenseits des Atomgitters dar. Wir beschäftigen uns in einem ersten Schritt mit den strukturellen Eigenschaften der eindimensionalen Ladungs- und Spindichtemodulation – den Streifen in den Kupferoxidebenen – welche die funktionalen Bauelemente aller Kuprat-Supraleiter sind. Es zeigt sich, dass die Konkurrenz zwischen dem ordnenden periodischen Potential des Atomgitters und dem Potential der zufällig verteilten Verunreinigungen auf großen Längenskalen in zwei Dimensionen immer zugunsten der Unordnung ausgeht. So sind die Auslenkungsfluktuationen der Streifen divergent und topologische Defekte lassen auch bei verschwindender Temperatur nur kurzreichweitige Translationsordnung zu. Der Einfluss von Quantenfluktuationen ändert nichts an diesem Ergebnis, welches in Einklang mit der Beobachtung von glasartigem Verhalten in Experimenten steht.
Im zweiten Schritt wird das Zusammenspiel von Unordnung und den elektronischen Freiheitsgraden auf den Streifen mit dem Modell gekoppelter eindimensionaler Elektronenflüssigkeiten, den Luttinger Flüssigkeiten (LF), untersucht. Renormierungsgruppenmethoden zeigen, dass – anders als im reinen System – die Ladungsdichtewellenkopplung zwischen den LF immer irrelevant ist. Durch Variation der Unordnungsstärke oder der Kopplungsparameter zwischen und auf den Streifen kann ein Delokalisierungsübergang vom ungeordneten Isolator zu einem stark anisotropen metallischen Zustand mit LF-artigem Transport ausgelöst werden. Dieser Zustand unterscheidet sich stark von seinem Gegenstück im reinen System und stellt doch eine mögliche zweidimensionale metallisch Phase dar, die nicht als Fermi-Flüssigkeit beschrieben werden kann.

Im Mittelpunkt von Teil zwei steht das ungeordnete planare Flussliniengitter als eine einfache Realisierung eines Vortexglases. Der kürzlich gefundene Ausdruck für die freie Energie bei einer speziellen Flusslinien-Wechselwirkung [EK01] hilft uns, die Existenz einer thermisch freien Phase über dem planaren Vortexglas auszuschließen. Dieses Resultat kann auf den Fall beliebiger repulsiver Wechselwirkungen ausgedehnt werden. Das verwandte XY Modell in einem Zufallsfeld zeigt bekanntermaßen sehr wohl den Übergang zu einer thermisch entpinnten Phase, allerdings ohne, wie wir berechnen, dabei Spuren in der freien Energie zu hinterlassen.
Die auf den ersten Blick unerwartete Abbildung des Flussliniengitters auf ein Modell der kombinatorischen Statistik, das 'Random Bond Dimer Model', ermöglicht die Untersuchungen des abschließenden Teils. Das Dimer Modell kann mittels eines kürzlich entwickelten polynomialen Algorithmus numerisch exakt behandelt werden, was einen wesentlichen Fortschritt im Vergleich zu herkömmlichen Monte Carlo Verfahren darstellt. Nach der Erweiterung der Abbildung auf thermodynamische Größen können die Vorhersagen der exakten Lösung und Simulationsdaten der Gruppe von C. Zeng (Washington, D.C.) verglichen werden. Es ergibt sich die erstaunlich genaue Übereinstimmung in allen untersuchten Größen: der Amplitude von Korrelationsfunktionen; der mittleren freien Energie, inneren Energie und der Entropie; den Momenten der unordnungsverteilten freien Energie; der

Wärmekapazität. Die neuen Resultate verdeutlichen den Modellcharakter des planaren Vortexglases, das trotz der einem Glas inhärenten Komplexität in vielen Aspekten noch 'lösbar' ist.

Erklärung

Ich versichere, dass ich die von mir vorgelegte Dissertation selbständig angefertigt, die benutzten Quellen und Hilfsmittel vollständig angegeben und die Stellen der Arbeit – einschließlich Tabellen, Karten und Abbildungen –, die anderen Werken im Wortlaut oder dem Sinn nach entnommen sind, in jedem Einzelfall als Entlehnung kenntlich gemacht habe; dass diese Dissertation noch keiner anderen Fakultät oder Universität zur Prüfung vorgelegen hat; dass sie – abgesehen von den angegebenen Teilpublikationen – noch nicht veröffentlicht worden ist sowie, dass ich eine solche Veröffentlichung vor Abschluss des Promotionsverfahrens nicht vornehmen werde. Die Bestimmungen dieser Promotionsordnung sind mir bekannt. Die von mir vorgelegte Arbeit ist von Dr. Thorsten Emig und Priv. Doz. Dr. S. Scheidl betreut worden.

Teilpublikationen:

- ☐ "Pinning of stripes in cuprate superconductors"
  S. Bogner and S. Scheidl, Phys. Rev. B **64**, 054517 (2001)
- ☐ "Delocalization in coupled Luttinger liquids"
  S. Scheidl, S. Bogner and T. Emig, Phys. Rev. B **65**, 224507 (2002)
- ☐ "Is there a Glass Transition in Planar Vortex Arrays?"
  T. Emig and S. Bogner, Phys. Rev. Lett. **90**, 185701 (2003)